Title
Expanding the Composition and Function of the Toxoplasma Inner Membrane Complex

Author
Back, Peter Sungmin

Publication Date
2023

Peer reviewed|Thesis/dissertation

UNIVERSITY OF CALIFORNIA

Los Angeles

Expanding the Composition and Function of the *Toxoplasma* Inner Membrane Complex

A dissertation submitted in partial satisfaction of the

requirements for the degree Doctor of Philosophy

in Molecular Biology

by

Peter Sungmin Back

2023

ABSTRACT OF THE DISSERTATION

Expanding the Composition and Function

of the *Toxoplasma* Inner Membrane Complex

by

Peter Sungmin Back

Doctor of Philosophy in Molecular Biology

University of California, Los Angeles, 2023

Professor Peter John Bradley, Chair

The superphylum Alveolata contains three remarkably diverse groups of protozoans: the free-living ciliates and dinoflagellates, and the parasitic apicomplexans. Despite their diversity in morphology and lifestyle, alveolates are taxonomically unified by the presence of alveoli, a peripheral membrane system situated underneath the plasma membrane. The phylum Apicomplexa has received extensive attention due to the medical and economic burdens caused by its parasitic constituents, which include *Toxoplasma gondii* (toxoplasmosis) and *Plasmodium spp.*(malaria). Importantly, *T. gondii* serves as a model organism for these apicomplexans and even alveolates due to its experimental tractability. Moreover, toxoplasmosis is a life-threatening disease for immunocompromised individuals and congenitally infected neonates, highlighting the desperate need to understand its biology and develop better therapeutics against this pathogen.

A hallmark structure of the Alveolata is the alveoli, called the inner membrane complex (IMC) in apicomplexan parasites. The IMC is a peripheral membrane-cytoskeletal system underlying the plasma membrane and governs essential functions in all facets of the parasite's intracellular lifestyle, including host cell invasion, replication, and egress. Specifically, it serves as a platform for the actin-myosin motor that powers gliding motility and provides a scaffold for daughter cells during replication. However, the sectioned organization of the IMC into multiple distinct subcompartments suggests additional functions not yet discovered for each compartment. Furthermore, even the well-established functions are not thoroughly understood, largely due to the scarcity of known IMC components. Here, we define a novel third role for the IMC and greatly expand the current catalog of daughter IMC proteins.

By characterizing the apical cap proteins AC9 and AC10, we demonstrate for the first time that the IMC apical cap critically stabilizes the apical complex, a cytoskeletal structure that controls parasite motility and secretory organelle exocytosis. We discover that AC9:AC10 performs this function by interacting with the MAP kinase ERK7 and concentrating it in the apical cap. Our subsequent dissection of the AC9:AC10:ERK7 complex revealed multiple independent interactions that organize the apical cap and uncovered an unusual mechanism of competitive inhibition that AC9 exerts on ERK7. This implicates the apical cap as not only an anchoring site for ERK7, but also as a regulatory center for its kinase activity.

We also explore the daughter cell scaffold by focusing on IMC29, pinpointing its precise timing of expression and describing its important function in coordinating the initiation stages of endodyogeny. We then use proximity labeling to identify a large array of novel IMC proteins, many of which localize exclusively to the nascent daughter cells. This firmly establishes the daughter IMC as a distinct subcompartment with its own cohort of proteins. Moreover, some of these proteins exhibited an interesting localization to the membrane interface between two daughter cells, launching a new area

of research that promises novel insights into endodyogeny. Together, this dissertation presents exciting findings into the composition and function of the *T. gondii* IMC, with potentially broader impacts for apicomplexan and alveolate cell biology.

The dissertation of Peter Sungmin Back is approved.

Oliver I. Fregoso

Kent L. Hill

Marcus Horwitz

Peter John Bradley, Committee Chair

University of California, Los Angeles

2023

Dedicated to my parents,

who lead difficult immigrant lives to make a better life for us.

To my Lighthouse Community Church family,

the people who gave me a place to belong.

TABLE OF CONTENTS

List of Figures

List of Tables

Acknowledgments

This dissertation is not only the culmination of my work, but also the testament of an extensive support system, my village.

The first person to thank has to be my PI, Dr. Peter Bradley, perhaps the most hands-on mentor I have ever experienced. The truly impressive part is how much I have enjoyed your direct mentorship. Your ability to balance challenging and caring for me is unparalleled, and I can sincerely say that you are simultaneously my boss, my colleague, my friend, and my parent (?!). Remember when I broke that microcentrifuge and we had to pry it open to get our mass spec samples? Or that time I contaminated a whole bottle of media with transgenic parasites? Those moments really brought out your nurturing side, never making me feel devalued. You even bought me a new microcentrifuge! Thank you for always going above and beyond for your students. In every part of my PhD – writing training grants, preparing for presentations, or designing experiments – I always felt like we were a team. I can only hope to become the kind of mentor you were to me, but I'm sure time will tell what kind of indelible mark you left on me as a scientist.

To the members of the Bradley lab, past and present. While every one of you played an important role in my PhD journey, I only have space to highlight a few. Thank you to Dr. Josh Beck, whose thin-section electron micrographs were used to illustrate the IMC structure in Chapter 1. To Andy, thank you for teaching me basically every lab-standard assay within 3 months and for launching so many projects, many of which made this dissertation possible. To Amara, thank you for putting up with me for 8-10 hours a day for >5 years. From meeting at UCLA interviews, taking the same classes, joining the Bradley lab together, and now with graduation on the horizon, it's impossible to separate my PhD experience from our friendship. I know we often joke that we see each other more than we

see anyone else ('besties' in your words, cringe). But I think one of the things that will feel most foreign after graduating is knowing that you're not in the next bay over. Alas, I will miss our spontaneous blaze, and now subway (rotisserie-style chicken!) lunches, our photography adventures, and out-of-the-blue political conversations. Thank you for not just being colleagues, but friends. Besties, I guess.

To the members of the Horwitz lab, thank you for treating me with the utmost patience and dealing with my young, undergraduate self. Specifically, to Mike and Marcus, thank you for sparking my interest in science. Even if I may have seemed a bit detached or made a lot of simple mistakes, I attribute much of my achievements to the foundations you set for me. To Sasa, Susana, and BJ, thank you for warmly welcoming me into your daily lunches and sharing your life with me; the lab became a second home for me as a result.

To the community at UCLA – Hallem lab, Fregoso lab, Hill lab, Zhou lab, and MBI – thank you for being good friends to me and good resources for me. Special thanks to Dr. Elissa Hallem, who was a formal member of my committee and was only removed for logistical reasons. Thank you for always writing me great reference letters, for being my rotation PI during the toughest first quarter of grad school, and for being a great advisor throughout the years. Shout out to the MBI admin team – Ashley, Stephanie, and Helen – for their amazing logistical support.

To my LCC community, you have been my second family. Most of you have fed me at least one meal, if not dozens. Some of you have thoughtfully invited me over for holidays, knowing that my family is overseas. A few of you have become my closest friends, opening up your life with me, supplementing my rent, being my roommates, playing games together, hanging out, and laughing. Thank you for keeping me sane during this long journey. To Becca, while this dissertation marks the end of a season for me, it's the beginning of another one for us. I'm glad the hours and hours we've logged on facetime are coming to an end, and I'm excited to log many more hours finally in person.

To my family, especially my parents, words cannot describe the gratitude I feel. Thank you for raising us and bringing us to the United States, at the expense of your own careers. I know the instability of your lives in Korea reflects the sacrifice you made to establish an American life for my brother and me. But I hope you are proud of the legacy of faith you have instilled in us. This dissertation is dedicated to you, hopefully a small glimpse that the sacrifice was all worth it.

Finally, I want to acknowledge all those who contributed to each chapter of this dissertation. In particular, I want to thank Dr. Michael Reese and Wil O'Shaughnessy, with whom we had an incredibly fruitful collaboration. The publications described in Chapters 2 and 3 would not have been possible without them, reflected by the co-first authorship and co-principal investigators.

Chapter 2 was originally published in *PNAS*. "Back, P.S.*, O'Shaughnessy, W.J.*, Moon, A.S., Dewangan, P.S., Hu, X., Sha, J., Wohlschlegel, J.A., Bradley, P.J.$^{+}$, Reese, M.L.$^{+}$, 2020. Ancient MAPK ERK7 is regulated by an unusual inhibitory scaffold required for Toxoplasma apical complex biogenesis. *PNAS*. 117, 12164–12173. https://doi.org/10.1073/pnas.1921245117." It is reprinted here with permission under the Creative Commons Attribution License 4.0 (CC BY). *P.S.B. and W.J.O. contributed equally to this work; $^{+}$P.J.B. and M.L.R. are co-principal investigators of this work. Author contributions: P.S.B., W.J.O., A.S.M., P.S.D., X.H., P.J.B., and M.L.R. designed research; P.S.B., W.J.O., A.S.M., P.S.D., X.H., and J.S. performed research; P.S.B., W.J.O., P.S.D., X.H., J.S., J.A.W., P.J.B., and M.L.R. analyzed data; and P.S.B., W.J.O., P.S.D., P.J.B., and M.L.R. wrote the paper. In addition to funding for the Reese lab, P.J.B. acknowledges funding from the NIH (National Institute of Allergy and Infectious Diseases R01 AI123360) and J.A.W. acknowledges NIH R01 GM089778. P.S.B. was funded by Ruth L. Kirschstein National Research Service Award GM007185.

Chapter 3 was originally published in *mBio*. "Back, P.S., O'Shaughnessy, W.J., Moon, A.S., Dewangan, P.S., Reese, M.L., Bradley, P.J., 2022. Multivalent Interactions Drive the Toxoplasma AC9:AC10:ERK7 Complex To Concentrate ERK7 in the Apical Cap. mBio 13, e02864-21.

https://doi.org/10.1128/mbio.02864-21." It is reprinted here with permission under the Creative Commons Attribution 4.0 International License 4.0. P.S.B. and W.J.O. contributed equally to this work. Author order was determined alphabetically. P.J.B. and M.L.R. are co-principal investigators for this work. This work was supported by the National Institute of Health (AI150715 to M.L.R. and AI064616 to P.J.B.). M.L.R. was also supported by the National Science Foundation (NSF; MCB1553334) and the Welch Foundation (I-2075-20210327). P.S.B. was supported by the Ruth L. Kirschstein National Research Service Award GM007185 and the Molecular Biology Institute (MBI) Whitcome Fellowship at UCLA.

Chapter 4 is adapted from a manuscript resubmitted to *mBio*. I would like to thank everyone who contributed to the work including Andy S. Moon, Rebecca R. Pasquarelli, Hannah N. Bell, Juan A. Torres, Allan L. Chen, Jihui Sha, Ajay A. Vashisht, James A. Wohlschlegel, and Peter J. Bradley. We would also like to thank Vern Carruthers for the MIC2 antibodies, Gustavo Arrizabalaga for the NHE3 antibody, and David Roos for the GRASP55-YFP plasmid as well as the members of the Bradley lab for helpful reading of the manuscript. This work was supported by NIH grants AI064616 to P.J.B. and GM089778 to J.A.W. P.S.B. and R.R.P. were supported by the Ruth L. Kirschstein National Research Service Award GM007185 and UCLA Molecular Biology Institute (MBI) Whitcome Fellowship. R.R.P. was additionally supported by the Ruth L. Kirschstein National Research Service Award AI007323.

Vita

Education

2013-2017	Bachelor of Science in Microbiology, Immunology, and Molecular Genetics Graduated with departmental honors in advanced research *University of California, Los Angeles*

Research Experience

June 2018 – 2023	Graduate Student Researcher, Laboratory of Dr. Peter Bradley *Department of Microbiology, Immunology, and Molecular Genetics, UCLA*
Spring 2018	Rotation Student, Laboratory of Dr. Oliver Fregoso *Department of Microbiology, Immunology, and Molecular Genetics, UCLA*
Winter 2018	Rotation Student, Laboratory of Dr. Peter Bradley *Department of Microbiology, Immunology, and Molecular Genetics, UCLA*
Fall 2017	Rotation Student, Laboratory of Dr. Elissa Hallem *Department of Microbiology, Immunology, and Molecular Genetics, UCLA*
2015 – 2017	Undergraduate Student Researcher, Laboratory of Dr. Marcus Horwitz *Department of Medicine, Infectious Diseases, UCLA* *Department of Microbiology, Immunology, and Molecular Genetics, UCLA*

Publications

Jan 2023	**Back PS**, Moon AS, Pasquarelli RR, Bell HN, Torres JA, Chen AL, Sha J, Vashisht AA, Wohlschlegel JA, Bradley PJ. IMC29 plays an important role in *Toxoplasma e*ndodyogeny and reveals new components of the daughter-enriched IMC proteome. *mBio*. 2023 Jan 9:e0304222.
Oct 2022	Souza ROO, Jacobs KN, **Back PS**, Bradley PJ, Arrizabalaga G. IMC10 and LMF1 mediate mitochondrial morphology by mitochondrion-pellicle contact sites in Toxoplasma gondii. *J Cell Sci*. 2022 Oct 31:jcs.260083.
Feb 2022	**Back PS***, O'Shaughnessy WJ*, Moon AS, Dewangan PS, Reese ML^{+}, Bradley PJ^{+}. Multivalent interactions drive the *Toxoplasma* AC9:AC10:ERK7 complex to concentrate ERK7 in the apical cap. *mBio*. 2022 Feb 22;13(1).
Feb 2021	Torres JA, Pasquarelli RR, **Back PS**, Moon AS, Bradley PJ. Identification and molecular dissection of IMC32, a conserved *Toxoplasma* inner membrane complex protein that is essential for parasite replication. *mBio*. 2021 Feb 16;12(1).
Jun 2020	**Back PS***, O'Shaughnessy WJ*, Moon AS, Dewangan PS, Hu X, Sha J, Wohlschlegel JA, Reese ML^{+}, Bradley PJ^{+}. Ancient MAPK ERK7 is regulated by an unusual inhibitory scaffold required for *Toxoplasma* apical complex biogenesis. *PNAS*. 2020 Jun 2;117(22).

Oct 2019	Choi CP, Moon AS, **Back PS**, Jami-Alahmadi Y, Vashisht AA, Wohlschlegel JA, Bradley PJ. A photoactivatable crosslinking system reveals protein interactions in the *Toxoplasma gondii* inner membrane complex. *PLoS Biology*. 2019 Oct 4;17(10).

Selected Conference Presentations

May 2022	"The alveolin protein IMC6 is critical for parasite replication and forms a network of cytoskeletal interactions to maintain parasite shape." International Congress of Toxoplasmosis (ToxoXVI). Riverside, California. Poster presentation
Oct 2021	"An essential IMC protein complex governs *Toxoplasma* invasion and egress." Southern California Eukaryotic Pathogens Conference. Online platform. Oral presentation.
Oct 2020	"An essential IMC protein governs *Toxoplasma* invasion and apical organelle organization." Southern California Eukaryotic Pathogens Conference. Online platform. Poster presentation.
Oct 2019	"An essential IMC protein governs *Toxoplasma* invasion and apical organelle organization." Southern California Eukaryotic Pathogens Conference. UC Riverside, CA. Selected for best oral presentation.
Sep 2019	"Identification and functional analysis of AC9, an essential apical cap protein." UCLA Molecular Biology Interdepartmental Program Retreat. Lake Arrowhead, CA. Selected for best poster presentation.
Jun 2019	"Identification and Functional Analysis of IMC29, a novel daughter-enriched *Toxoplasma* IMC Protein." International Congress of Toxoplasmosis (ToxoXV). Quindío, Colombia. Oral presentation.
Nov 2018	"Identification and Functional Analysis of IMC29, a Novel Daughter-Enriched *Toxoplasma* IMC protein." Southern California Eukaryotic Pathogens Conference. UC Riverside. Selected for best poster presentation.

Selected Awards and Fellowships

2022-2023	Dissertation Year Fellowship *UCLA Graduate Division*
2022	Mautner Graduate Awards for excellence in academics and research (https://bit.ly/3NFoZos)
2020-2021	Predoctoral Whitcome Fellowship *UCLA Molecular Biology Interdepartmental Program*
2018-2019	Cellular and Molecular Biology Training Grant *Ruth L. Kirschstein National Research Service Award GM007185*
2017	Departmental Honors for MIMG *UCLA*

Chapter 1

–

Introduction

1.1 *Toxoplasma gondii* is the causative agent of toxoplasmosis

1.1.1 Prevalence and transmission

Toxoplasma gondii is a widespread protozoan parasite that is able to infect virtually any warm-blooded mammal. In humans, its prevalence ranges from under 10% in some regions to an astonishing 90% in others, depending on several factors such as climate, sanitation, and diet (Pappas et al., 2009). The reason for this local variability in prevalence is the parasite's cyst-mediated mode of transmission. Cyst forms of the parasite are found either in undercooked meat (mainly pork and lamb) as tissue cysts or in food and water containing oocysts shed by cats (domestic or wild members of the family Felidae) (Montoya and Liesenfeld, 2004). Thus, consumption of cyst-contaminated food or water is believed to be the main route for human infections, and reduction of cyst transmission is key to curbing further spread of the parasite. Transmission of tissue cysts can be minimized by avoiding undercooked meat while oocysts can be filtered out during water purification processes. Oocyst viability is also dependent on environmental factors like climate and altitude, correlating higher prevalence rates to hot and humid regions of the world, particularly in lower altitudes.

For example, in the United States, prevalence remains relatively low at 11% (Jones et al., 2007; Pappas et al., 2009; Aguirre et al., 2019). Some East Asian countries such as South Korea tout an even lower prevalence of 6.7%, likely due to minimal consumption of undercooked meat, low frequency of domestic cats, high frequency of urban lifestyles, and high quality of water sanitation (Shin et al., 2009). In contrast, European countries such as Germany notoriously report high levels of prevalence of up to 84%, attributed primarily to the consumption of raw meat (Wilking et al., 2016). South American countries document high seroprevalence as well; for example, rural Brazil reported that 74.5% of pregnant women were seropositive mainly due to frequent contact with contaminated soil (Spalding

et al., 2005). Despite this variability, *T. gondii* is clearly an extremely widespread parasite found in most regions of the world.

1.1.2 Clinical manifestations and disease

In healthy children and adults, acute infections typically show little to no symptoms, often resembling mild flu-like symptoms. On rare occasions, parasites can infiltrate the eye and cause retinal lesions with intense inflammation, known as ocular toxoplasmosis (Montoya and Liesenfeld, 2004). This is observed in approximately 2% of all infected individuals, even in immunocompetent people as the eye is an immune privileged environment (Holland, 2003). In all other parts of the body, a competent immune system is effective at controlling the initial acute infection; however, this forces the parasites into a dormant, cyst form which establishes a chronic infection in the muscle, organ tissue, and brain (Jones et al., 2007). While these cysts are generally innocuous, they are believed to persist for the life of the immunocompetent human host. Concerningly, even for healthy people, recent studies have correlated asymptomatic *T. gondii* infections with greater cognitive decline in older individuals and increased chances of developing a whole host of medical conditions including cardiovascular disease, neurodegenerative disease, and opportunistic infections (Gajewski et al., 2014; Flegr et al., 2014). While this connection between chronic infection and other medical conditions is still tenuous, if true, *T. gondii* would become an even deadlier human pathogen, compounded by the glaring lack of treatment options for clearing latent cysts.

In contrast to healthy individuals, immunocompromised people are at high risk of developing severe acute toxoplasmosis. They can acquire the infection either through the normal transmission routes for a primary infection or through the reactivation of a latent infection. Reactivation can occur in two main medical situations: acquisition of an immunodeficient condition (e.g. HIV-mediated AIDS), and active suppression of immunity (e.g. post-transplant medication) (Montoya and Liesenfeld,

2004). In either case, the symptoms can be debilitating if left unmanaged and the disease fatal if left untreated. The most pronounced manifestation is encephalitis, which results in a number of neurologic abnormalities including ataxia, lethargy, and seizures (Luft et al., 1993). Notably, toxoplasmic encephalitis remains the leading cause of brain mass lesions in HIV-infected patients despite the overall success of antiretroviral therapies, though this is likely due to inaccessibility to the medication or noncompliance (Marra, 2018). Ocular toxoplasmosis is also more severe in these individuals, often displaying as recurrent lesions at the borders of retinal scars (Montoya and Liesenfeld, 2004). These lesions are likely the result of constant cycling of reactivation and latency, leading to tissue damage by both parasitic invasion and collateral damage from immune-directed inflammation.

Another group that experiences potentially life-threatening infections is neonates, who can acquire the infection by vertical transmission of a primary maternal infection, regardless of the mother's immune status (Torgerson and Mastroiacovo, 2013). Congenital toxoplasmosis can present with hydrocephalus, microcephaly, intracranial calcifications, chorioretinitis, blindness, and epilepsy (McAuley et al., 1994). Severe cases may even result in premature birth or miscarriages. The severity of the disease is largely determined by the timing of transmission. The chance of vertical transmission is greater during the later stages of pregnancy; however, the disease is typically more severe if the parasite is transmitted during the earlier gestational period (Goldstein et al., 2008). Furthermore, latent infections are at risk of reactivating in women who become immunocompromised during their pregnancy, which can then transmit to the fetus and cause congenital infection. Thus, neonates represent one of the most important groups to protect from this disease.

While an effective vaccine is yet to be developed, treatment options do exist, though they are limited to controlling the acute disease. For immunocompromised cases, and in rare instances for healthy individuals, a typical drug regimen includes pyrimethamine (Daraprim), sulfadiazine, and

folinic acid for 4-6 weeks. The main side effects are caused by pyrimethamine, which include bone marrow suppression and liver toxicity, especially when administered over a long period of time. Sulfadiazine may be substituted with clindamycin depending on the patient's specific sensitivities or allergies. An alternative drug combination is trimethoprim with sulfamethoxazole, though this is typically not as effective as the pyrimethamine regimen (Masters et al., 2003). Still others include atovaquone with azithromycin, but these have not been as extensively studied (Kovacs and The NIAID-Clinical Center Intramural AIDS Program, 1992). For pregnant women and congenital infections, public health education and serological screening of pregnant women remain the most reliable methods of disease prevention. If prevention methods are unsuccessful, early diagnosis and treatment have been shown to dramatically improve the clinical outcome of the infected newborn (Goldstein et al., 2008). If an acute infection is detected in women before the 16th week of pregnancy, spiramycin may be administered (Meroni et al., 2009). There appears to be compelling evidence of its efficacy to reduce parasite transmission in early gestational periods (Montoya et al., 2021). Thus, spiramycin is routinely used in Europe, Mexico and Canada, though it remains an experimental drug in the United States. If an infection is detected after the 16th week of pregnancy or if the fetus is found to be infected, the standard pyrimethamine regimen is implemented for the mother followed by continued treatment of the newborn for 12 months after birth. All the regimens mentioned may also be prescribed as prophylaxis, but its efficacy is controversial (Rajapakse et al., 2017). Thus, the severe lack of effective vaccines and treatments underscores the need for a deeper understanding of parasite biology to ultimately develop more effective, cheaper, and safer therapeutics against *T. gondii*.

1.2 *T. gondii* is a member of the phylum Apicomplexa and the superphylum Alveolata

1.2.1 *T. gondii* serves as a model organism for other apicomplexan parasites

The phylum Apicomplexa is comprised of over 5000 parasites, many of which cause significant medical and economic burdens worldwide. Other than *Toxoplasma*, human pathogens include *Plasmodium spp.* which causes malaria, and *Cryptosporidium spp.* which causes diarrheal disease (Mackintosh et al., 2004; Sow et al., 2016). Animal pathogens include *Eimeria spp.* and *Neospora spp.* which cause large numbers of abortions in livestock and extensive economic losses in these agricultural industries (Dubey, 2003; Lassen and Østergaard, 2012). *T. gondii* is considered a model organism for these apicomplexan parasites due to its ease of culturing in laboratory settings, amenability to genetic manipulation, and availability of robust assays for functional evaluation (Kim and Weiss, 2004). Recent studies have even developed complex *in vitro* systems that mimic the native host environment to better capture the intricacies of an *in vivo* infection. These include the advent of cat intestinal organoids that largely recapitulate the intestinal epithelial properties, and the use of human primary neuronal cells to more accurately explore the interface between parasite and the CNS (Genova et al., 2019; Mendez et al., 2021).

The *T. gondii* field has also developed several powerful approaches to knockout or knockdown endogenous genes or proteins, allowing researchers to determine the precise function of a protein (Jacot and Soldati-Favre, 2020). Most important was the advent of CRISPR/Cas9-based recombination, which further increased the efficiency of genetic engineering (Sidik et al., 2014). This has allowed the direct knockout of genes that were previously not possible and greatly accelerated the the development of system-wide genomic tools. For example, a recent genome-wide loss-of-function screen exploited the high efficiency of genetic recombination in *T. gondii* to disrupt every single gene in its genome and assign a corresponding fitness score (Sidik et al., 2016).

In addition, many of the key conditional knockdown and knockout systems were developed in *T. gondii*. First to be established was a tetracycline repressor-based system that conditionally controls the transcription of a gene of interest (Meissner et al., 2001). In this system, the gene of interest is placed under the control of a regulatable promoter containing seven tet-Operators, and the addition of anhydrotetracycline results in a transcriptional silencing of the gene. Another conditional system called the ligand-controlled destabilization domain (DD) allows rapid and reversible protein stabilization (Herm-Götz et al., 2007). In this system, the DD is fused to a gene of interest, and once expressed, the fusion protein is rapidly degraded unless stabilized by the synthetic ligand Shield-1. The third approach is a conditional knockout of the gene of interest (Andenmatten et al., 2013). In this, the DiCre recombinase is split into two inactive fragments fused to either the FRB or FKBP. The addition of rapamycin brings together FRB and FKBP to reconstitute the recombinase, which excises at loxP sites that flank the gene of interest. The fourth method also utilizes rapamycin induction but controls expression at the mRNA level (Pieperhoff et al., 2015). This system is called U1 small nuclear ribonucleic particles-mediated gene silencing, in which the addition of rapamycin results in the degradation of pre-mRNA. The most recent system to be developed is the auxin-inducible degron (AID), in which the addition of a plant hormone auxin results in a rapid degradation of the degron-fused protein of interest (Long et al., 2017b). Importantly, CRISPR/Cas9 recombineering has greatly enhanced the efficiency for all of these conditional systems as well. Such an impressive array of genetic tools with the choice to control gene expression at the genomic, transcriptomic, or protein level opens up countless areas of research that are unavailable to other apicomplexan parasites.

In an increasingly 'omics-forward era of research, *T. gondii* also represents a valuable model system to develop innovative system-wide tools that can be applied broadly. One example is a massive whole-cell proteomic experiment, in which virtually every protein was designated a subcellular location by subcellular fractionation and mass spectrometry (Barylyuk et al., 2020). Another example is the

adaptation of BioID, a protein-identification approach in which a promiscuous biotin ligase is fused to a bait protein and labels all nearby proteins in the native subcellular environment that can then be purified for mass spectrometry (A. L. Chen et al., 2015). Moreover, all of these 'omics datasets are available and easily accessible in the online resource ToxoDB (Kissinger et al., 2003; Harb and Roos, 2020). It is a user-friendly database that integrates all genomic, proteomic, and large-scale screens into one place; the importance of this tool cannot be overstated. Collectively, *T. gondii* has been instrumental in revealing crucial insights into apicomplexan parasites, and this field has the potential to continue developing broadly applicable tools that are relevant even outside the Apicomplexa.

1.2.2 *T. gondii* is a hallmark organism of the Alveolata

The phylum Apicomplexa belongs to the broader superphylum Alveolata, which in turn belongs to the Eukaryotic supergroup Stramenophila, Alveolata, Rhizaria (SAR) (Burki et al., 2020). The group Alveolata contains a diverse array of free-living dinoflagellates and ciliates, in addition to the intracellular apicomplexan parasites. Despite such fundamental differences in lifestyles, this alliance was designated based on rRNA sequencing and phylogenetic analyses (Wolters, 1991; Keeling et al., 2005). However, the most prominent characteristic that defines this group is the presence of membranous vesicles called 'alveoli' (Gould et al., 2008). While there is some structural variability between alveolates, all alveolar structures consist of a single or a series of flattened vesicles just underneath the plasma membrane (Kono et al., 2013). On the other hand, the functions of these structures vary widely to reflect the specific niche of each organism.

In ciliates, the single alveolar vesicle is located between the plasma membrane and epiplasm. It contains cytoskeletal proteins called plateins and primarily acts as a platform for ejectile structures like trichocysts and mucocysts (Hausmann and Kaiser, 1979; Kloetzel et al., 2003). It has also been shown to function in calcium storage, cilia movement and cell division (Plattner and Klauke, 2001).

In dinoflagellates, the homologous structure is called amphiesmal vesicles and can be found in two forms (Dodge and Crawford, 1969; Nevo and Sharon, 1969). In the first form, the vesicles contain cellulosic armored plates that are weaved together to create the theca of the cell and likely provide structural integrity. In the second form, the vesicles do not contain armored plates, resulting in 'naked' dinoflagellates; however, comparatively little is known about the function of this type of amphiesmal vesicles. In apicomplexans, the alveoli are called the inner membrane complex (IMC) and are typically organized as a series of rectangular plates along the body of the organism and capped by a single cone-shaped vesicle at the very apex (Scholtyseck, 1973; Morrissette et al., 1997). The apicomplexan IMC is the most extensively studied among the alveolates and has been shown to play critical roles in parasite motility, invasion into host cells, and intracellular replication (Blader et al., 2015). Overall, the presence of alveoli across such diverse organisms emphasizes the significance of this structure for the survival of all alveolates. Since the functions of alveoli in ciliates and dinoflagellates are much less understood, mechanisms that are uncovered by studying *T. gondii* promise to provide broad insights into the superphylum Alveolata.

1.3 Parasite morphology and specialized organelles

T. gondii differentiates into different forms depending on the stage of infection (Dubey et al., 1998). The bradyzoite is the slow-growing stage of the parasite and is found in tissue cysts of intermediate hosts (e.g. humans). The sporozoite is believed to be a specialized stage for invasion and is only found once parasites emerge from oocysts after going through sexual replication in the gut of the definitive host (cats). The tachyzoite is the rapidly proliferating stage of the parasite and is a result of differentiated bradyzoites; thus, tachyzoites can multiply by asexual replication if unhindered by the immune system. The acute infection is caused by tachyzoites, and its rapid growth facilitates robust experiments to tease apart the cell biology of the parasite.

The *T. gondii* tachyzoite measures approximately 2 μm wide and 5 μm long and resembles a banana in its shape. Interestingly, this shape is the basis for its taxonomic name. Originally identified by two groups in 1908, they used *Toxo* from the Greek word meaning "arc" or "bow" and *gondii* from the name of the rodent host "gundi" in which it was first discovered (Nicolle C. and Manceaux L., 1908; Splendore, A., 1908). As a protozoan parasite, it contains all of the typical eukaryotic organelles including a nucleus, endoplasmic reticulum (ER), Golgi apparatus and a single mitochondrion (Figure 1-1). Similar to other eukaryotic organisms, the *T. gondii* ER and Golgi primarily serve as production, processing, and trafficking centers for proteins that are primarily destined for the plasma membrane or the specialized secretory organelles in cellular respiration (Joiner and Roos, 2002). *T. gondii* contains a single mitochondrion and its function resembles that of other eukaryotes (Melo et al., 2000). However, its mitochondrial morphology is unique. In an extracellular parasite, the mitochondrion is

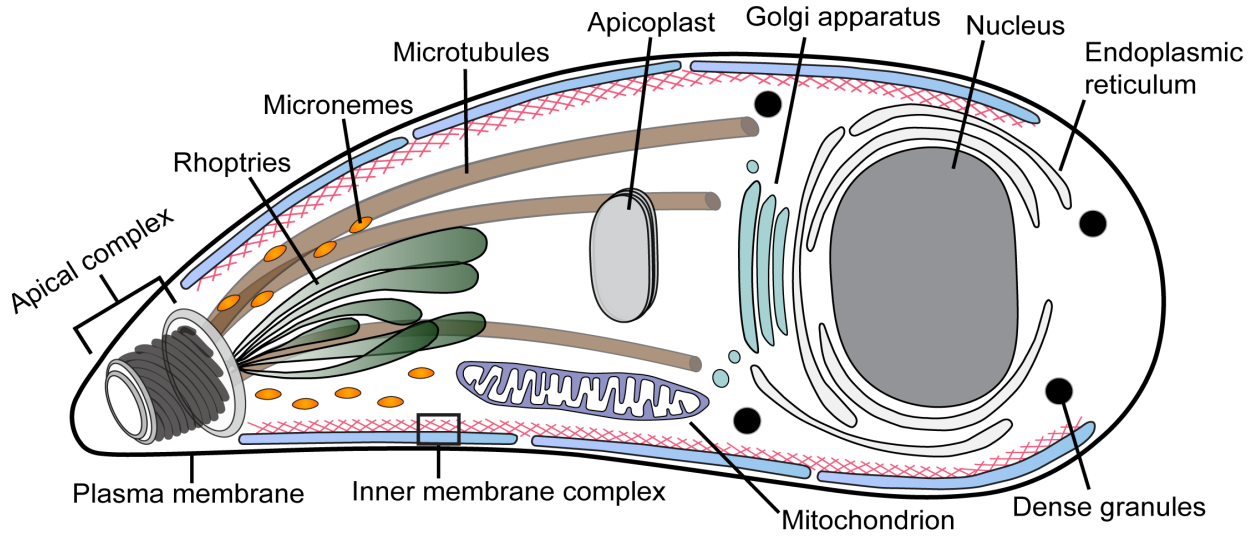

Figure 1-1. *T. gondii* morphology and specialized organelles.

Besides the typical eukaryotic organelles, several parasite-specific organelles are depicted. The cytoskeletal apical complex serves as a primary gateway for exocytosis, with secretion from the micronemes and rhoptries being released through the conoid. The dense granules also secrete proteins that remodel the parasitophorous vacuole. The apicoplast is an apicomplexan specific plastid organelle with essential metabolic functions. The inner membrane complex is a membrane (blue) and cytoskeletal (red) system underneath the plasma membrane with critical roles in motility and replication. Note that while the mitochondrion is illustrated here as a single concentrated stack, the mitochondrion of intracellular parasites displays a lasso-shape morphology that extends around the periphery of the parasite.

maintained in one concentrated region while in an intracellular parasite, the mitochondrion is stretched along the parasite periphery (Ovciarikova et al., 2017). Whether these morphological changes affect mitochondrial function is not yet understood. Besides these common organelles, *T. gondii* (and to some extent, all apicomplexan parasites) carries a set of specialized organelles that are required to invade its host cell and establish an intracellular environment.

The most striking of these is the apical complex, a group of cytoskeletal structures at the extreme apex of the parasite that includes the tubulin-based conoid, the flanking apical polar ring (APR), and two preconoidal rings (PCRs) (Morrissette and Sibley, 2002). As its name suggests, the apical complex gives the phylum Apicomplexa its name and is believed to be present in all members of the phylum. At the center of the apical complex is the conoid, which was one of the first apicomplexan-specific structures to be described due to the distinct basket-shaped ultrastructure (Scholtyseck et al., 1970). Interestingly, the conoid was presumed to be missing from Haemosporidia (e.g. *Plasmodium spp.*) until recent studies demonstrated the presence of a reduced conoid complex in multiple stages of *Plasmodium* (Levine et al., 1980; Wall et al., 2016, 2019; Koreny et al., 2021). Conoid-like structures have also been found in early-branching alveolates outside of Apicomplexa, suggesting that the apical complex is more broadly conserved than originally appreciated (Okamoto and Keeling, 2014; Füssy et al., 2017). In agreement with this, several groups have identified cilium-associated proteins in the apical complex, supporting its significance beyond Apicomplexa (Francia et al., 2012; de Leon et al., 2013; Francia et al., 2016; Wall et al., 2016; Lentini et al., 2019).

The apical complex has been assigned several putative functions, primarily by work in *T. gondii*. Numerous studies have attributed its role to regulating the release of proteins from the specialized secretory organelles called micronemes and rhoptries, which govern parasite motility, attachment, invasion, and egress (Blader et al., 2015). For example, calcium signaling cascades were found to coordinate both microneme secretion and conoid extrusion, supporting a link between the two

processes (Carmen et al., 2009). In addition, another group showed that the absence of the apical polar ring protein RNG2 eliminated microneme secretion and prevented host cell invasion (Katris et al., 2014). Besides its role in exocytosis, the apical complex is also considered to be the microtubule organizing center (MTOC) for a series of subpellicular microtubules that extend the majority of the parasite's length, which was demonstrated by characterizing the apical polar ring protein APR1 (Leung et al., 2017). Finally, the conoid has been implicated in initiating motility by several calmodulin-like proteins, the myosin motor protein MyoH, and the essential formin protein FRM1 (Graindorge et al., 2016; Long et al., 2017b; Tosetti et al., 2019). This was corroborated by identifying the protein CPH1, without which the conoid was deformed and parasites could not move or invade (Long et al., 2017a). In addition, a recent study identified two proteins Pcr4 and Pcr5 that are required to stabilize the preconoidal rings and allow parasite motility, in both *T. gondii* and *Plasmodium* ookinetes (Dos Santos Pacheco et al., 2022). Together, the apical complex is a highly conserved structure that is critical for multiple parasite-specific processes to ultimately drive parasite invasion.

Another set of specialized organelles is the secretory micronemes and rhoptries (Figure 1-1). The micronemes are rod-shaped organelles that are clustered near the apical end of the parasite (Carruthers and Tomley, 2008). They secrete transmembrane MIC proteins containing adhesin domains onto the surface of the parasite. These MIC adhesins are released in response to calcium signaling and function in attaching the parasite's plasma membrane to the surface of a host cell, allowing gliding motility through the action of the parasite's actin-myosin motor. The rhoptries are a series of 8-14 club-shaped organelles that also cluster in the apical end of the parasite. Rhoptry proteins are secreted at the site of parasite attachment to the host cell and form the moving junction, a complex through which the parasite invaginates the host plasma membrane forming a parasitophorous vacuole (PV) in the cytoplasm around the invading parasite. Rhoptry proteins have also been demonstrated to be injected into the host cell cytoplasm and directly modulate key host effectors, allowing the parasite

to avoid the host's immune response (Blader et al., 2015). The final secretory organelles are the dense granules, which release GRA proteins into the newly formed PV to remodel the environment for intracellular growth. A subset of GRAs traverse the PV membrane into the host cytoplasm, where they also control host factors to evade host immunity (Blader et al., 2015). Aside from the secretory organelles, *T. gondii* also contains a plastid organelle called the apicoplast. It is encased by four membranes with its own small genome and is believed to be the remnant of a secondary endosymbiotic event. As such, it has no photosynthetic function; however, it has retained some essential metabolic functions for parasite growth including the synthesis of isoprenoids, fatty acids and heme (Lim and McFadden, 2010). Importantly, due to its plant-like properties and distinct nature from higher order eukaryotic hosts, the apicoplast has been an attractive target for parasite-specific therapeutics (Soldati, 1999).

A hallmark organelle of apicomplexan parasites (and alveolate organisms) is the inner membrane complex (IMC). The *T. gondii* IMC is a peripheral membrane system that lies directly underneath the plasma membrane. It is a two-part structure composed of a series of membrane vesicles and an underlying network of cytoskeletal proteins (Mann and Beckers, 2001). The IMC has traditionally had two well-established roles: serving as a platform for the actin-myosin motor that powers gliding motility and forming a scaffold for daughter bud assembly during asexual replication. Section 1.5 of this chapter includes greater detail about the structure and function of the IMC, and Chapters 2 and 3 describe a newly discovered third role for the IMC in stabilizing the apical complex.

1.4 The lytic cycle

1.4.1 Host cell invasion

One principal reason for *T. gondii*'s wide range of hosts is its remarkable ability to invade any nucleated cell from a warm-blooded mammal. This is possible because the parasite carries an arsenal of invasion machinery that allows the indiscriminate entry of any host cell membrane. Invasion begins with the parasite loosely attaching itself to a host cell through its surface protein coat. The parasite's coat is covered with GPI-anchored surface antigens called SAGs, which are known to recognize and bind sulfated proteoglycans on the host cell (Carruthers et al., 2000). Upon attachment, the parasite releases a combination of microneme and rhoptry proteins that enable a tighter attachment to the host cell followed by the formation of a protein complex called the moving junction (MJ) at the site of host cell penetration. The major components of the MJ include the microneme protein apical membrane antigen 1 (AMA1), which is anchored in the parasite's plasma membrane, and the rhoptry neck proteins RON2, RON4, RON5, and RON8, which are anchored to the host cell's plasma membrane (Blader et al., 2015). AMA1 has been shown to interact directly with RON2 which spans the host plasma membrane, providing a firm link between the parasite and host cell (Besteiro et al., 2009). RON4, RON5 and RON8 are tethered to RON2 to form the RON complex on the cytoplasmic face of the host membrane and function in stabilizing the entire MJ structure. Intriguingly, RON4 and RON5 cooperate to recruit the host adaptor proteins ALIX, TSG101, CIN85, and CD2AP (Guérin et al., 2017). These host proteins have canonical roles in interacting with actin and tubulin to bridge membrane proteins with the underlying cytoskeleton, helping to maintain intercellular junctions (Johnson et al., 2008; Campos et al., 2016). RON8 was also shown to be involved in establishing a firm attachment to the host cell, without which the parasites could not invade properly (Straub et al., 2011). Thus, the prevailing model suggests that the RON complex provides a physical link between

the parasite and host, giving the parasite a strong enough grip to force itself through the MJ and into the host cell.

To push itself inward, the parasite uses a corkscrew-like motion, causing rotational progression to invaginate the host membrane (Bichet et al., 2014). Meanwhile, at the MJ-host junction, the host actin cytoskeleton is remodeled into a ring-shaped complex of F-actin and ARP2/3 (Gonzalez et al., 2009). This is believed to facilitate the invagination of the host plasma membrane at the site of entry. Remarkably, the MJ performs one final function in stripping all transmembrane proteins and lipid rafts from the host plasma membrane as the invading parasite adopts the host membrane to form its own parasitophorous vacuole (PV) membrane (Mordue et al., 1999). This crucial step yields a PV that lacks host receptors and thus avoids fusing with the host vesicular trafficking machinery – a clever method of avoiding detection and ultimately host lysosomal destruction.

As expected, active invasion undoubtedly requires efficient parasite motility. Many components of the apicomplexan actin-myosin motor machinery have been demonstrated to be essential for proper gliding motility (Frénal et al., 2017a). Surprisingly, one study observed competent but impaired invasion ability in the absence of some of these components (Egarter et al., 2014). However, it was recently shown that different myosin proteins contain redundant functions, suggesting a model that motility is indeed critical for invasion and that the absence of one myosin can be partially complemented by another to achieve invasion (Marq et al., 2014; Frénal et al., 2017a). The role of the apical complex adds another layer of complexity as a myosin protein was recently found to reside on the conoid (Graindorge et al., 2016). This gave rise to an updated model that the conoid motor machinery is primarily responsible for initiating parasite motility and thus provides the first active step of invasion, firmly establishing the essentiality of motility for invasion. Section 1.5.2.1 covers the actin-myosin motor complex in greater detail.

1.4.2 Replication via endodyogeny

Unlike its mammalian host, *T. gondii* replicates via an unusual process of cell division called endodyogeny. As alluded to by its name, endodyogeny involves the formation of two daughter cells that mature completely inside the maternal parasite, with the parent being degraded at the end of the process (Figure 1-2). This method of replication is unique to *T. gondii* tachyzoites and its closest apicomplexan relatives, but many variations of internal budding exist in other life stages or other apicomplexan parasites (Gubbels et al., 2021). For example, endodyogeny is the form of asexual replication for *T. gondii* when the parasite is infecting its intermediate hosts. This entails a single round of DNA replication and nuclear mitosis followed by the assembly of two daughter cells and cytokinesis (Francia and Striepen, 2014). In the feline definitive hosts, however, *T. gondii* undergoes sexual replication via endopolygeny followed by karyokinesis, in which more than two daughter buds are produced per round of division. Other apicomplexan parasites also employ replication mechanisms that occur fully within the maternal parasite, albeit with differences to the number and timing of DNA replication/segregation cycles before cytokinesis and emergence (White and Suvorova, 2018; Gubbels et al., 2021). For example, *Plasmodium spp.* utilize schizogony while *Sarcocystis neurona* utilizes endopolygeny. In contrast to endodyogeny, endopolygeny and schizogony involve multiple rounds of DNA replication and nuclear mitosis before daughter cell assembly and cytokinesis. While this dissertation will only focus on *T. gondii* endodyogeny, note that many of the fundamental steps are conserved throughout Apicomplexa.

Endodyogeny is initiated by centrosome duplication at the G1/S phase transition, as the parasite gears up to replicate its chromosomes. Unlike their mammalian counterparts, apicomplexan centrosomes are separated into two parts, the inner core and the outer core, which are duplicated and regulated independently of each other (Suvorova et al., 2015). The combination of this bipartite centrosome and the spindle MTOC is believed to encapsulate the complete mitotic spindle apparatus

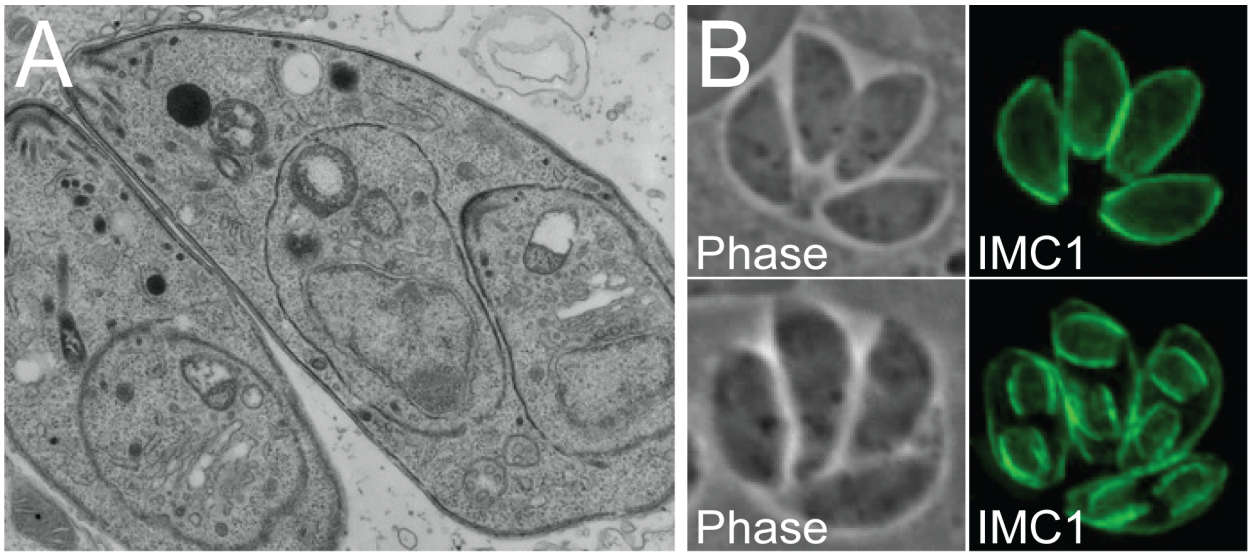

Figure 1-2. Endodyogeny is an internal replication system.

(A) Thin-section electron micrograph* depicts two daughter cells developing fully within the maternal cytoplasm. The membranes surrounding the daughter cells are the inner membrane complex (IMC) rather than the plasma membrane. (B) Immunofluorescence assays labeling IMC1, which localizes to both the maternal and daughter IMC, shows exactly two daughter buds per round of division.

*EM images were generated by courtesy of Josh Beck.

(White and Suvorova, 2018). The outer core of the centrosome, along with the associated centriole, is duplicated first and marks the launching of new daughter cytoskeletons (also called the daughter cell scaffold, DCS). The outer core contains a variety of conserved and *T. gondii*-specific components. The centriolar protein Centrin1 and its binding partner Sfi-1 localize specifically to the outer core along with Sas-6 (Suvorova et al., 2015). Disruption of Sfi-1 was shown to severely reduce the number of duplicated outer cores, implicating its role in this process. The outer core is also associated with several kinases that coordinate its duplication – the NIMA (never in mitosis-A)-related kinase Nek1-2, the Aurora kinase Ark3, the MAP (mitogen-activated protein) kinase MAPK-L1, and CDPK7. Among these, CDPK7 was implicated in positioning the duplicating centrosomes while Nek1-2 was shown to play key roles in properly segregating them (Chen and Gubbels, 2013; Morlon-Guyot et al., 2014). MAPK-L1 was localized to the pericentrolar matrix, just anterior to the outer core, and is believed to preserve the physical link between the centrosome and newly forming DCS (Suvorova et al., 2015). In contrast to these factors, Ark3 displays dynamic localization from the centrosomes to an IMC-

associated region on one side of developing daughter cells (Suvorova et al., 2015). It was also shown not to be involved in centrosome duplication and instead affected parasite morphology and intravacuolar rosette conformation, suggesting that its function is restricted to the IMC-associated region (Berry et al., 2016). Collectively, the centrosome appears to be tightly regulated by these kinases, and its early and essential role in replication indicates that this structure is a major regulator of apicomplexan cell cycle.

Upon duplication of the outer core, striated fiber assemblin proteins form an SFA fiber that provides a physical connection between the centrosome and the developing daughter cytoskeleton (Francia et al., 2012). Around the same time, the first elements of the DCS are recruited to the outer core, which include the IMC protein IMC15 and the protein trafficking GTPase Rab11B (Agop-Nersesian et al., 2010; Anderson-White et al., 2011). These are believed to coordinate the recruitment of the daughter cell scaffold components, especially since the latter transports Golgi-derived material into the daughter membrane vesicles. Rapidly after the assembly of the SFA fiber, the apical complex begins to be constructed. This is most clearly seen by the localization of the APR protein RNG2, which is recruited to recently duplicated centrosomes and almost immediately forms a ring-like structure, presumably the APR (Katris et al., 2014). The tubulin-based conoid is likely constructed around the same time, as seen by the localization of tubulin as well as conoid-associated proteins such as SAS6L and Centrin2 (Hu et al., 2006; de Leon et al., 2013; Lentini et al., 2019). Once formed, the base of the conoid (or perhaps the APR itself) is believed to connect directly to the SFA fiber to stabilize the DCS and provide a platform for future daughter components (Blader et al., 2015). Next to be incorporated are a number of IMC proteins, reviewed in greater detail in Section 1.5.2.2.

As DNA replication, mitosis, and cytokinesis of daughter cells occur concurrently in apicomplexans, the exact timing of S phase progression is difficult to determine. Thus, at some point after the outer cores duplicate, the inner core of the centrosome duplicates, followed by the

duplication of a structure called the centrocone. Unique to apicomplexan parasites, the centrocone is a specialized MTOC for spindle microtubules that is embedded in the nuclear membrane and is closely associated with the inner core (Gubbels et al., 2006). The two structures together are believed to constitute the entire spindle pole complex, essential for coordinating chromosome replication (White and Suvorova, 2018). To date, the *T. gondii* spindle pole complex is comprised of seven proteins: CEP250, CEP250-L1, CEP530, ECR1, Crk5, MORN1, and EB1. CEP250 is dually present in both the inner and outer cores and was recently shown to tether the two cores together while CEP250L-1 localizes exclusively to the inner core is critical for directing the formation and stability of the spindle pole complex (Suvorova et al., 2015; Chen and Gubbels, 2019; Tomasina et al., 2022). In contrast to both of these, CEP530 localizes to the interface between the inner and outer cores and was shown to function in coordinating karyokinesis with cytokinesis (Courjol and Gissot, 2018). Posterior to the inner core lies the centrocone, which contain the structural protein MORN1 as well as the regulatory factors ECR1 (essential for chromosome replication 1) and Crk5 (cyclin-dependent-related kinase 5) (Gubbels et al., 2006; Naumov et al., 2017). The presence of these proteins suggests that the centrocone is involved in coordinating the connection between the spindle poles and centrosomes, though this requires additional experimental support. Lastly, the microtubule end-binding protein EB1 associates with the spindle microtubules, where its role was attributed to the organization of the kinetochores to allow efficient and accurate mitosis (C.-T. Chen et al., 2015). Together, the current model suggests the following order of events – duplication of the outer core, the inner core, the centrocone, spindle-mediated chromosome replication, and finally the separation of the nuclear envelope. Note that *T. gondii* mitosis is closed, meaning their chromosomes replicate completely within the nuclear envelope. Thus, it is likely that some of these components are involved in segregating the nuclear envelope, but the mechanism is not well understood. Nevertheless, these initial stages of

division culminate in two distinct nodes with their own sets of daughter cell cytoskeleton and centrosome structure, with DNA replication still ongoing.

Just after the duplication of centrosomes, the Golgi apparatus is divided by lateral extension and medial fission (Pelletier et al., 2002). The centrosomes then migrate to the inner ends of the divided Golgi and associate with the apicoplast (Hartmann et al., 2006). This connection likely provides anchor points as the apicoplast then undergoes lateral extension (Striepen et al., 2000). As mentioned above, the daughter cell scaffold containing the apical complex, subpellicular microtubules and the IMC has already started building and now encapsulates the Golgi. Then, coordinated by the dynamin protein DrpA, the elongated apicoplast undergoes fission and is moved into each daughter cell (van Dooren et al., 2009). As the daughter IMC continues to assemble, the lasso-shaped mitochondrion begins making multiple contact sites with the IMC, a well-established phenomenon even in mature parasites (Ovciarikova et al., 2017; Souza et al., 2022). As DNA replication is completed and the nucleus begins to separate into each daughter cell, the endoplasmic reticulum (ER) forms multiple extensions along the nuclear envelope (Hager et al., 1999). Upon completion of nuclear division, the ER follows the nucleus into each daughter cell. Recent studies intriguingly showed that F-actin and the myosin motor MyoF are critical for multiple processes of organellar inheritance, including centrosome positioning, apicoplast segregation, Golgi organization and ER movement (Jacot et al., 2013; Carmeille et al., 2021). This importantly implicates a major role for the parasite's actin-myosin motor in driving organelle segregation, in addition to its well-established role in parasite motility. Once the ER is positioned within each daughter bud, the highly polarized secretory pathway is established and *de novo* construction of the secretory organelles can begin (dense granules, micronemes, and rhoptries) (Nishi et al., 2008). Reminiscent of the role of Rab11B in IMC biogenesis, the dynamin-related protein DrpB was shown to be required for building these secretory organelles (Breinich et al., 2009). In addition to *de novo* assembly, maternal organelles are also recycled into

daughter cells via a highly dynamic F-actin network (Periz et al., 2019). This recycling mechanism was also demonstrated for the IMC and plasma membrane suggesting that this is a common method of building new organelles (Ouologuem and Roos, 2014). While both *de novo* assembly and recycling undoubtedly occur, it is unclear the exact contribution of each process. Finally, the last step of division is mitochondrial entry into each daughter cell, which is excluded from the daughter cells until the very end for reasons not yet understood (Nishi et al., 2008). This is followed by fission and separation from the maternal mitochondrion, a process that requires another dynamin-related protein DrpC (Melatti et al., 2019).

While outside the scope of this dissertation, a large body of work has begun to elucidate how the apicomplexan cell cycle is regulated. Similar to other eukaryotic systems, one of the most important groups is the cyclin-dependent kinases (CDKs) and cyclins (Gubbels et al., 2008). Apicomplexans, however, also contain a group of Apetala 2 (AP2) transcription factors that bind to promotor elements to control gene expression (De Silva et al., 2008). Importantly, a recent global transcriptomics analysis demonstrated that *T. gondii* transcription is clustered in two waves, one for growth and house-keeping that occur during G1 and another for cell division and host cell invasion during the transition into S phase (Behnke et al., 2010). These subtranscriptomes appear to correlate well with the dynamics of endodyogeny and highlight the tight regulation of the cell cycle exhibited by apicomplexans.

1.4.3 Egress

Egress is an extremely coordinated process that depends largely on environmental cues. Two common signals to activate egress are a decrease in potassium (K^+) concentration within the host cell cytoplasm and acidification of the parasitophorous vacuole, though these two conditions may be linked. The decrease in K^+ concentration can be induced by several situations. One situation is a result of a cytotoxic $CD8^+$ T cell response (Persson et al., 2007). Activated T cells release perforin and

express Fas receptors, both of which induce damage to the infected host cell and cause a drop in intracellular K^+ that triggers parasite egress. Another situation involves the secretion of nucleotide triphosphate-degrading enzymes (NTPases), which impede the Na^+/K^+-ATPase pumps at the PV border from maintaining proper K^+, ultimately leading to egress (Stommel et al., 1997).

The second major signal for egress is the acidification of the parasitophorous vacuole. In parasite replication, studies have shown that vacuolar pH decreases during the final stages of replication, just prior to egress (Roiko et al., 2014). A major consequence of this is the activation of the perforin-like protein PLP1, which is secreted by the micronemes (Kafsack et al., 2009). Unlike other MIC proteins which traffic to the parasite's membrane surface, PLP1 is soluble and released into the PV. Importantly, it only functions in low pH where it is inserted into the PV membrane as well as the host plasma membrane to create pores, an essential process for parasites to egress (Roiko et al., 2014). Besides the two major signals, an additional one has been shown to occur only in the absence of an immune response. As parasites replicate within the PV, they constantly produce abscisic acid (ABA); at a certain threshold, the parasites are triggered to egress (Nagamune et al., 2008a). This appears to be an example of quorum sensing, but it remains unclear how ABA is sensed or how this signaling pathway intersects with the others mentioned above.

Once the signal to egress is received, it is transduced by two secondary messengers: cytoplasmic Ca^{2+} and cyclic guanosine monophosphate (cGMP). The Ca^{2+} pathway is a well-established mechanism that drives both egress and invasion (Nagamune et al., 2008b; Blader et al., 2015). Parasites are believed to contain many stores of calcium spanning the acidocalcisomes, the endoplasmic reticulum, and the mitochondria, which was determined by identifying numerous organelle-specific Ca^{2+} response channels (Lovett et al., 2002; Moreno and Docampo, 2003; Arrizabalaga et al., 2004; Luo et al., 2005). Ca^{2+} is then transduced through two well characterized Ca^{2+}-dependent protein kinases (CDPK1 and CDPK3) (Lourido et al., 2010; McCoy et al., 2012).

Global phosphoproteomic studies have identified hundreds of potential CDPK targets, most of which are involved in signaling cascades, exocytosis, the IMC, and components of the motor complex (Lourido et al., 2013; Treeck et al., 2014). As CDPKs belong to a family of kinases shared broadly in plants and ciliates, calcium-transduced functions are likely highly conserved and represent attractive drug targets.

The other secondary messenger is cGMP, and in apicomplexan parasites, the only known effector is protein kinase G (PKG) (Gurnett et al., 2002). While numerous studies have demonstrated that *T. gondii* PKG is essential for microneme secretion, motility, invasion, and egress, its precise mechanism of action is not fully understood. To date, PKG is believed to regulate microneme secretion by connecting phospholipase C (PLC) with calcium-dependent transduction via CDPK1 and CDPK3 (Brochet et al., 2014). In support of this, global phosphoproteomic analysis in *Plasmodium* parasites revealed that PKG substrates are mainly involved in cell signaling, proteolysis, gene regulation, and protein export (Alam et al., 2015). This may indicate a similar array of PKG targets in *T. gondii*, but this is yet to be determined. Moreover, it is unclear how these individual pathways relate to each other or are fine-tuned for specific environmental cues, but this is likely the focus of many ongoing studies.

Nonetheless, once an egress signal is received and transduced, the parasite undergoes a cascade of changes to emerge from the host cell and reinvade nearby host cells. The main consequence of signaling is the secretion of microneme proteins through the apical complex, including the adhesins involved in motility and PLP1 involved in perforating membranes. Once released, PLP1 assembles into pore-forming complexes that permeabilize the PV membrane and is also thought to permeabilize the host plasma membrane. At the same time, driven by the micronemal adhesins on the parasite surface, gliding motility is activated and the parasites burst out of the PV, rupturing the host cell in the process. Notably, the apical complex is again critical for this step due to its role in initiating motility

(discussed in Section 1.4.1 regarding invasion). Thus, egress is a carefully coordinated event that depends largely on external cues and is ultimately driven by microneme secretion and motility.

1.5 The inner membrane complex (IMC)

1.5.1 Structure and organization of the IMC

1.5.1.1 The IMC consists of multiple subcompartments

The IMC is a highly specialized membrane-cytoskeletal system that lies directly underneath the plasma membrane. It consists of two main portions – a series of flattened membrane vesicles (also called the alveoli) and an underlying network of intermediate filament-like proteins called the subpellicular network (Figure 1-3). The cytoskeletal network is also believed to associate with the array of 22 subpellicular microtubules that undergird the apical two-thirds of the parasite. The structure and composition of the IMC has been most extensively characterized in *T. gondii* and *Plasmodium spp.* (Harding and Meissner, 2014). The striking organization of the IMC vesicles in apicomplexan parasites has been seen by freeze-fracture EM for several decades (Porchet and Torpier, 1977; Meszoely et al., 1982). These studies revealed that the vesicles are arranged as three rows of rectangular plates fused together with a single cone-shaped vesicle that encircles the apical end. There are also openings at the extreme apex and base, housing the apical complex and basal complex, respectively, which are not strictly considered to be parts of the IMC.

Based on these historical EM studies and more recent proteomic characterizations, the IMC is delineated into multiple distinct subcompartments. Consistent with the organization of the membrane vesicle plates, the IMC is first separated into the apical cap, central body, and basal regions (Anderson-White et al., 2012). These subcompartment designations have been further supported by the identification of proteins with specific localization to each region (Beck et al., 2010; A. L. Chen et

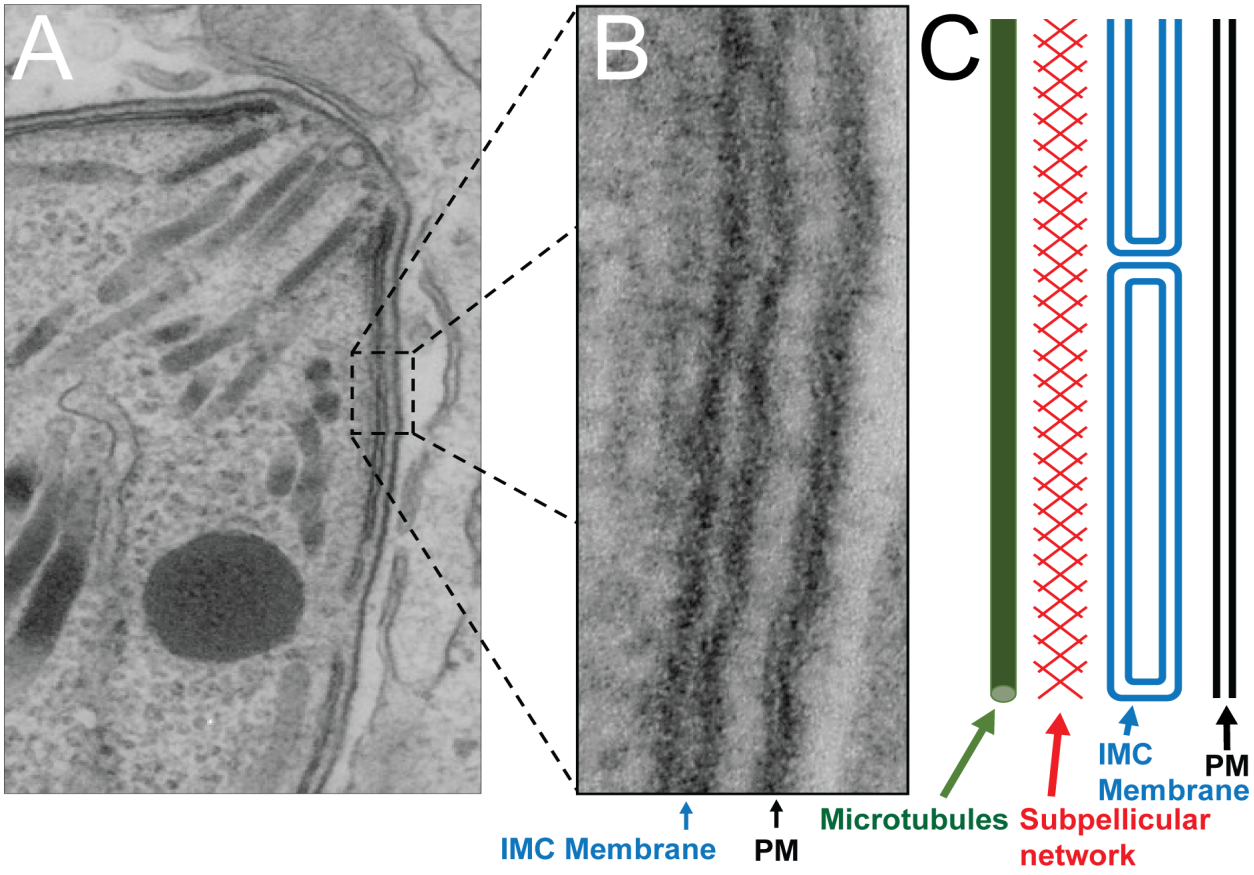

Figure 1-3. The inner membrane complex is a peripheral membrane-cytoskeletal system.

(A) Thin-section electron micrograph* and the close-up view in (B) highlights the 'triple membrane system' of the parasite pellicle. This includes the outer plasma membrane (PM) with the membrane vesicles of the IMC (alveoli) flattened against the PM. (C) Schematic of the IMC structure displays the plasma membrane (PM), the IMC membrane vesicles, the IMC subpellicular network, and the microtubules. Note that the IMC network and microtubules are not visible by this EM method.

*EM images were generated by courtesy of Josh Beck.

---

al., 2015; Chen et al., 2017). The subpellicular network represents another compartment of the IMC with a distinct set of proteins. First identified using detergent-extracted parasite ghosts, the network is composed of tightly interwoven 8-10 nm filaments (Mann and Beckers, 2001). Importantly, even in these ghosts, the distinct apical, medial, and basal regions could be observed, which was later supported by distinct protein localizations within the subcompartment boundaries (Anderson-White et al., 2012). A group of proteins that localize to the sutured junctions between the alveolar plates were also discovered (A. L. Chen et al., 2015; Chen et al., 2017). These IMC sutures proteins are remarkably further subdivided into those that run along both the longitudinal and transverse sutures or those that

are solely present on the transverse lines of the membrane boundaries. Moreover, many IMC proteins often localized to both the maternal and daughter IMC during division, suggesting that they function in multiple parts of the cell cycle (Hu et al., 2002; Mann et al., 2002). However, the discovery of a daughter-exclusive protein IMC29 indicated the existence of another group of proteins specific for the daughter cell scaffold (Chen et al., 2017). This was supported by the recent characterization of many new daughter components such as IMC32 and FBXO1 (Baptista et al., 2019; Torres et al., 2021). Importantly, each IMC subcompartment likely provides different functions for the parasite, but these are only beginning to be defined. Two of the best studied functions are described in Section 1.5.2.

1.5.1.2 Membrane vesicles of the IMC (alveoli): protein platforms

While the IMC membrane vesicles are well-known to serve as platforms for a large array of proteins, the composition of the membranes remains poorly understood. For example, the lumen of these vesicles is thought to contain stores of calcium that are likely released as part of the coordinated signal to secrete microneme proteins and activate motility. However, this was only postulated based on evidence from the related alveolate *Paramecium* and not substantiated by experiments in *T. gondii* (Ladenburger et al., 2009). In addition, one of the main components of classic eukaryotic membranes is lipids, though the type and composition vary widely across organisms, cell types, organelles, etc. (Harayama and Riezman, 2018). The lipid content of the IMC is only partially known. It was suggested that certain parts of the IMC membranes contain high concentrations of cholesterol (Coppens and Joiner, 2003; Johnson et al., 2007). These cholesterol-rich regions were correlated with stabilizing components of the actin-myosin motor and potentially with the cholesterol-binding protein NCR1 (Johnson et al., 2007; Lige et al., 2011). In addition, the heat shock protein Hsp20 was found to localize to the IMC membranes and shown to bind phosphoinositides, suggesting the presence of these types

of lipids as well (de Miguel et al., 2005, 2008). These are, however, only correlative studies, and further investigation into IMC lipids represents an important area of study.

The protein composition of the IMC membranes has been better defined in recent years. In addition to NCR1 and Hsp20, these include the four IMC sub-compartment proteins (ISP1-4), the S-acyltransferase DHHC2, and an array of gliding-associated proteins (GAP40, GAP45, GAP50, GAP70, GAP80, IAP1) (Gaskins et al., 2004; Beck et al., 2010, 2013; Fung et al., 2012; Frénal et al., 2010, 2013; Marq et al., 2014). ISP1 localizes exclusively to the cone-shaped apical cap, ISP2/ISP4 localize to the central body region, and ISP3 to the central plus basal section. While these sub-compartment distinctions hint at different functions, only ISP2 appears to be important for parasite fitness, as its disruption resulted in severe replication defects (Beck et al., 2010). Thus, the membrane vesicles are certainly involved in parasite replication, though elucidating the exact mechanisms will likely require the identification and functional study of additional membrane-anchored proteins. One interesting phenomenon is the gate-keeping function of ISP1. Upon its disruption, ISP2 and ISP3 were shown to relocalize to the apical cap, displaying a hierarchical targeting of proteins in the membranes. However, the functional significance of this flexible localization remains unknown. Many more IMC proteins have been identified using proximity labeling (A. L. Chen et al., 2015). These include IMC21, which is excluded from the apical region, as well as AC1 and AC6, which are present only in the apical cap. How these new proteins relate to the existing collection of membrane-anchored proteins remains to be seen.

IMC proteins are typically embedded in the membranes via transmembrane domains or anchored to membranes via lipid-based post-translational modifications. For example, DHHC2, GAP40, and GAP50 contain multiple transmembrane domains while GAP45, GAP70, GAP80, IAP1, Hsp20 and the ISPs contain residues that are predicted to be myristoylated and/or palmitoylated. Particularly for the latter group, extensive mutation and deletion analyses have revealed the importance

of these acylations for associating with the IMC alveoli (Beck et al., 2010; Frénal et al., 2010; De Napoli et al., 2013; Marq et al., 2014). Thus, these protein modifications represent another type of lipids present in these parasites and demonstrate that *T. gondii* has conserved this prevalent mechanism of protein anchoring. Somewhat surprisingly, while the acylations in Hsp20 were necessary for anchoring the protein to the maternal alveoli, they were dispensable for localizing to the daughter alveoli, suggesting a different method of incorporating proteins to the daughter IMC (De Napoli et al., 2013). In the case of GAP45, GAP70, and GAP80, the acylations restricted the localization of these components to the maternal IMC, leading to the hypothesis that this is a mechanism by which protein anchoring is temporally controlled (Frénal et al., 2010; Marq et al., 2014). Regardless, this also supports the existence of a distinct unknown process for anchoring IMC proteins to the nascent daughter cell scaffold. Identifying and investigating other daughter IMC proteins, particularly daughter-exclusive ones, will be important to clarify this mystery.

1.5.1.3 Subpellicular network (cytoskeleton): source of parasite strength

The subpellicular network lies underneath the IMC membranes and is composed of tightly interwoven 8-10 nm filaments (Figure 1-4) (Mann and Beckers, 2001). These filaments are believed to be comprised primarily of a family of intermediate filament-like proteins called alveolins (Anderson-White et al., 2011). *T. gondii* possesses 14 alveolin proteins (IMC1 and IMC3-15), which are defined by a conserved alveolin domain with signature motifs that are rich in proline and valine residues (Gould et al., 2008; Anderson-White et al., 2011). The alveolin domains are thought to mediate protein-protein interactions that form the filaments, but experimental evidence is lacking. Localizing each protein has largely reproduced the subcompartment divisions seen by membrane-anchored IMC proteins (Anderson-White et al., 2011; Dubey et al., 2017). IMC15 is initially recruited to the duplicating centrosomes early in division and then transitions to the budding cytoskeleton,

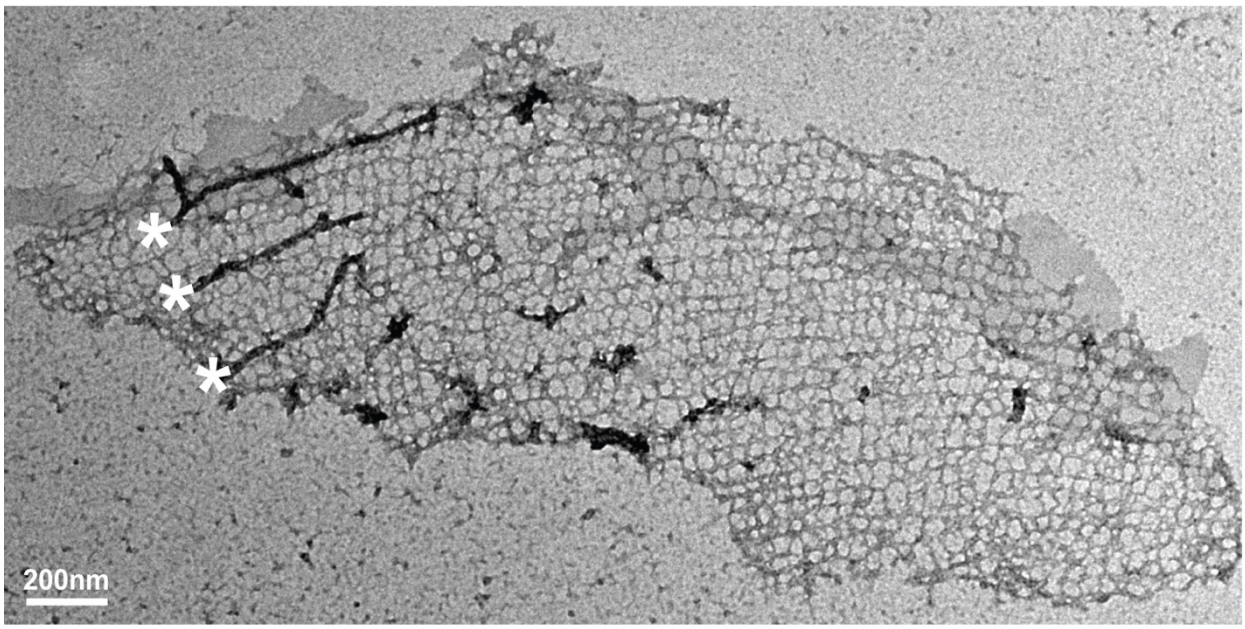

Figure 1-4. The organization of the subpellicular network.

Electron micrograph* of a detergent-extracted ghost illustrates the 8-10 nm filaments that are interwoven together to create the subpellicular network. White asterisks indicate remnants of the subpellicular microtubules that were fragmented during sample preparation.

*EM images were generated in collaboration with Qing Lou and Dr. Hong Zhou.

IMC1/3/4/6/10 are present in the central region of both the maternal and daughter buds, IMC5/8/9/13 are in basal complex of both maternal and daughter buds, IMC7/12/14 localize to the central body of mature parasites, and IMC11 is exclusively in the apical cap. Functional characterization of several of these have assigned putative functions for the IMC network. IMC7/12/14 were shown to provide tensile strength for the parasite (Dubey et al., 2017). As expected, based on its localization to the centrosomes, IMC15 was shown to be critical for restricting the number of daughter buds per round of division. In contrast, IMC14 was surprisingly shown to also be important for controlling the daughter number despite its localization in the maternal cytoskeleton. This suggests that the mature IMC may also provide scaffolding functions during division or that IMC14 may additionally be present in the DCS at subvisible levels. Lastly, although not validated, IMC1/3/4/6/10 are believed to be refractory to genetic disruption, likely providing very important or essential structural roles for the subpellicular network.

In addition to alveolins, many other detergent-insoluble IMC components have recently been identified, presumably contributing to the organization or function of the subpellicular network. PHIL1 is one such protein that localizes along the entire length of the parasite but is enriched in the apical cap (Gilk et al., 2006). Disrupting *PHIL1* resulted in morphologically abnormal parasites with impaired motility and overall fitness, consistent with the function of the network in providing structural integrity to the parasite (Barkhuff et al., 2011; Leung et al., 2014). In addition, IMC17-20, IMC22, and IMC24 localize solely to the central region of the maternal cytoskeleton while IMC23 localizes to the central region of both the maternal and daughter cytoskeleton (A. L. Chen et al., 2015). Additional ones that are in the central mature cytoskeleton include IMC26-28, with IMC28 exhibiting localization in the apical cap as well (Chen et al., 2017). While the cytoskeletal associations of IMC26-28 have not been validated, they were discovered from a purified cytoskeletal fraction, suggesting that they may also comprise the IMC network. Several proteins localize exclusively to the cytoskeleton of the apical cap, including AC2-AC5 and AC7-9, firmly distinguishing the apical cap as a distinct subcompartment (A. L. Chen et al., 2015; Chen et al., 2017). While the functions of these non-alveolin proteins have yet to be characterized, many were assigned fitness scores in a genome-wide CRISPR screen (GWCS) indicating they are likely dispensable for parasite fitness. One compelling hypothesis from this is that the subpellicular network contains a large number of proteins with redundant functions, allowing the parasite to preserve its structural integrity as it encounters various environmental conditions. Together, the subpellicular network performs multiple structural roles for maintaining parasite morphology and coordinating endodyogeny.

1.5.1.4 IMC sutures: what holds it all together

Recently, a group of proteins were localized to the sutures in the junctions between alveolar plates, defining another subdomain of the IMC. These include the IMC sutures proteins ISC1-6, the

transverse sutures proteins TSC1-5 as well as the S-acyltransferase DHHC14 (TSC1 is also called CBAP or SIP) (Tilley et al., 2014; Lentini et al., 2015; A. L. Chen et al., 2015; Chen et al., 2017; Dogga and Frénal, 2020). Of these, ISC1, ISC2, ISC4, ISC5 and TSC1-4 associate with the subpellicular network while ISC3, ISC6, and TSC5-6 associate with the membrane vesicles. This demonstrates that the sutures span the membrane and cytoskeleton portions of the IMC, consistent with other regions of the IMC. Like other membrane-associated proteins, ISC3, ISC6, TSC5, and TSC6 contain transmembrane domains. However, the mechanism by which the cytoskeletal sutures proteins are held in the subpellicular network or their interactions with each other remains unknown. Regardless, both portions of the sutures appear to provide a similar function for the parasite, as the disruption of either the membrane-bound *ISC3* and cytoskeletal *TSC1* resulted in similar phenotypes of abnormal parasite morphology, fitness defects in culture, and loss of virulence *in vivo*, though the ISC3-resultant defects were much more severe (Tilley et al., 2014; Lentini et al., 2015; Chen et al., 2017). These studies imply a more structural role for the sutures but additional investigation into the other sutures components will provide a deeper understanding.

1.5.1.5 Intramembranous particles (IMP): the bridge?

The IMC harbors another interesting structure that has been observed in freeze-fracture EM studies for decades. Named the intramembranous particles (IMPs), they are 9 nm particles arranged with distinct periodicity along every face of the IMC membrane vesicles (Morrissette et al., 1997). These are found in two different arrangements – one contains a double row of particles that are laterally spaced out in 32 nm increments. These IMP rows are believed to overlie the subpellicular microtubules, as 22 double rows correspond to 22 subpellicular microtubules. The second arrangement is a single row of particles, also spaced out by 32 nm and interspersed between the double rows. These are believed to overlie the filaments of the subpellicular network. Based on such

distinctive organization, the IMPs are thought to provide a physical connection between the subpellicular network and the alveolar vesicles, and perhaps even with the microtubules (Harding and Meissner, 2014). The protein composition of the IMPs had remained unknown until the characterization of the abovementioned GAPM proteins (Harding et al., 2019). While this requires further experimental investigation, the GAPMs represent the most likely candidates because they were shown to associate with both the membrane and cytoskeletal portions of the IMC (Bullen et al., 2009). Collectively, the apicomplexan IMC is a cooperative organelle composed of multiple structures that are interconnected to fulfill its essential functions in all aspects of the parasite's lytic cycle.

1.5.2 Functions of the IMC

1.5.2.1 Platform for the glideosome

The glideosome is an actin-myosin motor complex that is confined to the cortical space between the parasite's plasma membrane and IMC alveolar vesicles. It is conserved throughout the Apicomplexa and considered the main driver of gliding motility, which is essential for host cell invasion and egress (Frénal et al., 2017a). As in other eukaryotic systems, movement is powered by the myosin motor proteins and associated actin filaments. In apicomplexans, the myosin proteins are anchored to the IMC; they attach to the actin filaments, which are themselves attached to microneme-secreted adhesins on the parasite's surface. The moving force is actuated as the myosin motor passes the actin filaments down the length of the parasite, propelling the parasite forward.

In *T. gondii*, the main myosin protein responsible is MyoA and its supplemental factors ELC1 and ELC2 (essential light chain proteins) (Gaskins et al., 2004; Bookwalter et al., 2014). These interact with the myosin light chain MLC1, which anchors the entire motor complex to the IMC via the gliding-associated proteins GAP40, GAP45 and GAP50 (Herm-Götz et al., 2002; Frénal et al., 2010). The GAP complex is itself attached to the alveolar vesicles via transmembrane domains or N-terminal

acylations. Since this GAP complex is only present in the medial body region of the IMC, another IMC protein called GAP70 anchors MyoA to the apical cap, and yet another called GAP80 anchors the myosin motor protein MyoC to the basal complex (Marq et al., 2014). The most recently identified myosin is named MyoH and was suggested to initiate gliding motility, though this component is not anchored in the IMC and instead associates directly with the conoid microtubules (Graindorge et al., 2016). While the membrane anchoring provides some stability to the glideosome, this is likely not sufficient to provide ample motive force. One explanation to better stabilize the glideosome points to the cholesterol-rich regions of the alveolar vesicles that were shown to immobilize several components of the glideosome (Johnson et al., 2007). Another theory is that the GAPM proteins provide this stabilization as they have been shown to interact with both GAP45 and several alveolin proteins of the cytoskeletal network (Bullen et al., 2009). Nonetheless, the significance of the IMC in parasite motility, invasion, and egress is undisputed as it serves as an essential foundation for the glideosome.

1.5.2.2 Scaffold for daughter cells

Both the alveolar membranes and the subpellicular network of the IMC are critical for proper endodyogeny. This was illuminated through the careful study of numerous IMC components (Francia and Striepen, 2014; Harding and Meissner, 2014). The collection of these revealed the interesting phenomenon that IMC proteins are assembled onto the daughter cell scaffold in a specific sequence (Behnke et al., 2010). In a 'just-in-time' manner, proteins are deposited onto the daughter IMC at just the right time and at just the right place (Figure 1-5). This kind of cell-cycle dependence is likely important to maintain a tightly regulated replication system. Thus, each daughter protein (or groups of daughter proteins) may contain subtle functional differences that correspond to the temporal and spatial pattern of that protein. These nuances are just beginning to be teased apart in the field.

As discussed in Section 1.4.2, once the centrosomes have duplicated, the daughter cell scaffold initiates along the SFA fibers, starting with IMC15 and Rab11b. The fact that IMC15 is part of the cytoskeletal network and Rab11b is associated with the membrane vesicles argues that the network and alveoli develop concurrently. At this point, the earliest IMC components are recruited and arranged in an interesting 5-fold symmetry pattern around each centrosome (Engelberg et al., 2022). These proteins include FBXO1, AC9, AC10, IMC32, BCC0, and BCC3 (Baptista et al., 2019; Back et al., 2020; Torres et al., 2021; Back et al., 2022; Engelberg et al., 2022). FBXO1, IMC32, and BCC0 were shown to play critical roles in parasite replication, consistent with their early timing of expression to the scaffold. AC9 and AC10, on the other hand, localize to both the maternal and daughter apical caps and were shown to be completely dispensable for replication (determined by this study in Chapters 2 and 3). This suggests that early recruitment to the scaffold does not always entail direct involvement in daughter cell formation. After this initiation stage, BCC4 and MORN1 are recruited to form ring-like structures around the 5-fold symmetry, likely the foundation to ultimately form the basal complex (Gubbels et al., 2006; Engelberg et al., 2022). At a similar time to BCC4/MORN1, the ISPs are recruited to various subcompartments of the daughter alveoli, and ISP1 was shown to mimic the 5-fold symmetry of earlier daughter components (Beck et al., 2010; Fung et al., 2012; Engelberg

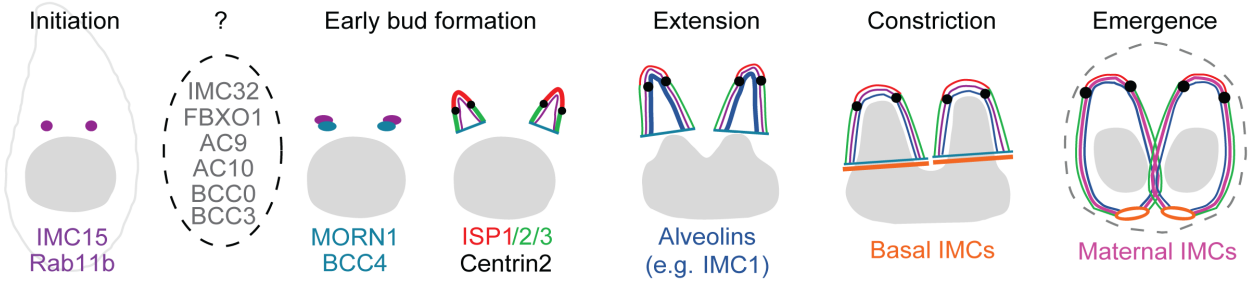

Figure 1-5. Building the daughter cell scaffold.

Diagram of the daughter cell scaffold from initiation to emergence, featuring the 'just-in-time' manner of depositing IMC proteins onto the forming daughter cells. Recent work has identified many novel components in the early stages of the scaffold (designated as '?'); however, their exact relationship to each other and to other known IMC proteins is still being resolved.

et al., 2022). While our understanding of the players that initiate the daughter scaffold is improving, this list of proteins is likely not exhaustive.

After the initiation stage, a recent model postulated that the scaffold then expands bidirectionally, with the apical cap growing in the apical direction while the remainder of the IMC along with the basal complex growing in the opposite direction. This extension stage is marked by the recruitment of a large cohort of proteins to various subdomains of the daughter cell scaffold. First, the alveolins IMC1/3/4/5/6/8/9/10/13 assemble onto the daughter subpellicular network as GAP40 and GAP50 are recruited to the daughter alveoli (Anderson-White et al., 2012). BCC2, BCC3, and BCC5 are also recruited but only to the basal complex (Engelberg et al., 2022). In addition, the GAPM proteins are likely deposited to the scaffold around this time, but they have not been directly compared to known IMC components (Harding et al., 2019). It also appears that some of the IMC sutures proteins are recruited to the daughter cell scaffold during this early extension stage as well, but a detailed comparison study has not been conducted (A. L. Chen et al., 2015). The presence of a sutures structure in daughter cells is further supported by the distinctive sutures localization of BCC3 and the S-acyltransferase DHHC14 (Dogga and Frénal, 2020; Engelberg et al., 2022).

As the daughter cells continue to elongate, the subpellicular microtubules begin extending downward from the apical complex. This marks the midpoint of daughter budding, during which the alveolins IMC5/8/9/13 redistribute to the basal complex (Anderson-White et al., 2011). Concurrently, the basal complex proteins BCC1 and BCC8, calcium binding protein Centrin2, which is initially near the centrosome, and the myosin protein MyoJ also appear at the basal complex (Hu, 2008; Frénal et al., 2017b). Up to this point, all proteins that were recruited had remained associated with the growing daughter cell scaffold. However, as the extension stage transitions into the late constriction stage, BCC4 was shown to be removed from the basal complex (Engelberg et al., 2022). Such tight regulation of protein expression supports the 'just-in-time' cell cycle model and suggests a highly specific

function for each protein. However, the mechanism behind this on-and-off sequence remains unknown; identifying the regulatory effectors that control this dynamic process is key to a more refined understanding of endodyogeny.

As the daughter cells finish the extension stage, the basal section of daughter cells begins to taper, ultimately leading to the constriction of the basal complex and two fully separated daughter cells (Gubbels et al., 2022). The importance of this constriction step was demonstrated by the conditional disruption of BCC4/MORN1 resulting in severe growth defects (Lorestani et al., 2010; Heaslip et al., 2010; Engelberg et al., 2022). More careful observation of these parasites revealed a shocking multi-headed phenotype, in which these mutant parasites have undergone several rounds of endodyogeny without separating at the basal complex. This was further supported by the conditional knockout of a MORN1-associated phosphatase, which phenocopied that of BCC4/MORN1 (Engelberg et al., 2016). This demonstrates that parasites can start the next round of division before the completion of cytokinesis, decoupling these steps of the replication cycle. Interestingly, while MyoJ was also shown to be responsible for constriction, MyoJ-KO parasites only displayed a mild fitness defect (Frénal et al., 2017b). As MyoJ is recruited to the basal complex during the final constriction stages, the early stages of scaffolding may be more consequential than the later ones. This is supported by the GWCS phenotype scores of BCC proteins, which tend to correlate more dispensable scores with proteins that appear later on in the basal complex (Sidik et al., 2016). Evidently, the basal complex has received much attention due to its prominent role in building the daughter cell scaffold. Characterizing its precise relationship with the other daughter structures (e.g. apical complex, subpellicular network, alveoli) will provide a more complete picture of endodyogeny.

The transition to the last daughter emergence stage is marked by the appearance of RNG1 at the apical polar ring, after which the maternal cytoskeleton begins to break down (Tran et al., 2010). The maternal cytoskeleton disassembly coincides with the incorporation of the maternal plasma

membrane into the nearly-complete daughter cells, a process that requires the small G-protein Rab11A (Agop-Nersesian et al., 2009). The forming plasma membrane on the daughter cells is then anchored to the outer membrane of the daughter alveoli by GAP45 in the central body section and by GAP70 in the apical cap section, events that are believed to establish a functional glideosome (Frénal et al., 2010). Finally, the alveolins IMC7/12/14 are recruited to the fully formed daughter cells and are speculated to differentiate the newly formed maternal IMC from the subsequent round of daughter buds (Anderson-White et al., 2011). Upon final emergence of daughter cells, a small residual body remains behind, which was long assumed to merely serve as an end-point reservoir for unincorporated material from the degraded maternal parasite. However, others had observed that the residual body maintains a constant connection between intravacuolar parasites, and importantly, it was recently identified as a site of organellar recycling (Caldas et al., 2010; O'Shaughnessy et al., 2021). Thus, the residual body is now hypothesized to provide key homeostatic functions during the cell cycle and thus warrants further exploration. Taken together, the IMC is central to coordinate every step of endodyogeny and a deeper understanding of its components promises to provide important cell biology insights and improved therapeutics against *T. gondii*.

1.6 Dissertation overview

Toxoplasma gondii is a widespread human pathogen that causes severe disease in immunocompromised individuals and congenitally infected neonates. It also serves as an important model organism for other members of the superphylum Alveolata, which comprise a diverse group of species including the causative agent of malaria as well as the free-living ciliates and dinoflagellates. The IMC is a signature structure of these alveolates, albeit with morphologies and functions as diverse as the organisms themselves. In apicomplexan parasites, the IMC is critical for all stages of the lytic cycle – motility, invasion, egress, and replication. However, the exact composition and mechanisms that drive these functions are still being resolved. For example, the various subcompartments of the IMC is thought to contain distinct roles, but its current functions have mainly been restricted to the central region of the IMC and the basal complex. This dissertation focuses on two understudied subcompartments of the IMC – the apical cap and the daughter IMC – leading to the discovery of a novel third role for the IMC as well as a substantial expansion of the known repertoire of IMC proteins. Chapter 2 demonstrates for the first time that the major function of the apical cap is to stabilize the apical complex. This is determined by analyzing the IMC protein AC9 and its essential interaction with the kinase ERK7. Chapter 3 follows up on this study to identify another apical cap protein AC10 that recruits both AC9 and ERK7 to the apical cap. Using deletion analysis and pairwise yeast-two-hybrid, the specific interactions that form the AC9:AC10:ERK7 complex were elucidated, establishing the apical cap as not only a structural anchor for ERK7 but also a regulatory center for its kinase activity. Chapter 4 explores IMC29, one of the earliest components of the daughter cell scaffold, and highlights its key role in coordinating endodyogeny. By exploiting its daughter-specific localization, many new daughter IMC proteins were identified, some of which also localized to a novel subregion of the IMC. Together, the goals of this work are to expand the composition of the apicomplexan IMC and elucidate key mechanisms that drive its involvement in the parasite's lytic cycle.

1.7 References

Agop-Nersesian, C., Egarter, S., Langsley, G., Foth, B.J., Ferguson, D.J.P., Meissner, M., 2010. Biogenesis of the Inner Membrane Complex Is Dependent on Vesicular Transport by the Alveolate Specific GTPase Rab11B. PLOS Pathogens 6, e1001029. https://doi.org/10.1371/journal.ppat.1001029

Agop-Nersesian, C., Naissant, B., Rached, F.B., Rauch, M., Kretzschmar, A., Thiberge, S., Menard, R., Ferguson, D.J.P., Meissner, M., Langsley, G., 2009. Rab11A-Controlled Assembly of the Inner Membrane Complex Is Required for Completion of Apicomplexan Cytokinesis. PLOS Pathogens 5, e1000270. https://doi.org/10.1371/journal.ppat.1000270

Aguirre, A.A., Longcore, T., Barbieri, M., Dabritz, H., Hill, D., Klein, P.N., Lepczyk, C., Lilly, E.L., McLeod, R., Milcarsky, J., Murphy, C.E., Su, C., VanWormer, E., Yolken, R., Sizemore, G.C., 2019. The One Health Approach to Toxoplasmosis: Epidemiology, Control, and Prevention Strategies. EcoHealth 16, 378–390. https://doi.org/10.1007/s10393-019-01405-7

Alam, M.M., Solyakov, L., Bottrill, A.R., Flueck, C., Siddiqui, F.A., Singh, S., Mistry, S., Viskaduraki, M., Lee, K., Hopp, C.S., Chitnis, C.E., Doerig, C., Moon, R.W., Green, J.L., Holder, A.A., Baker, D.A., Tobin, A.B., 2015. Phosphoproteomics reveals malaria parasite Protein Kinase G as a signalling hub regulating egress and invasion. Nat Commun 6, 7285. https://doi.org/10.1038/ncomms8285

Andenmatten, N., Egarter, S., Jackson, A.J., Jullien, N., Herman, J.-P., Meissner, M., 2013. Conditional genome engineering in Toxoplasma gondii uncovers alternative invasion mechanisms. Nat Methods 10, 125–127. https://doi.org/10.1038/nmeth.2301

Anderson-White, B., Beck, J.R., Chen, C.-T., Meissner, M., Bradley, P.J., Gubbels, M.-J., 2012. Chapter One - Cytoskeleton Assembly in Toxoplasma gondii Cell Division, in: Jeon, K.W. (Ed.), International Review of Cell and Molecular Biology. Academic Press, pp. 1–31. https://doi.org/10.1016/B978-0-12-394309-5.00001-8

Anderson-White, B.R., Ivey, F.D., Cheng, K., Szatanek, T., Lorestani, A., Beckers, C.J., Ferguson, D.J.P., Sahoo, N., Gubbels, M.-J., 2011. A family of intermediate filament-like proteins is sequentially assembled into the cytoskeleton of Toxoplasma gondii. Cell Microbiol 13, 18–31. https://doi.org/10.1111/j.1462-5822.2010.01514.x

Arrizabalaga, G., Ruiz, F., Moreno, S., Boothroyd, J.C., 2004. Ionophore-resistant mutant of Toxoplasma gondii reveals involvement of a sodium/hydrogen exchanger in calcium regulation. Journal of Cell Biology 165, 653–662. https://doi.org/10.1083/jcb.200309097

Back, P.S., O'Shaughnessy, W.J., Moon, A.S., Dewangan, P.S., Hu, X., Sha, J., Wohlschlegel, J.A., Bradley, P.J., Reese, M.L., 2020. Ancient MAPK ERK7 is regulated by an unusual inhibitory scaffold required for Toxoplasma apical complex biogenesis. Proceedings of the National Academy of Sciences 117, 12164–12173. https://doi.org/10.1073/pnas.1921245117

Back, P.S., O'Shaughnessy, W.J., Moon, A.S., Dewangan, P.S., Reese, M.L., Bradley, P.J., 2022. Multivalent Interactions Drive the Toxoplasma AC9:AC10:ERK7 Complex To Concentrate ERK7 in the Apical Cap. mBio 13, e02864-21. https://doi.org/10.1128/mbio.02864-21

Baptista, C.G., Lis, A., Deng, B., Gas-Pascual, E., Dittmar, A., Sigurdson, W., West, C.M., Blader, I.J., 2019. Toxoplasma F-box protein 1 is required for daughter cell scaffold function during parasite replication. PLOS Pathogens 15, e1007946. https://doi.org/10.1371/journal.ppat.1007946

Barkhuff, W.D., Gilk, S.D., Whitmarsh, R., Tilley, L.D., Hunter, C., Ward, G.E., 2011. Targeted Disruption of TgPhIL1 in Toxoplasma gondii Results in Altered Parasite Morphology and Fitness. PLOS ONE 6, e23977. https://doi.org/10.1371/journal.pone.0023977

Barylyuk, K., Koreny, L., Ke, H., Butterworth, S., Crook, O.M., Lassadi, I., Gupta, V., Tromer, E., Mourier, T., Stevens, T.J., Breckels, L.M., Pain, A., Lilley, K.S., Waller, R.F., 2020. A Comprehensive Subcellular Atlas of the Toxoplasma Proteome via hyperLOPIT Provides Spatial Context for Protein Functions. Cell Host & Microbe 28, 752-766.e9. https://doi.org/10.1016/j.chom.2020.09.011

Beck, J.R., Fung, C., Straub, K.W., Coppens, I., Vashisht, A.A., Wohlschlegel, J.A., Bradley, P.J., 2013. A Toxoplasma Palmitoyl Acyl Transferase and the Palmitoylated Armadillo Repeat Protein TgARO Govern Apical Rhoptry Tethering and Reveal a Critical Role for the Rhoptries in Host Cell Invasion but Not Egress. PLOS Pathogens 9, e1003162. https://doi.org/10.1371/journal.ppat.1003162

Beck, J.R., Rodriguez-Fernandez, I.A., Leon, J.C. de, Huynh, M.-H., Carruthers, V.B., Morrissette, N.S., Bradley, P.J., 2010. A Novel Family of Toxoplasma IMC Proteins Displays a Hierarchical Organization and Functions in Coordinating Parasite Division. PLOS Pathogens 6, e1001094. https://doi.org/10.1371/journal.ppat.1001094

Behnke, M.S., Wootton, J.C., Lehmann, M.M., Radke, J.B., Lucas, O., Nawas, J., Sibley, L.D., White, M.W., 2010. Coordinated Progression through Two Subtranscriptomes Underlies the Tachyzoite Cycle of Toxoplasma gondii. PLOS ONE 5, e12354. https://doi.org/10.1371/journal.pone.0012354

Berry, L., Chen, C.-T., Reininger, L., Carvalho, T.G., El Hajj, H., Morlon-Guyot, J., Bordat, Y., Lebrun, M., Gubbels, M.-J., Doerig, C., Daher, W., 2016. The conserved apicomplexan Aurora kinase TgArk3 is involved in endodyogeny, duplication rate and parasite virulence. Cellular Microbiology 18, 1106–1120. https://doi.org/10.1111/cmi.12571

Besteiro, S., Michelin, A., Poncet, J., Dubremetz, J.-F., Lebrun, M., 2009. Export of a Toxoplasma gondii Rhoptry Neck Protein Complex at the Host Cell Membrane to Form the Moving Junction during Invasion. PLOS Pathogens 5, e1000309. https://doi.org/10.1371/journal.ppat.1000309

Bichet, M., Joly, C., Hadj Henni, A., Guilbert, T., Xémard, M., Tafani, V., Lagal, V., Charras, G., Tardieux, I., 2014. The toxoplasma-host cell junction is anchored to the cell cortex to sustain parasite invasive force. BMC Biology 12, 773. https://doi.org/10.1186/s12915-014-0108-y

Blader, I.J., Coleman, B.I., Chen, C.-T., Gubbels, M.-J., 2015. Lytic Cycle of Toxoplasma gondii: 15 Years Later. Annu Rev Microbiol 69, 463–485. https://doi.org/10.1146/annurev-micro-091014-104100

Bookwalter, C.S., Kelsen, A., Leung, J.M., Ward, G.E., Trybus, K.M., 2014. A Toxoplasma gondii Class XIV Myosin, Expressed in Sf9 Cells with a Parasite Co-chaperone, Requires Two Light

Chains for Fast Motility *. Journal of Biological Chemistry 289, 30832–30841. https://doi.org/10.1074/jbc.M114.572453

Breinich, M.S., Ferguson, D.J.P., Foth, B.J., van Dooren, G.G., Lebrun, M., Quon, D.V., Striepen, B., Bradley, P.J., Frischknecht, F., Carruthers, V.B., Meissner, M., 2009. A Dynamin Is Required for the Biogenesis of Secretory Organelles in Toxoplasma gondii. Current Biology 19, 277–286. https://doi.org/10.1016/j.cub.2009.01.039

Brochet, M., Collins, M.O., Smith, T.K., Thompson, E., Sebastian, S., Volkmann, K., Schwach, F., Chappell, L., Gomes, A.R., Berriman, M., Rayner, J.C., Baker, D.A., Choudhary, J., Billker, O., 2014. Phosphoinositide Metabolism Links cGMP-Dependent Protein Kinase G to Essential Ca2+ Signals at Key Decision Points in the Life Cycle of Malaria Parasites. PLOS Biology 12, e1001806. https://doi.org/10.1371/journal.pbio.1001806

Bullen, H.E., Tonkin, C.J., O'Donnell, R.A., Tham, W.-H., Papenfuss, A.T., Gould, S., Cowman, A.F., Crabb, B.S., Gilson, P.R., 2009. A Novel Family of Apicomplexan Glideosome-associated Proteins with an Inner Membrane-anchoring Role*. Journal of Biological Chemistry 284, 25353–25363. https://doi.org/10.1074/jbc.M109.036772

Burki, F., Roger, A.J., Brown, M.W., Simpson, A.G.B., 2020. The New Tree of Eukaryotes. Trends in Ecology & Evolution 35, 43–55. https://doi.org/10.1016/j.tree.2019.08.008

Caldas, L.A., de Souza, W., Attias, M., 2010. Microscopic analysis of calcium ionophore activated egress of Toxoplasma gondii from the host cell. Veterinary Parasitology 167, 8–18. https://doi.org/10.1016/j.vetpar.2009.09.051

Campos, Y., Qiu, X., Gomero, E., Wakefield, R., Horner, L., Brutkowski, W., Han, Y.-G., Solecki, D., Frase, S., Bongiovanni, A., d'Azzo, A., 2016. Alix-mediated assembly of the actomyosin–tight junction polarity complex preserves epithelial polarity and epithelial barrier. Nat Commun 7, 11876. https://doi.org/10.1038/ncomms11876

Carmeille, R., Lomoriello, P.S., Devarakonda, P.M., Kellermeier, J.A., Heaslip, A.T., 2021. Actin and an unconventional myosin motor, TgMyoF, control the organization and dynamics of the endomembrane network in Toxoplasma gondii. PLOS Pathogens 17, e1008787. https://doi.org/10.1371/journal.ppat.1008787

Carmen, M.G.D., Mondragón, M., González, S., Mondragón, R., 2009. Induction and regulation of conoid extrusion in Toxoplasma gondii. Cellular Microbiology 11, 967–982. https://doi.org/10.1111/j.1462-5822.2009.01304.x

Carruthers, V.B., Håkansson, S., Giddings, O.K., Sibley, L.D., 2000. Toxoplasma gondii Uses Sulfated Proteoglycans for Substrate and Host Cell Attachment. Infection and Immunity 68, 4005–4011. https://doi.org/10.1128/IAI.68.7.4005-4011.2000

Carruthers, V.B., Tomley, F.M., 2008. Microneme Proteins in Apicomplexans, in: Burleigh, B.A., Soldati-Favre, D. (Eds.), Molecular Mechanisms of Parasite Invasion: Subcellular Biochemistry, Subcellular Biochemistry. Springer, New York, NY, pp. 33–45. https://doi.org/10.1007/978-0-387-78267-6_2

Chen, A.L., Kim, E.W., Toh, J.Y., Vashisht, A.A., Rashoff, A.Q., Van, C., Huang, A.S., Moon, A.S., Bell, H.N., Bentolila, L.A., Wohlschlegel, J.A., Bradley, P.J., 2015. Novel Components of the Toxoplasma Inner Membrane Complex Revealed by BioID. mBio 6, e02357-14. https://doi.org/10.1128/mBio.02357-14

Chen, A.L., Moon, A.S., Bell, H.N., Huang, A.S., Vashisht, A.A., Toh, J.Y., Lin, A.H., Nadipuram, S.M., Kim, E.W., Choi, C.P., Wohlschlegel, J.A., Bradley, P.J., 2017. Novel insights into the composition and function of the Toxoplasma IMC sutures. Cellular Microbiology 19, e12678. https://doi.org/10.1111/cmi.12678

Chen, C.-T., Gubbels, M.-J., 2019. TgCep250 is dynamically processed through the division cycle and is essential for structural integrity of the Toxoplasma centrosome. MBoC 30, 1160–1169. https://doi.org/10.1091/mbc.E18-10-0608

Chen, C.-T., Gubbels, M.-J., 2013. The Toxoplasma gondii centrosome is the platform for internal daughter budding as revealed by a Nek1 kinase mutant. Journal of Cell Science 126, 3344–3355. https://doi.org/10.1242/jcs.123364

Chen, C.-T., Kelly, M., Leon, J. de, Nwagbara, B., Ebbert, P., Ferguson, D.J.P., Lowery, L.A., Morrissette, N., Gubbels, M.-J., 2015. Compartmentalized Toxoplasma EB1 bundles spindle microtubules to secure accurate chromosome segregation. MBoC 26, 4562–4576. https://doi.org/10.1091/mbc.E15-06-0437

Coppens, I., Joiner, K.A., 2003. Host but Not Parasite Cholesterol Controls Toxoplasma Cell Entry by Modulating Organelle Discharge. MBoC 14, 3804–3820. https://doi.org/10.1091/mbc.e02-12-0830

Courjol, F., Gissot, M., 2018. A coiled-coil protein is required for coordination of karyokinesis and cytokinesis in Toxoplasma gondii. Cellular Microbiology 20, e12832. https://doi.org/10.1111/cmi.12832

de Leon, J.C., Scheumann, N., Beatty, W., Beck, J.R., Tran, J.Q., Yau, C., Bradley, P.J., Gull, K., Wickstead, B., Morrissette, N.S., 2013. A SAS-6-like protein suggests that the Toxoplasma conoid complex evolved from flagellar components. Eukaryot Cell 12, 1009–1019. https://doi.org/10.1128/EC.00096-13

de Miguel, N., Echeverria, P.C., Angel, S.O., 2005. Differential Subcellular Localization of Members of the Toxoplasma gondii Small Heat Shock Protein Family. Eukaryotic Cell 4, 1990–1997. https://doi.org/10.1128/EC.4.12.1990-1997.2005

de Miguel, N., Lebrun, M., Heaslip, A., Hu, K., Beckers, C.J., Matrajt, M., Dubremetz, J.F., Angel, S.O., 2008. Toxoplasma gondii Hsp20 is a stripe-arranged chaperone-like protein associated with the outer leaflet of the inner membrane complex. Biology of the Cell 100, 479–489. https://doi.org/10.1042/BC20080004

De Napoli, M.G., de Miguel, N., Lebrun, M., Moreno, S.N.J., Angel, S.O., Corvi, M.M., 2013. N-terminal palmitoylation is required for Toxoplasma gondii HSP20 inner membrane complex localization. Biochimica et Biophysica Acta (BBA) - Molecular Cell Research 1833, 1329–1337. https://doi.org/10.1016/j.bbamcr.2013.02.022

De Silva, E.K., Gehrke, A.R., Olszewski, K., León, I., Chahal, J.S., Bulyk, M.L., Llinás, M., 2008. Specific DNA-binding by Apicomplexan AP2 transcription factors. Proceedings of the National Academy of Sciences 105, 8393–8398. https://doi.org/10.1073/pnas.0801993105

Dodge, J.D., Crawford, R.M., 1969. Observations on the Fine Structure of the Eyespot and Associated Organelles in the Dinoflagellate Glenodinium Foliaceum. Journal of Cell Science 5, 479–493. https://doi.org/10.1242/jcs.5.2.479

Dogga, S.K., Frénal, K., 2020. Two palmitoyl acyltransferases involved sequentially in the biogenesis of the inner membrane complex of Toxoplasma gondii. Cellular Microbiology 22, e13212. https://doi.org/10.1111/cmi.13212

Dos Santos Pacheco, N., Brusini, L., Haase, R., Tosetti, N., Maco, B., Brochet, M., Vadas, O., Soldati-Favre, D., 2022. Conoid extrusion regulates glideosome assembly to control motility and invasion in Apicomplexa. Nat Microbiol 7, 1777–1790. https://doi.org/10.1038/s41564-022-01212-x

Dubey, J.P., 2003. Review of <italic>Neospora caninum</italic> and neosporosis in animals. Korean J Parasitol 41, 1–16. https://doi.org/10.3347/kjp.2003.41.1.1

Dubey, J.P., Lindsay, D.S., Speer, C.A., 1998. Structures of Toxoplasma gondiiTachyzoites, Bradyzoites, and Sporozoites and Biology and Development of Tissue Cysts. Clinical Microbiology Reviews 11, 267–299. https://doi.org/10.1128/CMR.11.2.267

Dubey, R., Harrison, B., Dangoudoubiyam, S., Bandini, G., Cheng, K., Kosber, A., Agop-Nersesian, C., Howe, D.K., Samuelson, J., Ferguson, D.J.P., Gubbels, M.-J., 2017. Differential Roles for Inner Membrane Complex Proteins across Toxoplasma gondii and Sarcocystis neurona Development. mSphere 2, e00409-17. https://doi.org/10.1128/mSphere.00409-17

Egarter, S., Andenmatten, N., Jackson, A.J., Whitelaw, J.A., Pall, G., Black, J.A., Ferguson, D.J.P., Tardieux, I., Mogilner, A., Meissner, M., 2014. The Toxoplasma Acto-MyoA Motor Complex Is Important but Not Essential for Gliding Motility and Host Cell Invasion. PLOS ONE 9, e91819. https://doi.org/10.1371/journal.pone.0091819

Engelberg, K., Bechtel, T., Michaud, C., Weerapana, E., Gubbels, M.-J., 2022. Proteomic characterization of the Toxoplasma gondii cytokinesis machinery portrays an expanded hierarchy of its assembly and function. Nat Commun 13, 4644. https://doi.org/10.1038/s41467-022-32151-0

Engelberg, K., Ivey, F.D., Lin, A., Kono, M., Lorestani, A., Faugno-Fusci, D., Gilberger, T.-W., White, M., Gubbels, M.-J., 2016. A MORN1-associated HAD phosphatase in the basal complex is essential for Toxoplasma gondii daughter budding. Cellular Microbiology 18, 1153–1171. https://doi.org/10.1111/cmi.12574

Flegr, J., Prandota, J., Sovičková, M., Israili, Z.H., 2014. Toxoplasmosis – A Global Threat. Correlation of Latent Toxoplasmosis with Specific Disease Burden in a Set of 88 Countries. PLOS ONE 9, e90203. https://doi.org/10.1371/journal.pone.0090203

Francia, M.E., Dubremetz, J.-F., Morrissette, N.S., 2016. Basal body structure and composition in the apicomplexans Toxoplasma and Plasmodium. Cilia 5, 3. https://doi.org/10.1186/s13630-016-0025-5

Francia, M.E., Jordan, C.N., Patel, J.D., Sheiner, L., Demerly, J.L., Fellows, J.D., Leon, J.C. de, Morrissette, N.S., Dubremetz, J.-F., Striepen, B., 2012. Cell Division in Apicomplexan Parasites Is Organized by a Homolog of the Striated Rootlet Fiber of Algal Flagella. PLOS Biology 10, e1001444. https://doi.org/10.1371/journal.pbio.1001444

Francia, M.E., Striepen, B., 2014. Cell division in apicomplexan parasites. Nature Reviews Microbiology 12, 125–136. https://doi.org/10.1038/nrmicro3184

Frénal, K., Dubremetz, J.-F., Lebrun, M., Soldati-Favre, D., 2017a. Gliding motility powers invasion and egress in Apicomplexa. Nature Reviews Microbiology 15, 645–660. https://doi.org/10.1038/nrmicro.2017.86

Frénal, K., Jacot, D., Hammoudi, P.-M., Graindorge, A., Maco, B., Soldati-Favre, D., 2017b. Myosin-dependent cell-cell communication controls synchronicity of division in acute and chronic stages of Toxoplasma gondii. Nat Commun 8, 15710. https://doi.org/10.1038/ncomms15710

Frénal, K., Polonais, V., Marq, J.-B., Stratmann, R., Limenitakis, J., Soldati-Favre, D., 2010. Functional Dissection of the Apicomplexan Glideosome Molecular Architecture. Cell Host & Microbe 8, 343–357. https://doi.org/10.1016/j.chom.2010.09.002

Frénal, K., Tay, C.L., Mueller, C., Bushell, E.S., Jia, Y., Graindorge, A., Billker, O., Rayner, J.C., Soldati-Favre, D., 2013. Global Analysis of Apicomplexan Protein S-Acyl Transferases Reveals an Enzyme Essential for Invasion. Traffic 14, 895–911. https://doi.org/10.1111/tra.12081

Fung, C., Beck, J.R., Robertson, S.D., Gubbels, M.-J., Bradley, P.J., 2012. Toxoplasma ISP4 is a central IMC Sub-compartment Protein whose localization depends on palmitoylation but not myristoylation. Molecular and Biochemical Parasitology 184, 99–108. https://doi.org/10.1016/j.molbiopara.2012.05.002

Füssy, Z., Masařová, P., Kručinská, J., Esson, H.J., Oborník, M., 2017. Budding of the Alveolate Alga Vitrella brassicaformis Resembles Sexual and Asexual Processes in Apicomplexan Parasites. Protist 168, 80–91. https://doi.org/10.1016/j.protis.2016.12.001

Gajewski, P.D., Falkenstein, M., Hengstler, J.G., Golka, K., 2014. Toxoplasma gondii impairs memory in infected seniors. Brain, Behavior, and Immunity 36, 193–199. https://doi.org/10.1016/j.bbi.2013.11.019

Gaskins, E., Gilk, S., DeVore, N., Mann, T., Ward, G., Beckers, C., 2004. Identification of the membrane receptor of a class XIV myosin in Toxoplasma gondii. Journal of Cell Biology 165, 383–393. https://doi.org/10.1083/jcb.200311137

Genova, B.M.D., Wilson, S.K., Dubey, J.P., Knoll, L.J., 2019. Intestinal delta-6-desaturase activity determines host range for Toxoplasma sexual reproduction. PLOS Biology 17, e3000364. https://doi.org/10.1371/journal.pbio.3000364

Gilk, S.D., Raviv, Y., Hu, K., Murray, J.M., Beckers, C.J.M., Ward, G.E., 2006. Identification of PhIL1, a Novel Cytoskeletal Protein of the Toxoplasma gondii Pellicle, through Photosensitized Labeling with 5-[125I]Iodonaphthalene-1-Azide. Eukaryotic Cell 5, 1622–1634. https://doi.org/10.1128/EC.00114-06

Goldstein, E.J.C., Montoya, J.G., Remington, J.S., 2008. Management of Toxoplasma gondii Infection during Pregnancy. Clinical Infectious Diseases 47, 554–566. https://doi.org/10.1086/590149

Gonzalez, V., Combe, A., David, V., Malmquist, N.A., Delorme, V., Leroy, C., Blazquez, S., Ménard, R., Tardieux, I., 2009. Host Cell Entry by Apicomplexa Parasites Requires Actin Polymerization in the Host Cell. Cell Host & Microbe 5, 259–272. https://doi.org/10.1016/j.chom.2009.01.011

Gould, S.B., Tham, W.-H., Cowman, A.F., McFadden, G.I., Waller, R.F., 2008. Alveolins, a new family of cortical proteins that define the protist infrakingdom Alveolata. Mol Biol Evol 25, 1219–1230. https://doi.org/10.1093/molbev/msn070

Graindorge, A., Frénal, K., Jacot, D., Salamun, J., Marq, J.B., Soldati-Favre, D., 2016. The Conoid Associated Motor MyoH Is Indispensable for Toxoplasma gondii Entry and Exit from Host Cells. PLOS Pathogens 12, e1005388. https://doi.org/10.1371/journal.ppat.1005388

Gubbels, M.-J., Coppens, I., Zarringhalam, K., Duraisingh, M.T., Engelberg, K., 2021. The Modular Circuitry of Apicomplexan Cell Division Plasticity. Frontiers in Cellular and Infection Microbiology 11.

Gubbels, M.-J., Ferguson, D.J.P., Saha, S., Romano, J.D., Chavan, S., Primo, V.A., Michaud, C., Coppens, I., Engelberg, K., 2022. Toxoplasma gondii's Basal Complex: The Other Apicomplexan Business End Is Multifunctional. Frontiers in Cellular and Infection Microbiology 12.

Gubbels, M.-J., Vaishnava, S., Boot, N., Dubremetz, J.-F., Striepen, B., 2006. A MORN-repeat protein is a dynamic component of the Toxoplasma gondii cell division apparatus. Journal of Cell Science 119, 2236–2245. https://doi.org/10.1242/jcs.02949

Gubbels, M.-J., White, M., Szatanek, T., 2008. The cell cycle and Toxoplasma gondii cell division: Tightly knit or loosely stitched? International Journal for Parasitology 38, 1343–1358. https://doi.org/10.1016/j.ijpara.2008.06.004

Guérin, A., Corrales, R.M., Parker, M.L., Lamarque, M.H., Jacot, D., El Hajj, H., Soldati-Favre, D., Boulanger, M.J., Lebrun, M., 2017. Efficient invasion by Toxoplasma depends on the subversion of host protein networks. Nat Microbiol 2, 1358–1366. https://doi.org/10.1038/s41564-017-0018-1

Gurnett, A.M., Liberator, P.A., Dulski, P.M., Salowe, S.P., Donald, R.G.K., Anderson, J.W., Wiltsie, J., Diaz, C.A., Harris, G., Chang, B., Darkin-Rattray, S.J., Nare, B., Crumley, T., Blum, P.S., Misura, A.S., Tamas, T., Sardana, M.K., Yuan, J., Biftu, T., Schmatz, D.M., 2002. Purification and Molecular Characterization of cGMP-dependent Protein Kinase from Apicomplexan Parasites: A NOVEL CHEMOTHERAPEUTIC TARGET *. Journal of Biological Chemistry 277, 15913–15922. https://doi.org/10.1074/jbc.M108393200

Hager, K.M., Striepen, B., Tilney, L.G., Roos, D.S., 1999. The nuclear envelope serves as an intermediary between the ER and Golgi complex in the intracellular parasite Toxoplasma gondii. Journal of Cell Science 112, 2631–2638. https://doi.org/10.1242/jcs.112.16.2631

Harayama, T., Riezman, H., 2018. Understanding the diversity of membrane lipid composition. Nat Rev Mol Cell Biol 19, 281–296. https://doi.org/10.1038/nrm.2017.138

Harb, O.S., Roos, D.S., 2020. ToxoDB: Functional Genomics Resource for Toxoplasma and Related Organisms. Methods Mol Biol 2071, 27–47. https://doi.org/10.1007/978-1-4939-9857-9_2

Harding, C.R., Gow, M., Kang, J.H., Shortt, E., Manalis, S.R., Meissner, M., Lourido, S., 2019. Alveolar proteins stabilize cortical microtubules in Toxoplasma gondii. Nat Commun 10, 401. https://doi.org/10.1038/s41467-019-08318-7

Harding, C.R., Meissner, M., 2014. The inner membrane complex through development of Toxoplasma gondii and Plasmodium. Cellular Microbiology 16, 632–641. https://doi.org/10.1111/cmi.12285

Hartmann, J., Hu, K., He, C.Y., Pelletier, L., Roos, D.S., Warren, G., 2006. Golgi and centrosome cycles in Toxoplasma gondii. Molecular and Biochemical Parasitology 145, 125–127. https://doi.org/10.1016/j.molbiopara.2005.09.015

Hausmann, K., Kaiser, J., 1979. Arrangement and structure of plates in the cortical alveoli of the hypotrich ciliate, Euplotes vannus. Journal of Ultrastructure Research 67, 15–22. https://doi.org/10.1016/S0022-5320(79)80013-1

Heaslip, A.T., Dzierszinski, F., Stein, B., Hu, K., 2010. TgMORN1 Is a Key Organizer for the Basal Complex of Toxoplasma gondii. PLOS Pathogens 6, e1000754. https://doi.org/10.1371/journal.ppat.1000754

Herm-Götz, A., Agop-Nersesian, C., Münter, S., Grimley, J.S., Wandless, T.J., Frischknecht, F., Meissner, M., 2007. Rapid control of protein level in the apicomplexan Toxoplasma gondii. Nat Methods 4, 1003–1005. https://doi.org/10.1038/nmeth1134

Herm-Götz, A., Weiss, S., Stratmann, R., Fujita-Becker, S., Ruff, C., Meyhöfer, E., Soldati, T., Manstein, D.J., Geeves, M.A., Soldati, D., 2002. Toxoplasma gondii myosin A and its light chain: a fast, single-headed, plus-end-directed motor. The EMBO Journal 21, 2149–2158. https://doi.org/10.1093/emboj/21.9.2149

Holland, G.N., 2003. Ocular toxoplasmosis: a global reassessment: . Part I: epidemiology and course of disease. American Journal of Ophthalmology 136, 973–988. https://doi.org/10.1016/j.ajo.2003.09.040

Hu, K., 2008. Organizational Changes of the Daughter Basal Complex during the Parasite Replication of Toxoplasma gondii. PLOS Pathogens 4, e10. https://doi.org/10.1371/journal.ppat.0040010

Hu, K., Johnson, J., Florens, L., Fraunholz, M., Suravajjala, S., DiLullo, C., Yates, J., Roos, D.S., Murray, J.M., 2006. Cytoskeletal Components of an Invasion Machine—The Apical Complex of Toxoplasma gondii. PLOS Pathogens 2, e13. https://doi.org/10.1371/journal.ppat.0020013

Hu, K., Mann, T., Striepen, B., Beckers, C.J.M., Roos, D.S., Murray, J.M., 2002. Daughter Cell Assembly in the Protozoan ParasiteToxoplasma gondii. MBoC 13, 593–606. https://doi.org/10.1091/mbc.01-06-0309

Jacot, D., Daher, W., Soldati-Favre, D., 2013. Toxoplasma gondii myosin F, an essential motor for centrosomes positioning and apicoplast inheritance. The EMBO Journal 32, 1702–1716. https://doi.org/10.1038/emboj.2013.113

Jacot, D., Soldati-Favre, D., 2020. CRISPR/Cas9-Mediated Generation of Tetracycline Repressor-Based Inducible Knockdown in Toxoplasma gondii, in: Tonkin, C.J. (Ed.), Toxoplasma Gondii: Methods and Protocols, Methods in Molecular Biology. Springer US, New York, NY, pp. 125–141. https://doi.org/10.1007/978-1-4939-9857-9_7

Johnson, R.I., Seppa, M.J., Cagan, R.L., 2008. The Drosophila CD2AP/CIN85 orthologue Cindr regulates junctions and cytoskeleton dynamics during tissue patterning. Journal of Cell Biology 180, 1191–1204. https://doi.org/10.1083/jcb.200706108

Johnson, T.M., Rajfur, Z., Jacobson, K., Beckers, C.J., 2007. Immobilization of the Type XIV Myosin Complex in Toxoplasma gondii. MBoC 18, 3039–3046. https://doi.org/10.1091/mbc.e07-01-0040

Joiner, K.A., Roos, D.S., 2002. Secretory traffic in the eukaryotic parasite Toxoplasma gondii : less is more. Journal of Cell Biology 157, 557–563. https://doi.org/10.1083/jcb.200112144

Jones, J.L., Kruszon-Moran, D., Sanders-Lewis, K., Wilson, M., 2007. Toxoplasma gondii Infection in the United States, 1999–2004, Decline from the Prior Decade. The American Journal of Tropical Medicine and Hygiene 77, 405–410. https://doi.org/10.4269/ajtmh.2007.77.405

Kafsack, B.F.C., Pena, J.D.O., Coppens, I., Ravindran, S., Boothroyd, J.C., Carruthers, V.B., 2009. Rapid Membrane Disruption by a Perforin-Like Protein Facilitates Parasite Exit from Host Cells. Science 323, 530–533. https://doi.org/10.1126/science.1165740

Katris, N.J., van Dooren, G.G., McMillan, P.J., Hanssen, E., Tilley, L., Waller, R.F., 2014. The Apical Complex Provides a Regulated Gateway for Secretion of Invasion Factors in Toxoplasma. PLoS Pathog 10, e1004074. https://doi.org/10.1371/journal.ppat.1004074

Keeling, P.J., Burger, G., Durnford, D.G., Lang, B.F., Lee, R.W., Pearlman, R.E., Roger, A.J., Gray, M.W., 2005. The tree of eukaryotes. Trends in Ecology & Evolution 20, 670–676. https://doi.org/10.1016/j.tree.2005.09.005

Kim, K., Weiss, L.M., 2004. Toxoplasma gondii: the model apicomplexan. Int J Parasitol 34, 423–432. https://doi.org/10.1016/j.ijpara.2003.12.009

Kissinger, J.C., Gajria, B., Li, L., Paulsen, I.T., Roos, D.S., 2003. ToxoDB: accessing the Toxoplasma gondii genome. Nucleic Acids Research 31, 234–236. https://doi.org/10.1093/nar/gkg072

Kloetzel, J.A., Baroin-Tourancheau, A., Miceli, C., Barchetta, S., Farmar, J., Banerjee, D., Fleury-Aubusson, A., 2003. Plateins: A Novel Family of Signal Peptide-Containing Articulins in Euplotid Ciliates1. Journal of Eukaryotic Microbiology 50, 19–33. https://doi.org/10.1111/j.1550-7408.2003.tb00102.x

Kono, M., Prusty, D., Parkinson, J., Gilberger, T.W., 2013. The apicomplexan inner membrane complex. Front Biosci (Landmark Ed) 18, 982–992. https://doi.org/10.2741/4157

Koreny, L., Zeeshan, M., Barylyuk, K., Tromer, E.C., Hooff, J.J.E. van, Brady, D., Ke, H., Chelaghma, S., Ferguson, D.J.P., Eme, L., Tewari, R., Waller, R.F., 2021. Molecular characterization of the conoid complex in Toxoplasma reveals its conservation in all apicomplexans, including Plasmodium species. PLOS Biology 19, e3001081. https://doi.org/10.1371/journal.pbio.3001081

Kovacs, J.A., The NIAID-Clinical Center Intramural AIDS Program, 1992. Efficacy of atovaquone in treatment of toxoplasmosis in patients with AIDS. The Lancet, Originally published as Volume 2, Issue 8820 340, 637–638. https://doi.org/10.1016/0140-6736(92)92172-C

Ladenburger, E.-M., Sehring, I.M., Korn, I., Plattner, H., 2009. Novel Types of Ca2+ Release Channels Participate in the Secretory Cycle of Paramecium Cells. Molecular and Cellular Biology 29, 3605–3622. https://doi.org/10.1128/MCB.01592-08

Lassen, B., Østergaard, S., 2012. Estimation of the economical effects of Eimeria infections in Estonian dairy herds using a stochastic model. Preventive Veterinary Medicine 106, 258–265. https://doi.org/10.1016/j.prevetmed.2012.04.005

Lentini, G., Dubois, D.J., Maco, B., Soldati-Favre, D., Frénal, K., 2019. The roles of Centrin 2 and Dynein Light Chain 8a in apical secretory organelles discharge of Toxoplasma gondii. Traffic 20, 583–600. https://doi.org/10.1111/tra.12673

Lentini, G., Kong-Hap, M., El Hajj, H., Francia, M., Claudet, C., Striepen, B., Dubremetz, J.-F., Lebrun, M., 2015. Identification and characterization of Toxoplasma SIP, a conserved apicomplexan cytoskeleton protein involved in maintaining the shape, motility and virulence of the parasite. Cellular Microbiology 17, 62–78. https://doi.org/10.1111/cmi.12337

Leung, J.M., He, Y., Zhang, F., Hwang, Y.-C., Nagayasu, E., Liu, J., Murray, J.M., Hu, K., 2017. Stability and function of a putative microtubule-organizing center in the human parasite Toxoplasma gondii. MBoC 28, 1361–1378. https://doi.org/10.1091/mbc.e17-01-0045

Leung, J.M., Rould, M.A., Konradt, C., Hunter, C.A., Ward, G.E., 2014. Disruption of TgPHIL1 Alters Specific Parameters of Toxoplasma gondii Motility Measured in a Quantitative, Three-Dimensional Live Motility Assay. PLOS ONE 9, e85763. https://doi.org/10.1371/journal.pone.0085763

Levine, N.D., Corliss, J.O., Cox, F.E.G., Deroux, G., Grain, J., Honigberg, B.M., Leedale, G.F., Loeblich, A.R., Lom, I.J., Lynn, D., Merinfeld, E.G., Page, F.C., Poljansky, G., Sprague, V., Vavra, J., Wallace, F.G., 1980. A Newly Revised Classification of the Protozoa*. The Journal of Protozoology 27, 37–58. https://doi.org/10.1111/j.1550-7408.1980.tb04228.x

Lige, B., Romano, J.D., Bandaru, V.V.R., Ehrenman, K., Levitskaya, J., Sampels, V., Haughey, N.J., Coppens, I., 2011. Deficiency of a Niemann-Pick, Type C1-related Protein in Toxoplasma Is Associated with Multiple Lipidoses and Increased Pathogenicity. PLOS Pathogens 7, e1002410. https://doi.org/10.1371/journal.ppat.1002410

Lim, L., McFadden, G.I., 2010. The evolution, metabolism and functions of the apicoplast. Philosophical Transactions of the Royal Society B: Biological Sciences 365, 749–763. https://doi.org/10.1098/rstb.2009.0273

Long, S., Anthony, B., Drewry, L.L., Sibley, L.D., 2017a. A conserved ankyrin repeat-containing protein regulates conoid stability, motility and cell invasion in Toxoplasma gondii. Nat Commun 8, 2236. https://doi.org/10.1038/s41467-017-02341-2

Long, S., Brown, K.M., Drewry, L.L., Anthony, B., Phan, I.Q.H., Sibley, L.D., 2017b. Calmodulin-like proteins localized to the conoid regulate motility and cell invasion by Toxoplasma gondii. PLOS Pathogens 13, e1006379. https://doi.org/10.1371/journal.ppat.1006379

Lorestani, A., Sheiner, L., Yang, K., Robertson, S.D., Sahoo, N., Brooks, C.F., Ferguson, D.J.P., Striepen, B., Gubbels, M.-J., 2010. A Toxoplasma MORN1 Null Mutant Undergoes Repeated Divisions but Is Defective in Basal Assembly, Apicoplast Division and Cytokinesis. PLOS ONE 5, e12302. https://doi.org/10.1371/journal.pone.0012302

Lourido, S., Jeschke, G.R., Turk, B.E., Sibley, L.D., 2013. Exploiting the Unique ATP-Binding Pocket of Toxoplasma Calcium-Dependent Protein Kinase 1 To Identify Its Substrates. ACS Chem. Biol. 8, 1155–1162. https://doi.org/10.1021/cb400115y

Lourido, S., Shuman, J., Zhang, C., Shokat, K.M., Hui, R., Sibley, L.D., 2010. Calcium-dependent protein kinase 1 is an essential regulator of exocytosis in Toxoplasma. Nature 465, 359–362. https://doi.org/10.1038/nature09022

Lovett, J.L., Marchesini, N., Moreno, S.N.J., Sibley, L.D., 2002. Toxoplasma gondii Microneme Secretion Involves Intracellular Ca2+ Release from Inositol 1,4,5-Triphosphate (IP3)/Ryanodine-sensitive Stores *. Journal of Biological Chemistry 277, 25870–25876. https://doi.org/10.1074/jbc.M202553200

Luft, B.J., Hafner, R., Korzun, A.H., Leport, C., Antoniskis, D., Bosler, E.M., Bourland, D.D., Uttamchandani, R., Fuhrer, J., Jacobson, J., Morlat, P., Vilde, J.-L., Remington, J.S., 1993. Toxoplasmic Encephalitis in Patients with the Acquired Immunodeficiency Syndrome. New England Journal of Medicine 329, 995–1000. https://doi.org/10.1056/NEJM199309303291403

Luo, S., Ruiz, F.A., Moreno, S.N.J., 2005. The acidocalcisome Ca2+-ATPase (TgA1) of Toxoplasma gondii is required for polyphosphate storage, intracellular calcium homeostasis and virulence. Molecular Microbiology 55, 1034–1045. https://doi.org/10.1111/j.1365-2958.2004.04464.x

Mackintosh, C.L., Beeson, J.G., Marsh, K., 2004. Clinical features and pathogenesis of severe malaria. Trends in Parasitology 20, 597–603. https://doi.org/10.1016/j.pt.2004.09.006

Mann, T., Beckers, C., 2001. Characterization of the subpellicular network, a filamentous membrane skeletal component in the parasite Toxoplasma gondii. Mol Biochem Parasitol 115, 257–268. https://doi.org/10.1016/s0166-6851(01)00289-4

Mann, T., Gaskins, E., Beckers, C., 2002. Proteolytic Processing of TgIMC1 during Maturation of the Membrane Skeleton of Toxoplasma gondii *. Journal of Biological Chemistry 277, 41240–41246. https://doi.org/10.1074/jbc.M205056200

Marq, J.-B., Jacot, D., Polonais, V., Soldati-Favre, D., 2014. Plasticity between MyoC- and MyoA-Glideosomes: An Example of Functional Compensation in Toxoplasma gondii Invasion. PLOS Pathogens 10, e1004504. https://doi.org/10.1371/journal.ppat.1004504

Marra, C.M., 2018. Chapter 9 - Central nervous system infection with Toxoplasma gondii, in: Brew, B.J. (Ed.), Handbook of Clinical Neurology, The Neurology of HIV Infection. Elsevier, pp. 117–122. https://doi.org/10.1016/B978-0-444-63849-6.00009-8

Masters, P.A., O'Bryan, T.A., Zurlo, J., Miller, D.Q., Joshi, N., 2003. Trimethoprim-Sulfamethoxazole Revisited. Archives of Internal Medicine 163, 402–410. https://doi.org/10.1001/archinte.163.4.402

McAuley, J., Boyer, K.M., Patel, D., Mets, M., Swisher, C., Roizen, N., Wolters, C., Stein, L., Stein, M., Schey, W., Remington, J., Meier, P., Johnson, D., Heydeman, P., Holfels, E., Withers, S., Mack, D., Brown, C., Patton, D., McLeod, R., 1994. Early and Longitudinal Evaluations of Treated Infants and Children and Untreated Historical Patients with Congenital Toxoplasmosis: The Chicago Collaborative Treatment Trial. Clinical Infectious Diseases 18, 38–72. https://doi.org/10.1093/clinids/18.1.38

McCoy, J.M., Whitehead, L., Dooren, G.G. van, Tonkin, C.J., 2012. TgCDPK3 Regulates Calcium-Dependent Egress of Toxoplasma gondii from Host Cells. PLOS Pathogens 8, e1003066. https://doi.org/10.1371/journal.ppat.1003066

Meissner, M., Brecht, S., Bujard, H., Soldati, D., 2001. Modulation of myosin A expression by a newly established tetracycline repressor-based inducible system in Toxoplasma gondii. Nucleic Acids Research 29, e115. https://doi.org/10.1093/nar/29.22.e115

Melatti, C., Pieperhoff, M., Lemgruber, L., Pohl, E., Sheiner, L., Meissner, M., 2019. A unique dynamin-related protein is essential for mitochondrial fission in Toxoplasma gondii. PLOS Pathogens 15, e1007512. https://doi.org/10.1371/journal.ppat.1007512

Melo, E.J.L., Attias, M., De Souza, W., 2000. The Single Mitochondrion of Tachyzoites of Toxoplasma gondii. Journal of Structural Biology 130, 27–33. https://doi.org/10.1006/jsbi.2000.4228

Mendez, O.A., Flores Machado, E., Lu, J., Koshy, A.A., 2021. Injection with Toxoplasma gondii protein affects neuron health and survival. eLife 10, e67681. https://doi.org/10.7554/eLife.67681

Meroni, V., Genco, F., Tinelli, C., Lanzarini, P., Bollani, L., Stronati, M., Petersen, E., 2009. Spiramycin Treatment of Toxoplasma gondii Infection in Pregnant Women Impairs the Production and the Avidity Maturation of T. gondii-Specific Immunoglobulin G Antibodies. Clinical and Vaccine Immunology 16, 1517–1520. https://doi.org/10.1128/CVI.00253-09

Meszoely, C.A.M., Erbe, E.F., Steere, R.L., Pacheco, N.D., Beaudoin, R.L., 1982. Plasmodium berghei: Architectural analysis by freeze-fracturing of the intraoocyst sporozoite's pellicular system. Experimental Parasitology 53, 229–241. https://doi.org/10.1016/0014-4894(82)90064-9

Montoya, J., Liesenfeld, O., 2004. Toxoplasmosis. The Lancet 363, 1965–1976. https://doi.org/10.1016/S0140-6736(04)16412-X

Montoya, J.G., Laessig, K., Fazeli, M.S., Siliman, G., Yoon, S.S., Drake-Shanahan, E., Zhu, C., Akbary, A., McLeod, R., 2021. A fresh look at the role of spiramycin in preventing a neglected disease: meta-analyses of observational studies. European Journal of Medical Research 26, 143. https://doi.org/10.1186/s40001-021-00606-7

Mordue, D.G., Håkansson, S., Niesman, I., David Sibley, L., 1999. Toxoplasma gondii Resides in a Vacuole That Avoids Fusion with Host Cell Endocytic and Exocytic Vesicular Trafficking Pathways. Experimental Parasitology 92, 87–99. https://doi.org/10.1006/expr.1999.4412

Moreno, S.N., Docampo, R., 2003. Calcium regulation in protozoan parasites. Current Opinion in Microbiology 6, 359–364. https://doi.org/10.1016/S1369-5274(03)00091-2

Morlon-Guyot, J., Berry, L., Chen, C.-T., Gubbels, M.-J., Lebrun, M., Daher, W., 2014. The Toxoplasma gondii calcium-dependent protein kinase 7 is involved in early steps of parasite division and is crucial for parasite survival. Cellular Microbiology 16, 95–114. https://doi.org/10.1111/cmi.12186

Morrissette, N.S., Murray, J.M., Roos, D.S., 1997. Subpellicular microtubules associate with an intramembranous particle lattice in the protozoan parasite Toxoplasma gondii. Journal of Cell Science 110, 35–42. https://doi.org/10.1242/jcs.110.1.35

Morrissette, N.S., Sibley, L.D., 2002. Cytoskeleton of Apicomplexan Parasites. Microbiol. Mol. Biol. Rev. 66, 21–38. https://doi.org/10.1128/MMBR.66.1.21-38.2002

Nagamune, K., Hicks, L.M., Fux, B., Brossier, F., Chini, E.N., Sibley, L.D., 2008a. Abscisic acid controls calcium-dependent egress and development in Toxoplasma gondii. Nature 451, 207–210. https://doi.org/10.1038/nature06478

Nagamune, K., Moreno, S.N., Chini, E.N., Sibley, L.D., 2008b. Calcium Regulation and Signaling in Apicomplexan Parasites, in: Burleigh, B.A., Soldati-Favre, D. (Eds.), Molecular Mechanisms of Parasite Invasion: Subcellular Biochemistry, Subcellular Biochemistry. Springer, New York, NY, pp. 70–81. https://doi.org/10.1007/978-0-387-78267-6_5

Naumov, A., Kratzer, S., Ting, L.-M., Kim, K., Suvorova, E.S., White, M.W., 2017. The Toxoplasma Centrocone Houses Cell Cycle Regulatory Factors. mBio 8, e00579-17. https://doi.org/10.1128/mBio.00579-17

Nevo, Z., Sharon, N., 1969. The cell wall of Peridinium westii, a non cellulosic glucan. Biochimica et Biophysica Acta (BBA) - Biomembranes 173, 161–175. https://doi.org/10.1016/0005-2736(69)90099-6

Nicolle C., Manceaux L., 1908. Sur une infection á corps de Leishman (ou organismes voisons) du gondi. CR Acad Sci. 147.

Nishi, M., Hu, K., Murray, J.M., Roos, D.S., 2008. Organellar dynamics during the cell cycle of Toxoplasma gondii. Journal of Cell Science 121, 1559–1568. https://doi.org/10.1242/jcs.021089

Okamoto, N., Keeling, P.J., 2014. The 3D Structure of the Apical Complex and Association with the Flagellar Apparatus Revealed by Serial TEM Tomography in Psammosa pacifica, a Distant Relative of the Apicomplexa. PLOS ONE 9, e84653. https://doi.org/10.1371/journal.pone.0084653

O'Shaughnessy, W.J., Hu, X., Henriquez, S.A., Reese, M.L., 2021. Toxoplasma ERK7 defends the apical complex from premature degradation. https://doi.org/10.1101/2021.12.09.471932

Ouologuem, D.T., Roos, D.S., 2014. Dynamics of the Toxoplasma gondii inner membrane complex. Journal of Cell Science 127, 3320–3330. https://doi.org/10.1242/jcs.147736

Ovciarikova, J., Lemgruber, L., Stilger, K.L., Sullivan, W.J., Sheiner, L., 2017. Mitochondrial behaviour throughout the lytic cycle of Toxoplasma gondii. Sci Rep 7, 42746. https://doi.org/10.1038/srep42746

Pappas, G., Roussos, N., Falagas, M.E., 2009. Toxoplasmosis snapshots: Global status of Toxoplasma gondii seroprevalence and implications for pregnancy and congenital toxoplasmosis. International Journal for Parasitology 39, 1385–1394. https://doi.org/10.1016/j.ijpara.2009.04.003

Pelletier, L., Stern, C.A., Pypaert, M., Sheff, D., Ngô, H.M., Roper, N., He, C.Y., Hu, K., Toomre, D., Coppens, I., Roos, D.S., Joiner, K.A., Warren, G., 2002. Golgi biogenesis in Toxoplasma gondii. Nature 418, 548–552. https://doi.org/10.1038/nature00946

Periz, J., Del Rosario, M., McStea, A., Gras, S., Loney, C., Wang, L., Martin-Fernandez, M.L., Meissner, M., 2019. A highly dynamic F-actin network regulates transport and recycling of micronemes in Toxoplasma gondii vacuoles. Nat Commun 10, 4183. https://doi.org/10.1038/s41467-019-12136-2

Persson, E.K., Agnarson, A.M., Lambert, H., Hitziger, N., Yagita, H., Chambers, B.J., Barragan, A., Grandien, A., 2007. Death Receptor Ligation or Exposure to Perforin Trigger Rapid Egress of the Intracellular Parasite Toxoplasma gondii. The Journal of Immunology 179, 8357–8365. https://doi.org/10.4049/jimmunol.179.12.8357

Pieperhoff, M.S., Pall, G.S., Jiménez-Ruiz, E., Das, S., Melatti, C., Gow, M., Wong, E.H., Heng, J., Müller, S., Blackman, M.J., Meissner, M., 2015. Conditional U1 Gene Silencing in Toxoplasma gondii. PLOS ONE 10, e0130356. https://doi.org/10.1371/journal.pone.0130356

Plattner, H., Klauke, N., 2001. Calcium in ciliated protozoa: Sources, regulation, and calcium-regulated cell functions, in: International Review of Cytology. Academic Press, pp. 115–208. https://doi.org/10.1016/S0074-7696(01)01003-8

Porchet, E., Torpier, G., 1977. [Freeze fracture study of Toxoplasma and Sarcocystis infective stages (author's transl)]. Z Parasitenkd 54, 101–124. https://doi.org/10.1007/BF00380795

Rajapakse, S., Weeratunga, P., Rodrigo, C., de Silva, N.L., Fernando, S.D., 2017. Prophylaxis of human toxoplasmosis: a systematic review. Pathogens and Global Health 111, 333–342. https://doi.org/10.1080/20477724.2017.1370528

Roiko, M.S., Svezhova, N., Carruthers, V.B., 2014. Acidification Activates Toxoplasma gondii Motility and Egress by Enhancing Protein Secretion and Cytolytic Activity. PLOS Pathogens 10, e1004488. https://doi.org/10.1371/journal.ppat.1004488

Scholtyseck, E., 1973. Die Deutung von Endodyogenie und Schizogonie bei Coccidien und anderen Sporozoen. Z. Parasitenk. 42, 87–104. https://doi.org/10.1007/BF00329787

Scholtyseck, E., Mehlhorn, H., Friedhoff, K., 1970. The fine structure of the conoid of sporozoa and related organisms. Z. F. Parasitenkunde 34, 68–94. https://doi.org/10.1007/BF00629180

Shin, D.-W., Cha, D.-Y., Hua, Q.J., Cha, G.-H., Lee, Y.-H., 2009. Seroprevalence of <italic>Toxoplasma gondii</italic> Infection and Characteristics of Seropositive Patients in General Hospitals in Daejeon, Korea. Korean J Parasitol 47, 125–130. https://doi.org/10.3347/kjp.2009.47.2.125

Sidik, S.M., Hackett, C.G., Tran, F., Westwood, N.J., Lourido, S., 2014. Efficient Genome Engineering of Toxoplasma gondii Using CRISPR/Cas9. PLOS ONE 9, e100450. https://doi.org/10.1371/journal.pone.0100450

Sidik, S.M., Huet, D., Ganesan, S.M., Huynh, M.-H., Wang, T., Nasamu, A.S., Thiru, P., Saeij, J.P.J., Carruthers, V.B., Niles, J.C., Lourido, S., 2016. A Genome-wide CRISPR Screen in Toxoplasma Identifies Essential Apicomplexan Genes. Cell 166, 1423-1435.e12. https://doi.org/10.1016/j.cell.2016.08.019

Soldati, D., 1999. The Apicoplast as a Potential Therapeutic Target in Toxoplasma and Other Apicomplexan Parasites. Parasitology Today 15, 5–7. https://doi.org/10.1016/S0169-4758(98)01363-5

Souza, R.O.O., Jacobs, K.N., Back, P.S., Bradley, P.J., Arrizabalaga, G., 2022. IMC10 and LMF1 mediate mitochondrial morphology by mitochondrion-pellicle contact sites in Toxoplasma gondii. Journal of Cell Science jcs.260083. https://doi.org/10.1242/jcs.260083

Sow, S.O., Muhsen, K., Nasrin, D., Blackwelder, W.C., Wu, Y., Farag, T.H., Panchalingam, S., Sur, D., Zaidi, A.K.M., Faruque, A.S.G., Saha, D., Adegbola, R., Alonso, P.L., Breiman, R.F., Bassat, Q., Tamboura, B., Sanogo, D., Onwuchekwa, U., Manna, B., Ramamurthy, T., Kanungo, S., Ahmed, S., Qureshi, S., Quadri, F., Hossain, A., Das, S.K., Antonio, M., Hossain, M.J., Mandomando, I., Nhampossa, T., Acácio, S., Omore, R., Oundo, J.O., Ochieng, J.B., Mintz, E.D., O'Reilly, C.E., Berkeley, L.Y., Livio, S., Tennant, S.M., Sommerfelt, H., Nataro, J.P., Ziv-Baran, T., Robins-Browne, R.M., Mishcherkin, V., Zhang, J., Liu, J., Houpt, E.R., Kotloff, K.L., Levine, M.M., 2016. The Burden of Cryptosporidium Diarrheal Disease among Children < 24 Months of Age in Moderate/High Mortality Regions of Sub-Saharan Africa and South Asia, Utilizing Data from the Global Enteric Multicenter Study (GEMS). PLOS Neglected Tropical Diseases 10, e0004729. https://doi.org/10.1371/journal.pntd.0004729

Spalding, S.M., Amendoeira, M.R.R., Klein, C.H., Ribeiro, L.C., 2005. Serological screening and toxoplasmosis exposure factors among pregnant women in South of Brazil. Rev. Soc. Bras. Med. Trop. 38, 173–177. https://doi.org/10.1590/S0037-86822005000200009

Splendore, A., 1908. Un nuovo protozoa parassita deconigli incontrato nelle lesioni anatomiche d'une malattia che ricorda in molti punti il Kala-azar dell'uoma. Rev Soc Sci Sao Paulo, Nota preliminiare pel 3, 109–112.

Stommel, E.W., Ely, K.H., Schwartzman, J.D., Kasper, L.H., 1997. Toxoplasma gondii:Dithiol-Induced Ca2+Flux Causes Egress of Parasites from the Parasitophorous Vacuole. Experimental Parasitology 87, 88–97. https://doi.org/10.1006/expr.1997.4187

Straub, K.W., Peng, E.D., Hajagos, B.E., Tyler, J.S., Bradley, P.J., 2011. The Moving Junction Protein RON8 Facilitates Firm Attachment and Host Cell Invasion in Toxoplasma gondii. PLOS Pathogens 7, e1002007. https://doi.org/10.1371/journal.ppat.1002007

Striepen, B., Crawford, M.J., Shaw, M.K., Tilney, L.G., Seeber, F., Roos, D.S., 2000. The Plastid of Toxoplasma gondii Is Divided by Association with the Centrosomes. Journal of Cell Biology 151, 1423–1434. https://doi.org/10.1083/jcb.151.7.1423

Suvorova, E.S., Francia, M., Striepen, B., White, M.W., 2015. A Novel Bipartite Centrosome Coordinates the Apicomplexan Cell Cycle. PLOS Biology 13, e1002093. https://doi.org/10.1371/journal.pbio.1002093

Tilley, L.D., Krishnamurthy, S., Westwood, N.J., Ward, G.E., 2014. Identification of TgCBAP, a Novel Cytoskeletal Protein that Localizes to Three Distinct Subcompartments of the Toxoplasma gondii Pellicle. PLOS ONE 9, e98492. https://doi.org/10.1371/journal.pone.0098492

Tomasina, R., Gonzalez, F.C., Martins-Duarte, É.S., Bastin, P., Gissot, M., Francia, M.E., 2022. Separate To Operate: the Centriole-Free Inner Core of the Centrosome Regulates the Assembly of the Intranuclear Spindle in *Toxoplasma gondii*. mBio 13, e01859-22. https://doi.org/10.1128/mbio.01859-22

Torgerson, P.R., Mastroiacovo, P., 2013. The global burden of congenital toxoplasmosis: a systematic review. Bull. World Health Organ. 91, 501–508. https://doi.org/10.2471/BLT.12.111732

Torres, J.A., Pasquarelli, R.R., Back, P.S., Moon, A.S., Bradley, P.J., 2021. Identification and Molecular Dissection of IMC32, a Conserved Toxoplasma Inner Membrane Complex Protein That Is Essential for Parasite Replication. mBio 12, e03622-20. https://doi.org/10.1128/mBio.03622-20

Tosetti, N., Dos Santos Pacheco, N., Soldati-Favre, D., Jacot, D., 2019. Three F-actin assembly centers regulate organelle inheritance, cell-cell communication and motility in Toxoplasma gondii. eLife 8, e42669. https://doi.org/10.7554/eLife.42669

Tran, J.Q., Leon, J.C. de, Li, C., Huynh, M.-H., Beatty, W., Morrissette, N.S., 2010. RNG1 is a late marker of the apical polar ring in Toxoplasma gondii. Cytoskeleton 67, 586–598. https://doi.org/10.1002/cm.20469

Treeck, M., Sanders, J.L., Gaji, R.Y., LaFavers, K.A., Child, M.A., Arrizabalaga, G., Elias, J.E., Boothroyd, J.C., 2014. The Calcium-Dependent Protein Kinase 3 of Toxoplasma Influences Basal Calcium Levels and Functions beyond Egress as Revealed by Quantitative Phosphoproteome Analysis. PLOS Pathogens 10, e1004197. https://doi.org/10.1371/journal.ppat.1004197

van Dooren, G.G., Reiff, S.B., Tomova, C., Meissner, M., Humbel, B.M., Striepen, B., 2009. A Novel Dynamin-Related Protein Has Been Recruited for Apicoplast Fission in Toxoplasma gondii. Current Biology 19, 267–276. https://doi.org/10.1016/j.cub.2008.12.048

Wall, R.J., Roques, M., Katris, N.J., Koreny, L., Stanway, R.R., Brady, D., Waller, R.F., Tewari, R., 2016. SAS6-like protein in Plasmodium indicates that conoid-associated apical complex proteins persist in invasive stages within the mosquito vector. Scientific Reports 6, 1–12. https://doi.org/10.1038/srep28604

Wall, R.J., Zeeshan, M., Katris, N.J., Limenitakis, R., Rea, E., Stock, J., Brady, D., Waller, R.F., Holder, A.A., Tewari, R., 2019. Systematic analysis of Plasmodium myosins reveals differential expression, localisation, and function in invasive and proliferative parasite stages. Cellular Microbiology 21, e13082. https://doi.org/10.1111/cmi.13082

White, M.W., Suvorova, E.S., 2018. Apicomplexa Cell Cycles: Something Old, Borrowed, Lost, and New. Trends in Parasitology 34, 759–771. https://doi.org/10.1016/j.pt.2018.07.006

Wilking, H., Thamm, M., Stark, K., Aebischer, T., Seeber, F., 2016. Prevalence, incidence estimations and risk factors of Toxoplasma gondii infection in Germany: a representative, cross-sectional, serological study. Sci Rep 6, 22551. https://doi.org/10.1038/srep22551

Wolters, J., 1991. The troublesome parasites — molecular and morphological evidence that Apicomplexa belong to the dinoflagellate-ciliate clade. Biosystems, Papers presented at the 8th Biennial Conference of the International Society for Evolutionary Protistology 25, 75–83. https://doi.org/10.1016/0303-2647(91)90014-C

Chapter 2

–

Ancient MAPK ERK7 is regulated by an unusual inhibitory scaffold required for *Toxoplasma* apical complex biogenesis

Ancient MAPK ERK7 is regulated by an unusual inhibitory scaffold required for *Toxoplasma* apical complex biogenesis

Peter S. Back[a,1], William J. O'Shaughnessy[b,1], Andy S. Moon[c], Pravin S. Dewangan[b], Xiaoyu Hu[b], Jihui Sha[d], James A. Wohlschlegel[d], Peter J. Bradley[a,c,2], and Michael L. Reese[b,e,2]

[a]Molecular Biology Institute, University of California, Los Angeles, CA 90095; [b]Department of Pharmacology, University of Texas Southwestern Medical Center, Dallas, TX 75390; [c]Department of Molecular Microbiology and Immunology, University of California, Los Angeles, CA 90095; [d]Department of Biological Chemistry, David Geffen School of Medicine, University of California, Los Angeles, CA 90095; and [e]Department of Biochemistry, University of Texas Southwestern Medical Center, Dallas, TX 75390

Edited by Stephen M. Beverley, Washington University School of Medicine in St. Louis, St. Louis, MO, and approved April 16, 2020 (received for review December 6, 2019)

Apicomplexan parasites use a specialized cilium structure called the apical complex to organize their secretory organelles and invasion machinery. The apical complex is integrally associated with both the parasite plasma membrane and an intermediate filament cytoskeleton called the inner-membrane complex (IMC). While the apical complex is essential to the parasitic lifestyle, little is known about the regulation of apical complex biogenesis. Here, we identify AC9 (apical cap protein 9), a largely intrinsically disordered component of the *Toxoplasma gondii* IMC, as essential for apical complex development, and therefore for host cell invasion and egress. Parasites lacking AC9 fail to successfully assemble the tubulin-rich core of their apical complex, called the conoid. We use proximity biotinylation to identify the AC9 interaction network, which includes the kinase extracellular signal-regulated kinase 7 (ERK7). Like AC9, ERK7 is required for apical complex biogenesis. We demonstrate that AC9 directly binds ERK7 through a conserved C-terminal motif and that this interaction is essential for ERK7 localization and function at the apical cap. The crystal structure of the ERK7–AC9 complex reveals that AC9 is not only a scaffold but also inhibits ERK7 through an unusual set of contacts that displaces nucleotide from the kinase active site. ERK7 is an ancient and autoactivating member of the mitogen-activated kinase (MAPK) family and its regulation is poorly understood in all organisms. We propose that AC9 dually regulates ERK7 by scaffolding and concentrating it at its site of action while maintaining it in an "off" state until the specific binding of a true substrate.

kinase | scaffold | intrinsically disordered protein | cilium

Cilia are ancient eukaryotic organelles that organize signal-transduction cascades and mediate cell motility. These functions are driven by the cooperation of cytoskeleton and membrane structures and require specialized signaling and trafficking machinery for their biogenesis and maintenance (1–3). In apicomplexan parasites, the cilium is thought to have evolved to form the "apical complex" (4–7), which organizes the parasites' invasion machinery and for which the phylum is named. Apicomplexa include the causative agents of malaria, toxoplasmosis, and cryptosporidiosis, which all invade mammalian cells to cause disease. Like more typical eukaryotic cilia, the apical complex is composed of specialized microtubule structures inserted into the plasma membrane (8). In addition, the apical complex is the site of secretion of specialized organelles called micronemes and rhoptries that mediate the parasites' attachment to and invasion of host cells. In the asexual stage of most apicomplexans, secretion is thought to occur through a tubulin-rich structure in the apical complex called the conoid (8, 9). The apical complex is also intimately associated with an intermediate filament cytoskeleton called the inner-membrane complex (IMC) that scaffolds the apicomplexan cell, ensuring its correct morphology. The IMC anchors the parasite actin-based motility machinery (10), powering the parasite's motility as it glides across and invades host cells. While the IMC extends the length of the parasite, it has clearly segregated apical, medial, and basal subdomains that are defined by specific protein localization (11, 12). In *Toxoplasma gondii*, the IMC "apical cap" comprises the anterior-most ∼1 μm of the IMC, just basal to the apical complex. The apical cap appears to be a site at which actin regulators (13) and subcomponents of the parasite invasion machinery concentrate (14). While a number of IMC proteins have been genetically manipulated and evaluated phenotypically, their biochemical functions have been understudied.

In the present work, we identify one component of the *T. gondii* apical IMC, apical cap protein 9 (AC9), as essential to the parasite lytic cycle. We found that loss of AC9 results in parasites that are entirely unable to egress from their host cells or invade new cells. These deficiencies are attributable to the failure of the

Significance

Apicomplexan parasites include organisms that cause widespread and devastating human diseases such as malaria, cryptosporidiosis, and toxoplasmosis. These parasites are named for a structure, called the "apical complex," that organizes their invasion and secretory machinery. We found that two proteins, apical cap protein 9 (AC9) and an enzyme called ERK7, work together to facilitate apical complex assembly. Intriguingly, ERK7 is an ancient molecule that is found throughout Eukaryota, though its regulation and function are poorly understood. AC9 is a scaffold that concentrates ERK7 at the base of the developing apical complex. In addition, AC9 binding likely confers substrate selectivity upon ERK7. This simple competitive regulatory model may be a powerful but largely overlooked mechanism throughout biology.

Author contributions: P.S.B., W.J.O., A.S.M., P.S.D., X.H., P.J.B., and M.L.R. designed research; P.S.B., W.J.O., A.S.M., P.S.D., X.H., and J.S. performed research; P.S.B., W.J.O., P.S.D., X.H., J.S., J.A.W., P.J.B., and M.L.R. analyzed data; and P.S.B., W.J.O., P.S.D., P.J.B., and M.L.R. wrote the paper.

The authors declare no competing interest.

This article is a PNAS Direct Submission.

Data deposition: The crystal structure of the ERK7–AC9 complex reported in this paper has been deposited in the Protein Data Bank, https://www.pdb.org (PDB ID code 6V6A).

[1]P.S.B. and W.J.O. contributed equally to this work.

[2]To whom correspondence may be addressed. Email: pbradley@ucla.edu or michael.reese@utsouthwestern.edu.

This article contains supporting information online at https://www.pnas.org/lookup/suppl/doi:10.1073/pnas.1921245117/-/DCSupplemental.

First published May 14, 2020.

parasites to form a functional apical complex, as the conoids are entirely missing in mature parasites and regulated secretion is disrupted. These data provide insight into the functions of the IMC apical cap in regulating parasite development. Using proximity biotinylation, we defined the AC9 interaction network, which includes extracellular signal-regulated kinase 7 (ERK7), a conserved mitogen-activated protein kinase (MAPK) that regulates ciliogenesis in Metazoa (15, 16), and which we have recently shown is required for conoid formation (17). We demonstrated that AC9 is required for the correct localization of ERK7 at the apical cap, and that this scaffolding interaction is essential for apical complex maturation. Finally, we solved the crystal structure of the ERK7–AC9 complex, which revealed that the AC9 C terminus wraps around the kinase and inserts into the active site, inhibiting it. ERK7 orthologs are found in all eukaryotes with ciliated cells, though the pathways it regulates are largely unknown. Furthermore, ERK7 is autoactivating (18), raising the question how this ancient kinase is regulated. Here, we have identified an essential inhibitory interaction for the *T. gondii* ERK7. Moreover, our data highlight a simple competitive mechanism by which protein–protein interactions can ensure the fidelity and specificity of a signaling network.

Results

Loss of AC9 Blocks Host Cell Invasion and Egress and Parasite Conoid Assembly. AC9 (TGGT1_246950) was initially identified by proximity biotinylation as an apically localized interactor of the IMC suture component ISC4 (19), though AC9 function was not further investigated in the previous study. We were unable to obtain an AC9 knockout parasite strain using CRISPR-Cas9, and thus we chose to assess its function using the auxin-inducible degron (AID) system (20, 21). We endogenously tagged the C terminus of AC9 with an AID-3×HA (hemagglutinin) tag ($AC9^{AID}$). $AC9^{AID}$ faithfully localized to the apical cap (Fig. 1*A*) and addition of 3-indoleacetic acid (IAA) ($AC9^{AID/IAA}$) resulted in efficient degradation of the protein (Fig. 1*A* and *SI Appendix*, Fig. S1*A*). Loss of AC9 completely blocked the parasites' ability to form plaques, which was rescued by the expression of a non-degradable copy of AC9 (Fig. 1*B*). We found that $AC9^{AID/IAA}$ parasites replicated normally but failed to egress from their host cells. Instead, $AC9^{AID/IAA}$ parasites appeared to replicate until their vacuoles separated from the monolayer, which we found floating in the medium (Fig. 1*C*). This phenotype is similar to the knockout of parasite perforin-like protein 1 (22), and suggested a block in egress. Egress can be induced by treatment with the calcium ionophore A23187 (23). While $AC9^{AID}$ parasites efficiently egressed from host cells after ionophore treatment, $AC9^{AID/IAA}$ were completely unresponsive (Fig. 1*D*). Loss of AC9 also blocked parasite invasion of host cells (Fig. 1*E*). Invasion and egress require secretion from specialized organelles called micronemes (24). The microneme protein MIC2 is shed from the parasite plasma membrane after secretion, and the levels of this protein in media can be used as a surrogate for secretion (23). Loss of AC9 blocked both basal and ionophore-induced release of MIC2, though levels of GRA39, which is constitutively secreted through a different route, are unaffected (Fig. 1*F*). Taken together, our data show that AC9 is required for efficient microneme secretion, and its loss blocks the parasite lytic cycle.

As AC9 impacts invasion and microneme secretion, we reasoned the observed phenotypes may be due to changes in parasite ultrastructure upon AC9 degradation. To test this hypothesis, we used immunofluorescence to compare available apical markers in $AC9^{AID}$ and $AC9^{AID/IAA}$ parasites. Strikingly, loss of AC9 resulted in a disorganization of the rhoptry secretory organelles (Fig. 2*A*). These organelles are usually bundled and polarized with their necks pointing apically (marked by RON11). In $AC9^{AID/IAA}$ parasites, however, the rhoptries are detached from the parasite's apex and the necks are no longer consistently apically oriented (Fig. 2*A*). Thus, both the micronemes and rhoptries are impacted in the absence of AC9. In *Toxoplasma*, a tubulin-rich structure called the conoid forms the core of the apical complex (8) and is the site at which microneme and rhoptry secretion is thought to occur (9, 25). Partial disruptions in the conoid structure have recently been associated with loss of parasite motility, invasion, and egress (26–28). Thus, we tested whether the conoid marker SAS6L (4) was altered upon AC9 degradation. In normally developed $AC9^{AID}$ parasites, we observed distinct apical SAS6L foci in both mother and developing daughter parasites (Fig. 2*B*). Strikingly, in $AC9^{AID/IAA}$ parasites, the mother SAS6L signal was missing, while the daughter cells' was maintained (Fig. 2*B*). These data strongly suggest that AC9 is required for maturation of the parasite conoid, and that the invasion and egress phenotypes we observed upon AC9 degradation (Fig. 1) are driven by conoid loss.

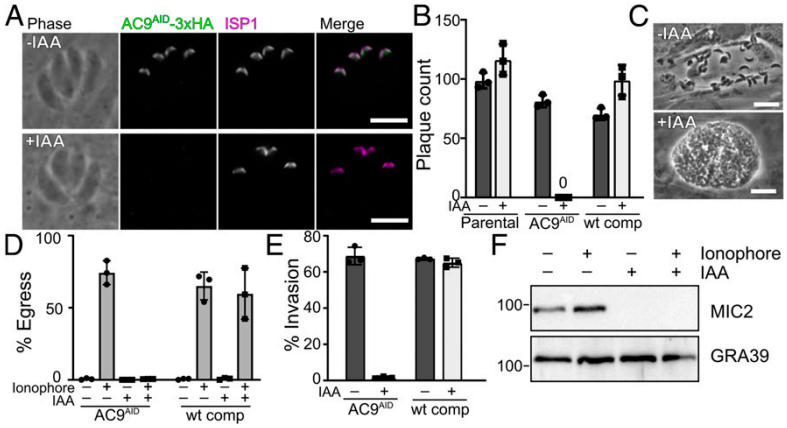

Fig. 1. AC9 is required to complete the parasite lytic cycle. (*A*) $AC9^{AID}$-3×HA (green) localizes to the apical cap (magenta) and is lost when parasites are treated with IAA. (Scale bars, 5 μm.) (*B*) Quantification of plaque number comparing growth of parental, $AC9^{AID}$, and WT-complemented $AC9^{AID}$ parasites grown with and without IAA. (*C*) $AC9^{AID}$ parasites naturally egress from host cells in –IAA but are found as floating vacuoles when grown in IAA. (Scale bars, 20 μm.) (*D*) Quantification of egress of the indicated strains induced by a calcium ionophore and grown in ±IAA. (*E*) Quantification of invasion of the indicated strains grown in ±IAA. (*F*) Western blot of soluble secreted proteins from $AC9^{AID}$ and $AC9^{AID/IAA}$. Microneme secretion was tracked with anti-MIC2 and the constitutively secreted dense granule protein GRA39 was used as a control. All error bars are SD.

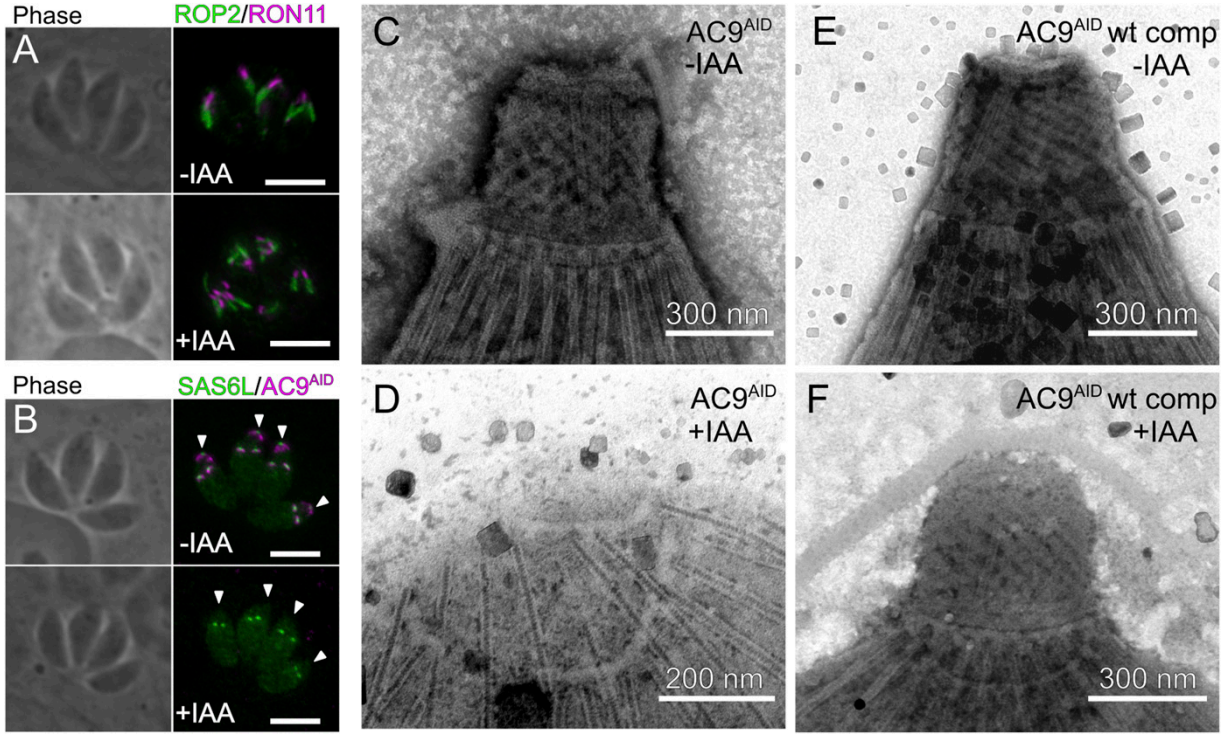

Fig. 2. Loss of AC9 disrupts the parasite apical complex. (*A*) AC9^{AID} and AC9$^{AID/IAA}$ parasites were stained with ROP2 (green) and RON11 (magenta). (*B*) AC9^{AID} and AC9$^{AID/IAA}$ parasites were stained with antibodies to the HA tag (magenta) and the conoid marker SAS6L (green). Arrowheads indicate the position of the maternal apical complex. (Scale bars, 5 μm.) (*D–F*) TEM images of the apical complex from negatively stained detergent-extracted (*C*) AC9^{AID} parasites, (*D*) AC9$^{AID/IAA}$ parasites, and AC9^{AID} WT-complemented parasites grown in (*E*) −IAA and (*F*) +IAA.

We next sought to directly examine the effect of AC9 loss on the ultrastructure of the mature parasite conoid. Many parasite cytoskeletal structures, including the apical complex, are preserved after detergent extraction (29). We detergent extracted AC9^{AID} and AC9$^{AID/IAA}$ parasites to create cytoskeleton "ghosts" and imaged them using negative-stained transmission electron microscopy (TEM). While we observed an extended conoid in AC9^{AID} parasites (Fig. 2*C*), we found that the conoid was completely absent in AC9$^{AID/IAA}$ parasites (Fig. 2*D*). As expected, expression of nondegradable AC9 rescued this phenotype (Fig. 2 *E* and *F*). Importantly, the ultrastructural changes appear to be specific to the loss of the conoid in AC9$^{AID/IAA}$ parasites, as our TEM images show that the parasites have maintained their 22 cortical microtubules (Fig. 2*D*). Intriguingly, we noted that AC9^{AID} tagging appears to have exacerbated an artifact of EM sample preparation of the parasite cytoskeleton in which the base of the conoid partially detaches from the apical polar ring (*SI Appendix*, Fig. S1). We assessed the basal (−IAA) level of AC9^{AID} protein, and found that AC9^{AID} levels are ∼40% of the levels of AC9 tagged with only a 3×HA in the same OsTIR1-expressing parental line (*SI Appendix*, Fig. S1). Such basal degradation has been uncovered as a common artifact of the AID system (30, 31). Notably, AC9^{AID}(wild-type [WT] complement) conoids were indistinguishable from the parental strain, suggesting that reduced AC9 protein levels may be driving the apparent defect in conoid ultrastructure (Fig. 1 and *SI Appendix*, Fig. S1). Nevertheless, despite any potential structural differences, the AC9^{AID} parasites showed no phenotype in secretion, invasion, or egress when untreated with IAA, in stark contrast to the effect of complete AC9 degradation (Fig. 1). Taken together, our data indicate AC9 has a critical role in maintaining apical complex ultrastructure.

Proximity Biotinylation Reveals AC9 Interacts with the MAP Kinase ERK7. We next sought to identify protein partners that collaborate with AC9 to facilitate parasite conoid assembly and/or maintenance. To this end, we endogenously tagged the protein with BirA* (AC9^{BioID}) (12, 32). After 24-h growth in 150 μM biotin, we could detect biotin labeling in the apical cap with fluorescent streptavidin, demonstrating active BirA* at this location (*SI Appendix*, Fig. S2*A*). While AC9 is predicted to be ∼70% intrinsically disordered, it has an ∼150-residue N-terminal predicted coiled-coil domain, which we reasoned may indicate it is a component of the IMC cytoskeleton. The IMC cytoskeleton is stable after detergent extraction (19), and we found that AC9 copurified with cytoskeletal, rather than membranous, components of the IMC (*SI Appendix*, Fig. S2*B*). This demonstrates AC9 is associated with the intermediate filament cytoskeleton of the apical cap, which we exploited to increase the specificity of our biotin identification (BioID) experiments (*SI Appendix*, Fig. S2*B*). We grew AC9^{BioID} parasites in biotin, lysed them in 1% Triton X-100, and separated the cytoskeleton from solubilized membrane and cytosolic components by sedimentation at 14,000 × *g*. We then purified the biotinylated proteins using streptavidin resin, which were identified by liquid chromatography-tandem mass spectrometry (LC-MS/MS) (Dataset S1). Our dataset was of high quality, as the top candidates were enriched in known apical cap proteins (12, 19). In addition, our top hit was previously undescribed (TGGT1_292950). To validate that TGGT1_292950 is, indeed, an apical cap protein, we epitope tagged the endogenous gene with 3×HA. The resulting protein colocalizes with the

apical cap marker ISP1 (*SI Appendix*, Fig. S2*C*), leading us to name the gene apical cap protein 10 (AC10).

Among the top candidates from our BioID dataset was the MAP kinase ERK7 (TGGT1_233010). We recently demonstrated that ERK7 localizes to the apical cap, and that its loss-of-function phenotype is essentially identical to what we have observed for AC9 (17). We therefore prioritized investigating the function of this interaction. AC9 and ERK7 colocalize at the apical cap (Fig. 3*A*) and proximity-ligation immunofluorescence (33) demonstrated that they are closely associated at this site (Fig. 3*B*). ERK7 is a member of an early-branching MAPK family that is conserved throughout eukaryotes (34, 35) and has been implicated as a facilitator of ciliogenesis in Metazoa (15, 16) and Apicomplexa (17), though little is known about its signaling cascade and regulatory interactions in any organism. AC9 is conserved among coccidian parasites, though the overall protein sequences are highly divergent (21 to 55% identity). The region of highest conservation is in the AC9 C terminus (Fig. 3*C*). Analysis across all sequenced coccidian genera demonstrated that 16 of the most C-terminal 33 residues in AC9 are invariant.

To test whether the AC9 C terminus was indeed the site of ERK7 binding, we bacterially expressed and purified several AC9 constructs N-terminally fused to yeast SUMO as a carrier protein. We found that $AC9_{401–452}$ was robustly pulled down by the glutathione S-transferase (GST)-ERK7 kinase domain (*SI Appendix*, Fig. S3), demonstrating that the two proteins interact directly. The AC9 C terminus is predicted to be intrinsically disordered, suggesting that it associates with the ERK7 kinase domain in an extended conformation. MAPKs interact with their substrates and regulatory partners through docking interactions that involve short linear motifs, usually 10 to 15 residues (36–38). We reasoned AC9 may be interacting through such a motif and tested whether shorter regions of the AC9 C terminus were sufficient to bind ERK7. Surprisingly, we found that neither $AC9_{401–430}$ nor $AC9_{431–452}$ were detectable after pull down by GST-ERK7 (*SI Appendix*, Fig. S3). We therefore reasoned that the entire well-conserved portion of AC9, comprising $AC9_{419–452}$ (Fig. 3*C*), was required for the interaction. We measured the binding of fluorescein-labeled $AC9_{419–452}$ to recombinantly express and purify ERK7 kinase domain by fluorescence anisotropy. $AC9_{419–452}$ bound ERK7 with a K_D of 34 ± 2 nM (Fig. 3*D*),

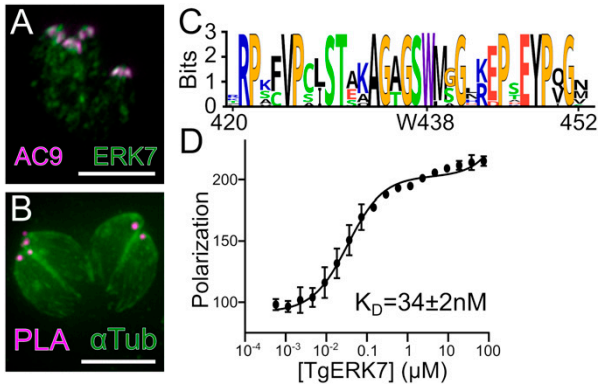

Fig. 3. AC9 tightly binds ERK7. (*A*) ERK7-Ty (green) colocalizes with AC9-HA (magenta) at the apical cap. (*B*) Proximity ligation (magenta) of ERK7 and AC9 reveal bright foci at the parasite apical cap. Parasites are counterstained with anti–β-tubulin (note that this antibody does not stain the apical complex, likely due to antigen accessibility). (Scale bars, 5 μm.) (*C*) Sequence logo for $AC9_{419–452}$ highlights invariant C-terminal residues. (*D*) Binding of $AC9_{419–452}$ to $ERK7_{1–358}$ was measured by fluorescence polarization and the K_D was calculated from global fit of three replicate experiments of three technical replicates each.

which is an affinity consistent with a strong MAPK docking-site interaction (36, 39).

AC9 Is Required for ERK7 Localization and Function in Parasites. Given their interaction, we reasoned that AC9 may be an ERK7 substrate. Available phosphoproteomic data report nine phosphosites on AC9 [ToxoDBv46, https://toxodb.org/toxo/ (40)]. To test the relevance of these sites to our observed phenotypes, we complemented the $AC9^{AID}$ strain by expressing a nonphosphorylatable allele, in which each of these Ser/Thr had been mutated to Ala (*SI Appendix*, Fig. S4*A*). This mutant protein correctly localized to the apical cap (*SI Appendix*, Fig. S4*B*) and fully rescued the ability of the $AC9^{AID}$ parasites to form plaques (*SI Appendix*, Fig. S4*C*), demonstrating that phosphorylation of these sites is not required for AC9 function.

We identified ERK7 as a component of the cytoskeletal fraction of AC9-interacting proteins (*SI Appendix*, Fig. S2 and Dataset S1), but ERK7 has no domains that would be predicted to interact with the cytoskeleton on its own. We therefore reasoned that AC9 may act as a scaffold that recruits ERK7 to the apical cap cytoskeleton. Consistent with this model, the ERK7 protein was lost from the apical cap upon AC9 degradation (Fig. 4*A*), and this localization is rescued in the AC9 WT complement (Fig. 4*B*). Importantly, AID-mediated degradation of ERK7 has no effect on AC9 localization (*SI Appendix*, Fig. S5*A*). These data suggest that a major function of AC9 is to recruit ERK7 to the apical cap. To directly test this model, we sought an AC9 mutant that retained its own localization but did not bind ERK7. While we were unable to obtain stable strains expressing deletions of the AC9 C terminus, we found that mutation of three Ser/Thr to Glu ($AC9^{3×Glu}$; Ser419-Glu, Thr420Glu, Ser437Glu) reduced in vitro AC9 affinity for ERK7 by ~200-fold (Fig. 4*C*). $AC9^{3×Glu}$ localized correctly when expressed in the background of the $AC9^{AID}$ strain (Fig. 4 *D* and *E*), though it was unable to rescue the $AC9^{AID/IAA}$ plaque phenotype (Fig. 4*F*). In addition, while ERK7 localized to the apical cap in $AC9^{AID/3×Glu}$ parasites, this localization was lost upon addition of IAA and degradation of the wild-type $AC9^{AID}$ copy (Fig. 4*D*), as was the tubulin-rich conoid (Fig. 4*E* and *SI Appendix*, Fig. S5*B*). Therefore, interaction with AC9 is necessary for ERK7 concentration at the apical cap. Importantly, ERK7 protein was still found in the parasite cytosol after AC9 degradation, demonstrating that expression of ERK7 is not sufficient for conoid development (Fig. 4*E* and *SI Appendix*, Fig. S5*B*). These data suggest that ERK7 must be present at the apical cap to function, and demonstrate that a critical function for AC9 is to control ERK7 localization.

AC9 Binds ERK7 in an Unusual Inhibitory Conformation. To better define the nature of the AC9–ERK7 interaction, we solved the cocrystal structure of $AC9_{419–452}$ bound to the ERK7 kinase domain to 2.1 Å (Fig. 5 and *SI Appendix*, Table S1). To our surprise, the AC9 C terminus forms extensive contacts with ERK7 and wraps around the kinase from the MAPK docking site (the CD domain) to the substrate-recognition region (Fig. 5). Strikingly, AC9 binding encompasses all major MAPK-interacting and regulatory regions except for the F site (41). MAPK docking-site interactions are typically defined by a cluster of positively charged residues in the docking motif that interact with an acidic cluster in the kinase CD domain adjacent to van der Waals interactions between complementary hydrophobic surfaces in the two partners (36, 42, 43). Remarkably, the only MAPK-interacting protein from *Toxoplasma* previously described is a secreted effector, GRA24, that binds mammalian p38 with a canonical docking-site interaction (44); there are no regulatory partners known for the parasite's MAPKs.

In stark contrast to more typical docking-site interactors, AC9 does not make extensive side-chain interactions with the MAPK CD domain. AC9 Phe424, Val425, and Leu428 make weak van der Waals interactions with the ERK7 CD domain (contacts >3.5 Å).

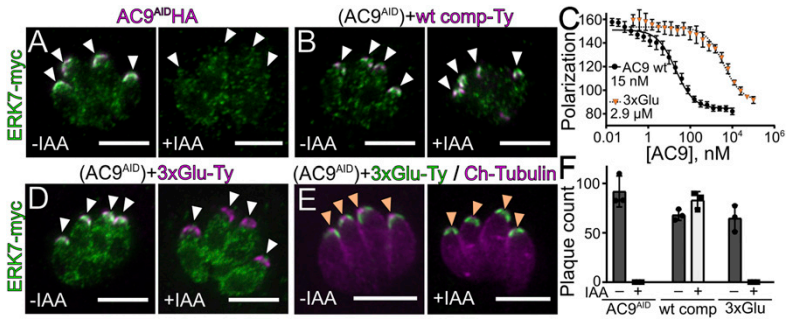

Fig. 4. AC9 is a scaffold that drives ERK7 apical localization. (*A* and *B*) ERK7-3×myc (green) localization is lost upon degradation of (*A*) $AC9^{AID}$-3×HA with growth in IAA (magenta), which is rescued in the (*B*) AC9 WT complement. White arrowheads indicate the apical cap. (*C*) K_i of WT $AC9_{401–452}$ and 3×Glu $AC9_{401–452}$ was determined by competition with fluorescein-labeled $AC9_{419–452}$; 95% CI: WT, 13.4 to 17.7 nM; 3×Glu, 2.4 to 3.6 μM. (*D*) ERK7-3×myc (green) localization was compared in 3×Glu-complemented (magenta) parasites as in *A* and *B*. (*E*) Growth of 3×Glu-complemented (green) $AC9^{AID}$ parasites expressing mCherry-tubulin (magenta) with or without IAA. Orange arrowheads indicate the expected location of conoid foci. (*F*) Quantification of plaque number comparing growth of $AC9^{AID}$, WT-complemented $AC9^{AID}$, and 3xGlu-complemented $AC9^{AID}$ parasites grown with and without IAA. (Scale bars, 5 μm.) All error bars are SD.

Only two polar AC9 side chains make close contact with the ERK7 CD domain (Fig. 5*B* and *SI Appendix*, Fig. S6): AC9 Arg421 is salt bridged with ERK7 Glu147 (3.0 Å), while AC9 Thr430 hydrogen bonds with ERK7 Glu96 (2.3 Å). Most of the ERK7 side chains in the CD domain that interact with AC9 do so through backbone hydrogen bonds. Mutation of the "basic patch" (e.g., MNK Arg5, Lys6 in Fig. 5*C*) of typical motifs that bind the MAPK CD domain abrogates their binding (36). Consistent with the idea that AC9 forms a suboptimal ERK7 docking-site interaction, mutation of the two basic residues in the AC9 CD-interacting motif (Arg421 and Lys423) to Ala only reduces affinity for ERK7 by approximately fourfold (Fig. 5*H*).

The C-terminal nine residues of AC9 (444 to 452) appear to act as a pseudosubstrate, as these residues make close contacts with the ERK7 substrate-recognition subdomain (Fig. 5*D*). These interactions are centered around the invariant AC9 Pro449, which appears to mimic the required Pro in a true MAPK substrate and packs against ERK7 Trp185 (3.4 Å). Intriguingly, the C terminus of AC9 makes contacts with a conserved basic cluster (ERK7 Arg184, 2.8 Å; Arg187, 2.9 Å) adjacent to the kinase APE motif. This cluster normally coordinates the pTyr in active MAPKs (Fig. 5*E*), indicating AC9 binding partially displaces the ERK7 activation loop. Notably, the ERK7-binding motif in AC9 is of an invariant length at the C terminus in all AC9 sequences (Fig. 3*C*) and the interaction with the AC9 C-terminal carboxylate helps explain this conservation.

Most striking of the AC9 interactions with ERK7, however, is the insertion of AC9 Trp438 into the ERK7 active site (Fig. 5*F*). The Trp438 side chain has displaced nucleotide and Mg^{2+} in our structure; even though the crystals formed in 1 mM ADP and 10 mM $MgCl_2$, there is no density consistent with either. In fact, the Trp438 side chain appears to be acting as a nucleotide mimic, a surprising function for a protein residue. The Trp438 indole ring makes π–cation interactions (3.2 Å) with the catalytic VAIK Lys42 that normally coordinates the ATP β-phosphate. In addition, the indole ring hydrogen bonds with the DFG Asp154 (2.7 Å), which normally coordinates nucleotide through a bound Mg^{2+}. The AC9 loop flanking Trp438 inserts from above the ERK7 CD domain, pushing the kinase Gly loop into an open conformation without disrupting its overall secondary structure. Thus, the AC9-bound conformation of the ERK7 active site is substantially different from that typical of an active kinase, such as ERK2 (Fig. 5*G* and *SI Appendix*, Fig. S7 *A* and *B*). Furthermore, our structure fully explains the loss of affinity of the $AC9^{3×Glu}$ mutant for ERK7. While neither Ser419 nor Thr420 makes side-chain contacts, Ser437 is buried in the active site next to Trp438. Mutation of Ser437 to Glu, however, would clash with ERK7 Asp98 (*SI Appendix*, Fig. S7*C*), consistent with the 200-fold drop in affinity we observed.

Taken together, our structural data strongly suggested that AC9 acts not only as a scaffold for ERK7 but likely serves as a competitive inhibitor of its kinase activity. Indeed, we found that *Toxoplasma* ERK7 phosphorylation of the generic substrate myelin basic protein (MBP) was completely blocked by the addition of 10 μM $AC9_{401–452}$ to the reaction (Fig. 6*A*). Because the interactions AC9 makes with *Toxoplasma* ERK7 side chains are broadly conserved among MAPKs (*SI Appendix*, Fig. S6), we reasoned AC9 may be a promiscuous inhibitor. Surprisingly, this was not the case. While AC9 robustly inhibits *Toxoplasma* ERK7 activity, it had no effect on the ability of another *Toxoplasma* MAPK (TgMAPK2), rat ERK7, or rat ERK2 to phosphorylate MBP (Fig. 6*A*). It thus seems likely that the specificity of AC9 for TgERK7 is due to a combination of surface complementarity and the ability of TgERK7 to adopt a conformation able to recognize AC9.

As described above, AC9 binds ERK7 with an extended interface that buries ∼1,650 $Å^2$. While the AC9–ERK7 interaction is reasonably strong (15 to 35 nM; Figs. 3*D* and 4*C*), protein–peptide interactions can achieve similar affinities with substantially smaller buried surfaces. For instance, Grb2-SH2 binds $Shc1_{423–435}$ with a K_D of 18 nM (45) with a 404-$Å^2$ interface (46). Similarly, the Cbl-TKB domain binds $APS_{609–621}$ with a K_D of 43 nM with a 629-$Å^2$ interface (47). These data suggest the AC9–ERK7 interface is formed by a distributed series of weak interactions, which is consistent with our mutagenesis data. Mutation of residues usually critical to recognizing the MAPK CD domain only modestly affected AC9 affinity ($AC9_{R231A/K232A}$; Fig. 5*H*). Even mutation of Trp438 yielded a protein with a respectable, albeit weakened, affinity of 1.6 μM (Fig. 5*H*). In addition, these distributed interactions (CD domain, active site, activation loop/pseudosubstrate) appear to act cooperatively to enable AC9 to capture ERK7 in an optimal conformation for binding. Truncated versions of AC9 showed no measurable binding to the kinase (*SI Appendix*, Fig. S3).

Given these observations, we reasoned that AC9 may be displaced by a substrate that can engage the CD domain with a physiologically relevant affinity. While there are yet no known substrates of *Toxoplasma* ERK7, we tested available peptides with known affinities to metazoan MAPKs for ERK7 binding. Even though there is no homologous sequence in *Toxoplasma*, we found that rat $MEK2_{4–16}$ binds *Toxoplasma* ERK7 with a K_D of ∼12 μM (Fig. 6*B*). Note that physiological MAPK docking-site interactions range in affinity from 0.5 to 50 μM (39, 48, 49) and MEK2 engages its cognate partner, ERK2, with an ∼8 μM K_D.

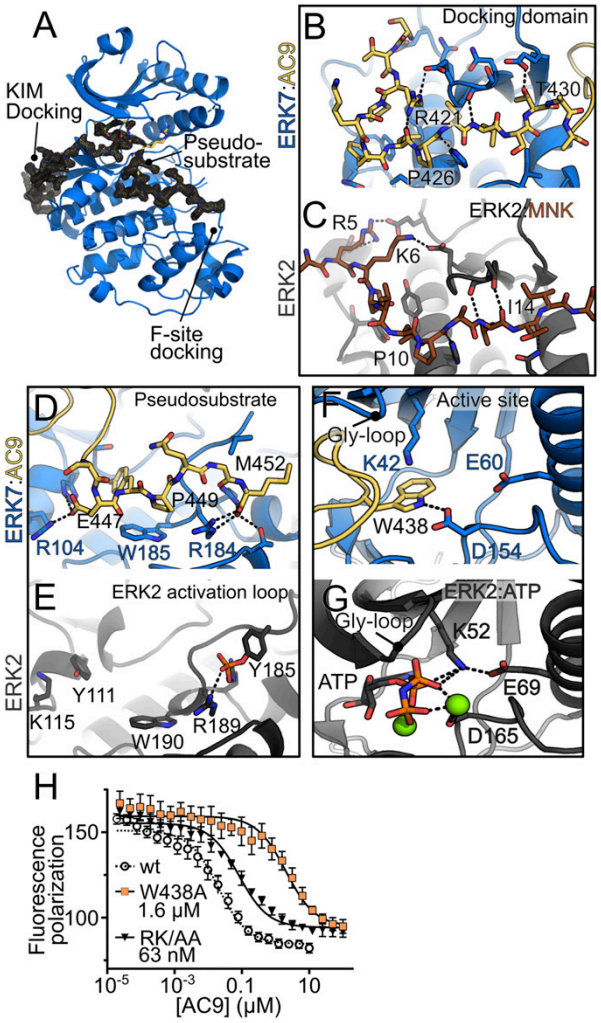

Fig. 5. AC9 binds ERK7 in an inhibitory conformation. (*A*) Overview of AC9–ERK7 interaction. ERK7 is blue. A 1.5σ $2F_O - F_C$ electron density map (black) is shown around AC9 (yellow). (*B–G*) Contacts between AC9 (yellow) and ERK7 (blue) are compared with ERK2 (gray) at (*B* and *C*) the MAPK-docking domain, (*D* and *E*) activation loop/substrate binding site, and (*F* and *G*) kinase active site. (*H*) K_I of AC9 mutants was determined by competition with fluorescein-labeled wild-type AC9. Wild-type competition curve (K_I 15 nM) is shown for comparison; 95% CI: $AC9_{W438A}$, 1.3 to 2.0 μM; $AC9_{R421A/K423A}$ (RK/AA), 55 to 74 nM. ERK2 images are from PDB ID codes 4H3Q (*C*) and 6OPG (*E* and *G*). All error bars are SD.

We chose to modify a well-characterized mammalian MAPK substrate, ELK1, which requires CD-domain interaction for efficient phosphorylation (50). As expected, we could not detect measurable phosphorylation of an $ELK1_{300–428}$ construct, which lacks an ERK7-binding motif. A chimeric ELK1 construct that contains the MEK2-docking motif ($ELK1_{MEK2\text{-}D}$), however, was phosphorylated by ERK7 at levels similar to the generic substrate MBP in the absence of AC9 (Fig. 6*C*). While ERK7 phosphorylation of MBP was efficiently inhibited by AC9, substantial levels of $ELK1_{MEK2\text{-}D}$ phosphorylation remained even in the presence of 10 μM AC9 (Fig. 6*C*). Thus, AC9 inhibition of ERK7 can be successfully released by competition with even a modest-affinity docking-site interaction.

Notably, ERK7 family members are unusual in the MAPK family as they are able to autophosphorylate their activation loops (18), and thus bypass the need for a MAPK kinase for their activation. We have previously found that ERK7 kinase activity is required for conoid formation (17). Our data therefore suggest that AC9 has the dual roles of concentrating *Toxoplasma* ERK7 at the apical cap and regulating its kinase activity and substrate specificity (Fig. 6*D*).

Discussion

We have identified AC9 as an essential cytoskeletal scaffold of the *Toxoplasma* ERK7 kinase. Remarkably, inducing AC9 degradation phenocopies loss of ERK7 and results in parasites that mature without conoids, thereby interrupting the lytic cycle. We found that AC9 is required for ERK7 localization to the apical cap and identified a mutant that could not bind and recruit ERK7, and therefore did not rescue any of the AC9 loss-of-function phenotypes (Fig. 4). Surprisingly, our crystal structure of the ERK7–AC9 complex revealed that AC9 is also a competitive inhibitor of ERK7 kinase activity. Usually, genetic ablation of an inhibitor would be expected to present the opposite phenotype from its target. Because ERK7 kinase activity is required for conoid formation (17), our data suggest that AC9 inhibition of the kinase is not permanent. Instead, we propose that AC9 binding to ERK7 represents an unusual mechanism of ensuring kinase specificity (Fig. 6*D*). Because ERK7 is autoactivating, its regulation by a phosphatase would be insufficient to ensure signaling fidelity, especially when the kinase is maintained at a high local concentration at the apical cap. While the full AC9 C terminus binds tightly to ERK7 (Fig. 3*D*), this is due to cooperative binding of distributed contacts (Fig. 5); neither $AC9_{401–430}$, which occupies the CD domain, nor $AC9_{431–452}$, which occupies the active and pseudosubstrate sites, is sufficient for ERK7 binding (*SI Appendix*, Fig. S3). We therefore propose that an ERK7 substrate with both a strong kinase-interacting motif and substrate site would successfully compete with AC9 for kinase binding during phosphorylation (Fig. 6*D*). Alternatively, an ERK7-activating factor may transiently displace AC9, allowing substrate binding. In either of these cases, the regulated release of AC9 inhibition would define ERK7 activity. Determining ERK7 substrates as well as other regulatory factors will not only provide the opportunity to directly test these models but will also allow us to define how ERK7 facilitates ciliogenesis in parasites (17) and other organisms (15, 16).

A striking feature of the AC9 inhibition of ERK7 is its specificity. Even though AC9 makes contacts with conserved sites, we found that it does not inhibit other *Toxoplasma* or mammalian MAPKs, including the rat ERK7 ortholog. These data suggest that the kinase dynamics, rather than final contact sites, are contributing to specificity of the inhibition. This has clear implications for the design of specific inhibitors of parasite ERK7. Moreover, the AC9–ERK7 interaction may represent a generalized mechanism of inhibiting ancient signaling molecules such as ERK7. ERK7 is the earliest-branching member of the MAPK family (51), and is unusual in its autoactivation (18). Notably, cyclin-dependent kinases (CDKs) are also regulated by inhibitory proteins (52), and are related to the MAPKs (51). Like the ERK7–AC9 interaction, the cell-cycle inhibitor p27 is intrinsically disordered and binds CDK2 through a distributed surface. Also like AC9, p27 inserts itself into the kinase active site and displaces nucleotide (*SI Appendix*, Fig. S7*C*) (53). However, there are notable differences between the two inhibitory interactions. First, AC9 occupies the MAPK CD domain, which is not present in CDKs. Also, while our structure demonstrates that AC9 insertion pushes the ERK7 Gly loop into an inactive conformation (Fig. 5 and *SI Appendix*, Fig. S7), p27 replaces the first β-strand in CDK2, destroying the Gly-loop structure (*SI Appendix*, Fig. S7*C*). Finally, while both ERK7 and AC9 protein levels appear to be maintained stably at the apical cap throughout the cell cycle, p27 is degraded

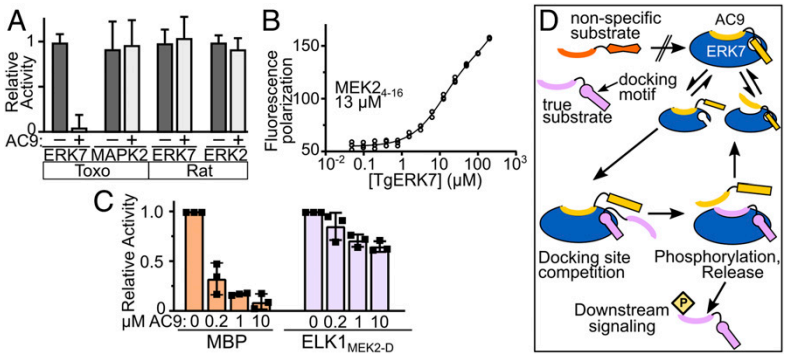

Fig. 6. AC9 is an inhibitory regulator of ERK7 kinase activity. (*A*) Quantification of phosphorylation of MBP by the indicated kinases in the presence and absence of 10 μM $AC9_{401–452}$, normalized to activity without AC9. (*B*) Binding of kinase-interacting-motif from rat MEK2 to TgERK7 was measured by fluorescence polarization; 95% CI: 10.5 to 14.5 μM. (*C*) Quantification of TgERK7 phosphorylation of MBP or a chimeric ELK1/$MEK2_{4–16}$ substrate in the presence of the indicated $AC9_{401–452}$ concentration ($n = 3$ biological replicates). (*D*) Model for AC9 regulation of ERK7 specificity. AC9 occupies the ERK7 active site, preventing the binding of nonspecific substrates. However, the AC9 docking-site interaction is suboptimal and can be competed off by true ERK7 substrates, which are released after phosphorylation, allowing AC9 to rebind. All error bars are SD.

at the G_1/S transition, releasing its inhibition of CDK2 (54). Nevertheless, the convergent evolution of specific protein inhibitors of two branches of the CMGC family suggests that there may be additional genetically encoded kinase inhibitors that remain unidentified throughout Eukaryota. Identifying such inhibitors would refine our understanding of cellular signaling architecture and provide potential platforms on which specific therapeutics may be designed.

Materials and Methods

Sequence Analysis. Sequences for AC9 from *T. gondii*, *Hammondia hammondi*, *Neospora caninum*, *Cyclospora cayetanensis*, *Cystoisospora suis*, *Eimeria* spp., and *Sarcocystis neurona* were retrieved from ToxoDBv43 (https://toxodb.org/toxo/) using the basic local alignment search tool (BLAST). The AC9 sequence from *Besnoitia besnoiti* was identified by BLAST and retrieved from UniProt. The protein sequences were aligned with Clustal Omega (55). The AC9 sequence logo was generated with WebLogo (56).

PCR and Plasmid Generation. All PCRs were conducted using Phusion polymerase (NEB) using primers listed in Dataset S2. Constructs were assembled using Gibson master mix (NEB). Point mutations were created by the Phusion mutagenesis protocol. $AC9^{AID}$ tagging constructs were generated using a PCR-amplified homology-directed repair template (P1-2) and a CRISPR-Cas9 pU6-Universal plasmid with a protospacer against the 3′ untranslated region of the gene of the interest (P3-4). AC9-BirA*, ERK7, and AC10 C-terminal tagging constructs were generated using P1-4, P5-8, and P9-12, respectively. To generate the wild-type complementation construct, the complete AC9-coding sequence was PCR-amplified from complementary DNA and cloned into a UPRT-locus knockout vector driven by the ISC6 promoter. Both the 3×Glu and the phosphorylation mutants were constructed using synthetic genes (Quintara Biosciences) and cloned into the pISC6-UPRT vector (Dataset S2).

Chemicals and Antibodies. 3-Indoleacetic acid (heteroauxin; Sigma-Aldrich; I2886) was used at 500 μM from a 500 mM stock in 100% ethanol. A23187 (Sigma-Aldrich; C5722) was used at 1 to 2 μM, dissolved from a 2 mM stock in dimethyl sulfoxide (DMSO). The HA epitope was detected with mouse monoclonal antibody (mAb) HA.11 (BioLegend; MMS-101P), rabbit polyclonal antibody (pAb) anti-HA (Invitrogen; 71-5500), or rat monoclonal 3F10 (Sigma-Aldrich; 11867423001). The Ty1 epitope was detected with mouse mAb BB2 (57). The c-Myc epitope was detected with mouse mAb 9E10 (58) or rabbit pAb anti-Myc (Invitrogen; PA1981). His_6-tagged proteins were recognized with mouse anti-His_6 (R&D Systems; MAB050). Biotinylated proteins were detected with Alexa Fluor 488-streptavidin (Molecular Probes; S32354) and captured with Streptavidin High-Capacity Agarose Beads (Thermo Scientific; PI20359). *Toxoplasma*-specific antibodies include rabbit anti–β-tubulin (17), mouse mAb anti-ISP1 7E8 (11), rabbit pAb anti-SAG1 (59), mouse mAb anti–F1-ATPase beta subunit 5F4 (60), mouse mAb anti-MIC2 (gift from Vern Carruthers, University of Michigan, Ann Arbor, MI), rat pAb anti-GRA39 (61), rabbit pAb anti-ROP2, rat pAb anti-RON11 (60), mouse mAb anti-SAS6L (4), mouse mAb anti-IMC1 45.15 (62), and mouse mAb anti-ISP3 (11).

Immunofluorescence. Human foreskin fibroblasts (HFF) were grown on coverslips in 24-well plates until confluent and were infected with parasites. The cells were rinsed once with phosphate-buffered saline (PBS), fixed with 3.7% formaldehyde in PBS, washed, permeabilized with 0.1% Triton X-100, blocked with 3% bovine serum albumin (BSA) for 1 h, and incubated with primary antibodies for a minimum of 2 h. Secondary antibodies used were conjugated to Alexa Fluor 488 or Alexa Fluor 594 (Thermo Scientific). The coverslips were mounted in Vectashield (Vector Labs) and viewed with an Axio Imager.Z1 fluorescence microscope (Zeiss). For proximity-ligation assays, cells were fixed in 4% paraformaldehyde/4% sucrose followed by permeabilization in 0.1% Triton X-100 for 10 min. Blocking, antibody incubations, and proximity ligation were conducted according to the manufacturer's directions (Sigma-Aldrich) using rabbit polyclonal anti-HA (63) and mouse m2 anti-FLAG (Sigma-Aldrich; F1804) as primary antibodies. Cells were counterstained with Alexa Fluor 647-conjugated rabbit anti–β-tubulin, mounted in Vectashield, and imaged on a Nikon Ti2E microscope.

Western Blotting. Parasites were lysed in Laemmli sample buffer with 100 mM dithiothreitol (DTT) and heated at 100 °C for 10 min. Proteins were separated by sodium dodecyl sulfate/polyacrylamide-gel electrophoresis (SDS/PAGE), transferred to nitrocellulose, and probed with primary antibodies and the corresponding secondary antibody conjugated to horseradish peroxidase. Western blots were imaged using SuperSignal West Pico Substrate (Pierce) and imaged on a ChemiDoc XRS+ (Bio-Rad). Band intensities were quantified using the manual volume tool in the Image Lab Software of ChemiDoc XRS+.

Plaque Assays. HFF monolayers were supplemented with ±500 μM IAA before allowing equal numbers of freshly lysed, extracellular parasites of a given strain (grown in –IAA) to infect and form plaques for 7 d. Cells were then fixed with ice-cold methanol and stained with crystal violet. Plaque number was counted manually and analyzed by Prism (GraphPad). All plaque assays were performed in triplicate for each condition.

Invasion Assays. Invasion assays were performed as previously described (22). Parasites were grown for 30 h ±IAA and intracellular parasites were collected by scraping and passaging through a 27-gauge needle. Equivalent parasite numbers were resuspended in Endo buffer (64) and settled onto coverslips with HFF monolayers for 20 min. Endo buffer was then replaced with warm D1 media (Dulbecco's modified Eagle's medium, 20 mM Hepes, 1% fetal bovine serum) and incubated at 37 °C for 30 min. Coverslips were then fixed and blocked, and extracellular parasites were stained with anti-SAG1 antibodies. The samples were then permeabilized, and all parasites were stained with anti-F1B ATPase antibodies and incubated with secondary antibodies. Parasites were scored as invaded (SAG1+, F1B– ATPase–) or not (SAG1+, F1B+) by fluorescence microscopy. Invasion assays were performed

in triplicate, at least 10 fields were counted for each replicate, and the average for each replicate was calculated as a percentage.

Egress Assays. Parasites were grown on a monolayer on coverslips for 34 h ±IAA until most vacuoles contained 16 or 32 parasites. Coverslips were washed twice with prewarmed PBS and incubated with A23187 (or DMSO control) diluted in PBS at 37 °C for 2 min. Coverslips were then fixed and stained with rabbit anti-IMC12 antibodies. At least 10 fields of ~200 vacuoles per field were counted for three replicate coverslips for each condition.

Microneme Secretion. Microneme-secretion assays were performed as previously described (23). Briefly, parasites were grown for 30 h and intracellular parasites were collected by mechanical release through a 27-gauge needle. After washing twice in D1 media, parasites were resuspended in prewarmed D1 media and induced with 1 μM A23187 for 10 min at 37 °C. Secretion was arrested by cooling on ice, and parasites were pelleted at 1,000 × *g* for 5 min at 4 °C. The supernatant was collected and centrifuged again at 1,000 × *g*. Secreted proteins in the resulting supernatant were assessed by SDS/PAGE and Western blot analysis.

Detergent Fractionation and Streptavidin Purification. The IMC cytoskeletal fraction was isolated by 1% Triton X-100 fractionation as described (65). Extracellular parasites were lysed in 1% Triton X-100, 50 mM Tris·HCl (pH 7.4), 150 mM NaCl buffer supplemented with cOmplete Protease Inhibitor Mixture (Roche) and incubated on ice for 30 min. Lysates were centrifuged, and equivalent loads of the total, supernatant, and pellet samples were run on SDS/PAGE and immunoblotted, using IMC1 and ISP3 as cytoskeletal and soluble controls, respectively. For streptavidin purification of BioID samples, parasites were grown for 24 h in media supplemented with 150 μM biotin. The cytoskeletal fraction was solubilized in 1% SDS and diluted to RIPA conditions, biotinylated proteins were purified using Streptavidin High-Capacity Agarose (Pierce), and the proteins were identified via mass spectrometry.

Mass Spectrometry. Purified proteins bound to streptavidin beads were reduced, alkylated, and digested by sequential addition of lys-C and trypsin proteases (66, 67). Samples were then desalted using C18 tips (Pierce) and fractionated online using a 75-μm inner-diameter fritted fused silica capillary column with a 5-μm pulled electrospray tip and packed in-house with 15 cm of Luna C18(2) 3-μm reversed-phase particles. The gradient was delivered by an EASY-nLC 1000 Ultra-High-Pressure Liquid-Chromatography System (Thermo Scientific). MS/MS spectra were collected on a Q-Exactive mass spectrometer (Thermo Scientific) (68, 69). Data analysis was performed using ProLuCID and DTASelect2 implemented in Integrated Proteomics Pipeline IP2 (Integrated Proteomics Applications) (70–72). Database searching was performed using a FASTA protein database containing *T. gondii* GT1-translated open reading frames downloaded from ToxoDB on February 23, 2016. Protein and peptide identifications were filtered using DTASelect and required a minimum of two unique peptides per protein and a peptide-level false positive rate of less than 5% as estimated by a decoy database strategy. Candidates were ranked by normalized spectral abundance factor values comparing $AC9^{BioID}$ versus control samples (73).

Transmission Electron Microscopy. To prepare parasite ghosts for TEM, parasites were first incubated with 20 μM calcium ionophore in Hank's buffered saline solution at 37 °C for 10 min. The parasite suspension was allowed to adhere to a grid, after which membranes were extracted by addition of 0.5% Triton X-100 for 3 to 4 min. The samples were then stained with 2% phosphotungstic acid (pH 7.4). All TEM images were acquired on a Tecnai G2 Spirit transmission electron microscope (FEI) equipped with an LaB_6 source at 120 kV.

Protein Expression and Purification. Unless otherwise noted, proteins were expressed as N-terminal fusions to His_6-SUMO. All proteins were expressed in Rosetta2 (DE3) bacteria overnight at 16 °C after induction with 300 mM isopropyl β-D-1-thiogalactopyranoside. TgERK7 for crystallography and binding was coexpressed with λ-phosphatase. For His_6-tagged proteins, cells were resuspended in 50 mM Tris (pH 8.6), 500 mM NaCl, 15 mM imidazole and lysed by sonication. His_6-tagged protein was affinity-purified using Ni-NTA resin (Qiagen), which was washed with binding buffer. Protein was eluted in 20 mM Tris (pH 8.6), 100 mM NaCl, 150 mM imidazole. $ERK7_{2–358}$ and AC9 constructs were further purified as follows. Protein was diluted 1:1 with 20 mM Tris (pH 8.6) and purified by anion exchange on a HiTrap Q column. The resulting peaks were pooled and incubated with ULP1 protease for 30 min, after which they were diluted 1:1 in water and the cleaved SUMO was separated from the protein of interest by anion exchange. The flow-through was concentrated and purified by size-exclusion chromatography and flash-frozen in 10 mM Hepes (pH 7.0), 300 mM NaCl for storage. GST and GST-ERK7 kinase domain (residues 2 to 358) were affinity-purified using glutathione Sepharose (GE) and eluted with 10 mM glutathione, which was removed by dialysis in storage buffer before concentration and flash freezing.

GST Pull Downs. Purified GST and GST-$ERK7_{2–358}$ were bound to glutathione Sepharose (GE) in 10 mM Hepes (pH 7.0), 300 mM NaCl, 10 mM DTT. Equimolar amounts of purified SUMO fusions of $AC9_{401–452}$, $AC9_{401–430}$, or $AC9_{431–452}$ (with an additional disordered linker composed of $AC9_{401–405}$) were incubated with the glutathione resin for 5 to 10 min and washed four times in binding buffer. The bound protein was removed by boiling in 1× SDS sample buffer, separated by SDS/PAGE, and detected by Western blot analysis with mouse anti-His_6 (Sigma).

Fluorescence Polarization. $AC9_{419–452}$ with an additional N-terminal Cys was purified as above, and allowed to react overnight with fluorescein-5-maleimide (Molecular Probes). Free fluorescein was removed by sequential buffer exchange with an ND-10 desalting column and then by a 3-kDa molecular mass cutoff centrifugal concentrator. Binding affinity was measured by serially diluting $ERK7_{2–358}$ against 10 nM fluorescein-AC9 in 20-μL volumes in a 384-well plate, and fluorescence polarization was measured in a BioTek Synergy plate reader. MEK2 binding was conducted in the same manner by titrating ERK7 against 100 nM fluorescein-labeled synthetic $MEK2_{4–16}$ peptide (gift from Melanie Cobb, University of Texas (UT) Southwestern, Dallas, TX). Competition experiments were conducted by titrating unlabeled AC9 constructs against 10 nM fluorescein-AC9 and 100 nM ERK7. All curves were globally fit in GraphPad Prism (to single-site binding or single-site inhibition, as appropriate) from biological triplicates of independent experiments composed of triplicate samples; 95% CIs for all fit affinities are indicated in the figure legends.

Protein Crystallization. A 1:1 $ERK7_{2–358}$:$AC9_{419–452}$ complex at 9 mg/mL total protein with 10 mM $MgCl_2$, 1 mM ADP, 10 mM DTT was mixed 1:1 in a sitting drop with 0.15 M DL-malic acid (pH 7.0), 20% polyethylene glycol 3350. Crystals were flash-frozen in a cryoprotectant of reservoir with 25% ethylene glycol.

Data Collection, Structure Determination, and Refinement. The diffraction data were collected at the UT Southwestern Structural Biology core with the Rigaku MicroMax-003 high-brilliancy CuK-α X-ray generator, equipped with a Rigaku HyPix direct photon detector, and processed using the CrysAlisPro software package. A model of *Toxoplasma* ERK7 was created in Modeler v9.14 (74) using Protein Data Bank (PDB) ID code 3OZ6 and used as a search model for molecular replacement in Phaser (75). Cycles of manual rebuilding in Coot (76) and refinement in PHENIX (77) led to a final 2.1-Å structure of the ERK7–AC9 complex (PDB ID code 6V6A). The structure was evaluated with MolProbity (78).

In Vitro Kinase Assays. The kinase assays comparing the specificity of AC9 inhibition were run using 1 μM indicated kinases, 5 mM $MgCl_2$, 200 μM cold ATP, 10 mM DTT, 1 mg/mL BSA, 300 mM NaCl, 20 mM Hepes (pH 7.0), 10% glycerol. TgERK7, rat ERK7, and TgMAPK2 were bacterially expressed as His_6-SUMO fusions and purified without phosphatase treatment. The coding sequence for rat ERK7 was a gift of Marsha Rosner, University of Chicago, Chicago, IL. Activated rat ERK2 was a gift of Melanie Cobb. Reactions were started by adding a hot ATP mix that contained 10 μCi [γ-^{32}P]ATP and 5 μg MBP. The 25-μL reactions were incubated at a 30 °C water bath for 30 min. Reactions were stopped by adding 9 μL 4× SDS buffer; 20-μL samples were then run on an SDS/polyacrylamide gel. The gels were Coomassie-stained, and the MBP band was excised and radioactivity was quantified using a scintillation counter. Recombinant ELK1 and $ELK1_{MEK2\text{-}D}$ were expressed as His_6-SUMO fusions and purified according to the same protocol as AC9. Competition assays were performed as above, with 200 nM TgERK7, 100 μM cold ATP, 10 μM either MBP or $ELK1_{MEK2}$ substrates, and varying concentrations of $AC9_{401–452}$. These assays were imaged by phosphorimager (FujiFilm; FLA-5100) and quantified using the ImageJ gel quantification tool (79).

Figure Generation. Data plotting and statistical analyses were conducted in GraphPad Prism v8.3. All error bars are mean-centered SD. All figures were created in Inkscape v0.92.

Data Availability. All data used in the study are included in the paper and Datasets S1 and S2 and the crystal structure of the ERK7–AC9 complex has been deposited in the PDB (ID code 6V6A). All plasmids and parasite strains developed in this study will be made available upon request.

ACKNOWLEDGMENTS. We thank Betsy Goldsmith and Melanie Cobb for guiding discussions; Vasant Muralidharan, Vinnie Taggliabracci, and Ben Weaver for helpful comments on the manuscript; the UT Southwestern Electron Microscopy core facility for assistance with data collection; and Zhe Chen and the UT Southwestern Structural Biology Lab for assistance with data collection and processing. X-ray data were collected on shared equipment funded by NIH Grant S10 OD025018. M.L.R. acknowledges funding from the Welch Foundation (I-1936-20170325) and National Science Foundation (MCB1553334). X.H. was funded, in part, by Cancer Prevention and Research Institute of Texas Training Grant RP160157. P.J.B. acknowledges funding from the NIH (National Institute of Allergy and Infectious Diseases R01 AI123360) and J.A.W. acknowledges NIH R01 GM089778. P.S.B. was funded by Ruth L. Kirschstein National Research Service Award GM007185.

1. J. F. Reiter, M. R. Leroux, Genes and molecular pathways underpinning ciliopathies. *Nat. Rev. Mol. Cell Biol.* **18**, 533–547 (2017).
2. H. Ishikawa, W. F. Marshall, Intraflagellar transport and ciliary dynamics. *Cold Spring Harb. Perspect. Biol.* **9**, a021998 (2017).
3. S. Werner, A. Pimenta-Marques, M. Bettencourt-Dias, Maintaining centrosomes and cilia. *J. Cell Sci.* **130**, 3789–3800 (2017).
4. J. C. de Leon *et al*., A SAS-6-like protein suggests that the *Toxoplasma* conoid complex evolved from flagellar components. *Eukaryot. Cell* **12**, 1009–1019 (2013).
5. R. J. Wall *et al*., SAS6-like protein in *Plasmodium* indicates that conoid-associated apical complex proteins persist in invasive stages within the mosquito vector. *Sci. Rep.* **6**, 28604 (2016).
6. M. E. Francia, J.-F. Dubremetz, N. S. Morrissette, Basal body structure and composition in the apicomplexans *Toxoplasma* and *Plasmodium*. *Cilia* **5**, 3 (2016).
7. M. E. Francia *et al*., Cell division in apicomplexan parasites is organized by a homolog of the striated rootlet fiber of algal flagella. *PLoS Biol.* **10**, e1001444 (2012).
8. K. Hu, D. S. Roos, J. M. Murray, A novel polymer of tubulin forms the conoid of *Toxoplasma gondii*. *J. Cell Biol.* **156**, 1039–1050 (2002).
9. M. G. Del Carmen, M. Mondragón, S. González, R. Mondragón, Induction and regulation of conoid extrusion in *Toxoplasma gondii*. *Cell. Microbiol.* **11**, 967–982 (2009).
10. A. Keeley, D. Soldati, The glideosome: A molecular machine powering motility and host-cell invasion by Apicomplexa. *Trends Cell Biol.* **14**, 528–532 (2004).
11. J. R. Beck *et al*., A novel family of *Toxoplasma* IMC proteins displays a hierarchical organization and functions in coordinating parasite division. *PLoS Pathog.* **6**, e1001094 (2010).
12. A. L. Chen *et al*., Novel components of the *Toxoplasma* inner membrane complex revealed by BioID. *MBio* **6**, e02357-14 (2015).
13. A. Hunt *et al*., Differential requirements for cyclase-associated protein (CAP) in actin-dependent processes of *Toxoplasma gondii*. *eLife* **8**, e50598 (2019).
14. K. Frénal *et al*., Functional dissection of the apicomplexan glideosome molecular architecture. *Cell Host Microbe* **8**, 343–357 (2010).
15. K. Miyatake, M. Kusakabe, C. Takahashi, E. Nishida, ERK7 regulates ciliogenesis by phosphorylating the actin regulator CapZIP in cooperation with Dishevelled. *Nat. Commun.* **6**, 6666 (2015).
16. A. Kazatskaya *et al*., Primary cilium formation and ciliary protein trafficking is regulated by the atypical MAP kinase MAPK15 in *Caenorhabditis elegans* and human cells. *Genetics* **207**, 1423–1440 (2017).
17. W. J. O'Shaughnessy, X. Hu, T. Beraki, M. McDougal, M. L. Reese, Loss of a conserved MAPK causes catastrophic failure in assembly of a specialized cilium-like structure in *Toxoplasma gondii*. *Mol. Biol. Cell* **31**, 881–888 (2020).
18. M. K. Abe *et al*., ERK7 is an autoactivated member of the MAPK family. *J. Biol. Chem.* **276**, 21272–21279 (2001).
19. A. L. Chen *et al*., Novel insights into the composition and function of the *Toxoplasma* IMC sutures. *Cell. Microbiol.* **19**, cmi.12678 (2017).
20. K. Nishimura, T. Fukagawa, H. Takisawa, T. Kakimoto, M. Kanemaki, An auxin-based degron system for the rapid depletion of proteins in nonplant cells. *Nat. Methods* **6**, 917–922 (2009).
21. K. M. Brown, S. Long, L. D. Sibley, Plasma membrane association by N-acylation governs PKG function in *Toxoplasma gondii*. *MBio* **8**, e00375-17 (2017).
22. B. F. C. Kafsack *et al*., Rapid membrane disruption by a perforin-like protein facilitates parasite exit from host cells. *Science* **323**, 530–533 (2009).
23. V. B. Carruthers, L. D. Sibley, Mobilization of intracellular calcium stimulates microneme discharge in *Toxoplasma gondii*. *Mol. Microbiol.* **31**, 421–428 (1999).
24. P. Sharma, C. E. Chitnis, Key molecular events during host cell invasion by apicomplexan pathogens. *Curr. Opin. Microbiol.* **16**, 432–437 (2013).
25. N. J. Katris *et al*., The apical complex provides a regulated gateway for secretion of invasion factors in *Toxoplasma*. *PLoS Pathog.* **10**, e1004074 (2014).
26. E. Nagayasu, Y.-C. Hwang, J. Liu, J. M. Murray, K. Hu, Loss of a doublecortin (DCX)-domain protein causes structural defects in a tubulin-based organelle of *Toxoplasma gondii* and impairs host-cell invasion. *Mol. Biol. Cell* **28**, 411–428 (2017).
27. S. Long *et al*., Calmodulin-like proteins localized to the conoid regulate motility and cell invasion by *Toxoplasma gondii*. *PLoS Pathog.* **13**, e1006379 (2017).
28. S. Long, B. Anthony, L. L. Drewry, L. D. Sibley, A conserved ankyrin repeat-containing protein regulates conoid stability, motility and cell invasion in *Toxoplasma gondii*. *Nat. Commun.* **8**, 2236 (2017).
29. K. Hu *et al*., Cytoskeletal components of an invasion machine—The apical complex of *Toxoplasma gondii*. *PLoS Pathog.* **2**, e13 (2006).
30. S. Li, X. Prasanna, V. T. Salo, I. Vattulainen, E. Ikonen, An efficient auxin-inducible degron system with low basal degradation in human cells. *Nat. Methods* **16**, 866–869 (2019).
31. K. M. Sathyan *et al*., An improved auxin-inducible degron system preserves native protein levels and enables rapid and specific protein depletion. *Genes Dev.* **33**, 1441–1455 (2019).
32. K. J. Roux, D. I. Kim, B. Burke, BioID: A screen for protein-protein interactions. *Curr. Protoc. Protein Sci.* **74**, 19.23.1-19.23.14 (2013).
33. O. Söderberg *et al*., Direct observation of individual endogenous protein complexes in situ by proximity ligation. *Nat. Methods* **3**, 995–1000 (2006).
34. M. K. Abe *et al*., ERK8, a new member of the mitogen-activated protein kinase family. *J. Biol. Chem.* **277**, 16733–16743 (2002).
35. D. Sang *et al*., Ancestral reconstruction reveals mechanisms of ERK regulatory evolution. *eLife* **8**, e38805 (2019).
36. T. Tanoue, M. Adachi, T. Moriguchi, E. Nishida, A conserved docking motif in MAP kinases common to substrates, activators and regulators. *Nat. Cell Biol.* **2**, 110–116 (2000).
37. W. Peti, R. Page, Molecular basis of MAP kinase regulation. *Protein Sci.* **22**, 1698–1710 (2013).
38. H. Enslen, R. J. Davis, Regulation of MAP kinases by docking domains. *Biol. Cell* **93**, 5–14 (2001).
39. Á. Garai *et al*., Specificity of linear motifs that bind to a common mitogen-activated protein kinase docking groove. *Sci. Signal.* **5**, ra74 (2012).
40. M. Treeck, J. L. Sanders, J. E. Elias, J. C. Boothroyd, The phosphoproteomes of *Plasmodium falciparum* and *Toxoplasma gondii* reveal unusual adaptations within and beyond the parasites' boundaries. *Cell Host Microbe* **10**, 410–419 (2011).
41. P. D. Mace *et al*., Structure of ERK2 bound to PEA-15 reveals a mechanism for rapid release of activated MAPK. *Nat. Commun.* **4**, 1681 (2013).
42. C. I. Chang, B. E. Xu, R. Akella, M. H. Cobb, E. J. Goldsmith, Crystal structures of MAP kinase p38 complexed to the docking sites on its nuclear substrate MEF2A and activator MKK3b. *Mol. Cell* **9**, 1241–1249 (2002).
43. G. Gógl, I. Törő, A. Reményi, Protein-peptide complex crystallization: A case study on the ERK2 mitogen-activated protein kinase. *Acta Crystallogr. D Biol. Crystallogr.* **69**, 486–489 (2013).
44. E. Pellegrini *et al*., Structural basis for the subversion of MAP kinase signaling by an intrinsically disordered parasite secreted agonist. *Structure* **25**, 16–26 (2017).
45. P. Nioche *et al*., Crystal structures of the SH2 domain of Grb2: Highlight on the binding of a new high-affinity inhibitor. *J. Mol. Biol.* **315**, 1167–1177 (2002).
46. K. Ogura *et al*., Solution structure of the SH2 domain of Grb2 complexed with the Shc-derived phosphotyrosine-containing peptide. *J. Mol. Biol.* **289**, 439–445 (1999).
47. J. Hu, S. R. Hubbard, Structural characterization of a novel Cbl phosphotyrosine recognition motif in the APS family of adapter proteins. *J. Biol. Chem.* **280**, 18943–18949 (2005).
48. A. J. Bardwell, M. Abdollahi, L. Bardwell, Docking sites on mitogen-activated protein kinase (MAPK) kinases, MAPK phosphatases and the Elk-1 transcription factor compete for MAPK binding and are crucial for enzymic activity. *Biochem. J.* **370**, 1077–1085 (2003).
49. C. A. Taylor IV *et al*., Functional divergence caused by mutations in an energetic hotspot in ERK2. *Proc. Natl. Acad. Sci. U.S.A.* **116**, 15514–15523 (2019).
50. S. H. Yang, P. R. Yates, A. J. Whitmarsh, R. J. Davis, A. D. Sharrocks, The Elk-1 ETS-domain transcription factor contains a mitogen-activated protein kinase targeting motif. *Mol. Cell. Biol.* **18**, 710–720 (1998).
51. G. Manning, D. B. Whyte, R. Martinez, T. Hunter, S. Sudarsanam, The protein kinase complement of the human genome. *Science* **298**, 1912–1934 (2002).
52. C. J. Sherr, J. M. Roberts, CDK inhibitors: Positive and negative regulators of G1-phase progression. *Genes Dev.* **13**, 1501–1512 (1999).
53. A. A. Russo, P. D. Jeffrey, A. K. Patten, J. Massagué, N. P. Pavletich, Crystal structure of the p27Kip1 cyclin-dependent-kinase inhibitor bound to the cyclin A-Cdk2 complex. *Nature* **382**, 325–331 (1996).
54. M. Pagano *et al*., Role of the ubiquitin-proteasome pathway in regulating abundance of the cyclin-dependent kinase inhibitor p27. *Science* **269**, 682–685 (1995).
55. F. Sievers *et al*., Fast, scalable generation of high-quality protein multiple sequence alignments using Clustal Omega. *Mol. Syst. Biol.* **7**, 539 (2011).
56. G. E. Crooks, G. Hon, J.-M. Chandonia, S. E. Brenner, WebLogo: A sequence logo generator. *Genome Res.* **14**, 1188–1190 (2004).
57. P. Bastin, Z. Bagherzadeh, K. R. Matthews, K. Gull, A novel epitope tag system to study protein targeting and organelle biogenesis in *Trypanosoma brucei*. *Mol. Biochem. Parasitol.* **77**, 235–239 (1996).
58. G. I. Evan, G. K. Lewis, G. Ramsay, J. M. Bishop, Isolation of monoclonal antibodies specific for human c-myc proto-oncogene product. *Mol. Cell. Biol.* **5**, 3610–3616 (1985).
59. J. L. Burg, D. Perelman, L. H. Kasper, P. L. Ware, J. C. Boothroyd, Molecular analysis of the gene encoding the major surface antigen of *Toxoplasma gondii*. *J. Immunol.* **141**, 3584–3591 (1988).
60. J. R. Beck *et al*., A *Toxoplasma* palmitoyl acyl transferase and the palmitoylated Armadillo repeat protein TgARO govern apical rhoptry tethering and reveal a critical role for the rhoptries in host cell invasion but not egress. *PLoS Pathog.* **9**, e1003162 (2013).

61. S. M. Nadipuram *et al*., In vivo biotinylation of the *Toxoplasma* parasitophorous vacuole reveals novel dense granule proteins important for parasite growth and pathogenesis. *MBio* **7**, e00808-16 (2016).
62. M. J. Wichroski, J. A. Melton, C. G. Donahue, R. K. Tweten, G. E. Ward, *Clostridium septicum* alpha-toxin is active against the parasitic protozoan *Toxoplasma gondii* and targets members of the SAG family of glycosylphosphatidylinositol-anchored surface proteins. *Infect. Immun.* **70**, 4353–4361 (2002).
63. T. Beraki *et al*., Divergent kinase regulates membrane ultrastructure of the *Toxoplasma* parasitophorous vacuole. *Proc. Natl. Acad. Sci. U.S.A.* **116**, 6361–6370 (2019).
64. T. Endo, K. Yagita, Effect of extracellular ions on motility and cell entry in *Toxoplasma gondii*. *J. Protozool.* **37**, 133–138 (1990).
65. C. P. Choi *et al*., A photoactivatable crosslinking system reveals protein interactions in the *Toxoplasma gondii* inner membrane complex. *PLoS Biol.* **17**, e3000475 (2019).
66. P. Kaiser, J. Wohlschlegel, Identification of ubiquitination sites and determination of ubiquitin-chain architectures by mass spectrometry. *Methods Enzymol.* **399**, 266–277 (2005).
67. J. A. Wohlschlegel, Identification of SUMO-conjugated proteins and their SUMO attachment sites using proteomic mass spectrometry. *Methods Mol. Biol.* **497**, 33–49 (2009).
68. A. Michalski *et al*., Mass spectrometry-based proteomics using Q Exactive, a high-performance benchtop quadrupole Orbitrap mass spectrometer. *Mol. Cell. Proteomics* **10**, M111.011015 (2011).
69. C. D. Kelstrup, C. Young, R. Lavallee, M. L. Nielsen, J. V. Olsen, Optimized fast and sensitive acquisition methods for shotgun proteomics on a quadrupole Orbitrap mass spectrometer. *J. Proteome Res.* **11**, 3487–3497 (2012).
70. D. L. Tabb, W. H. McDonald, J. R. Yates III, DTASelect and contrast: Tools for assembling and comparing protein identifications from shotgun proteomics. *J. Proteome Res.* **1**, 21–26 (2002).
71. T. Xu *et al*., ProLuCID: An improved SEQUEST-like algorithm with enhanced sensitivity and specificity. *J. Proteomics* **129**, 16–24 (2015).
72. D. Cociorva, D. L. Tabb, J. R. Yates, Validation of tandem mass spectrometry database search results using DTASelect. *Curr. Protoc. Bioinformatics*, chap. 13, unit 13.4 (2007).
73. L. Florens *et al*., Analyzing chromatin remodeling complexes using shotgun proteomics and normalized spectral abundance factors. *Methods* **40**, 303–311 (2006).
74. A. Sali, T. L. Blundell, Comparative protein modelling by satisfaction of spatial restraints. *J. Mol. Biol.* **234**, 779–815 (1993).
75. A. J. McCoy *et al*., Phaser crystallographic software. *J. Appl. Crystallogr.* **40**, 658–674 (2007).
76. P. Emsley, B. Lohkamp, W. G. Scott, K. Cowtan, Features and development of Coot. *Acta Crystallogr. D Biol. Crystallogr.* **66**, 486–501 (2010).
77. P. D. Adams *et al*., PHENIX: A comprehensive Python-based system for macromolecular structure solution. *Acta Crystallogr. D Biol. Crystallogr.* **66**, 213–221 (2010).
78. V. B. Chen *et al*., MolProbity: All-atom structure validation for macromolecular crystallography. *Acta Crystallogr. D Biol. Crystallogr.* **66**, 12–21 (2010).
79. J. Schindelin *et al*., Fiji: An open-source platform for biological-image analysis. *Nat. Methods* **9**, 676–682 (2012).

Supplemental Figures

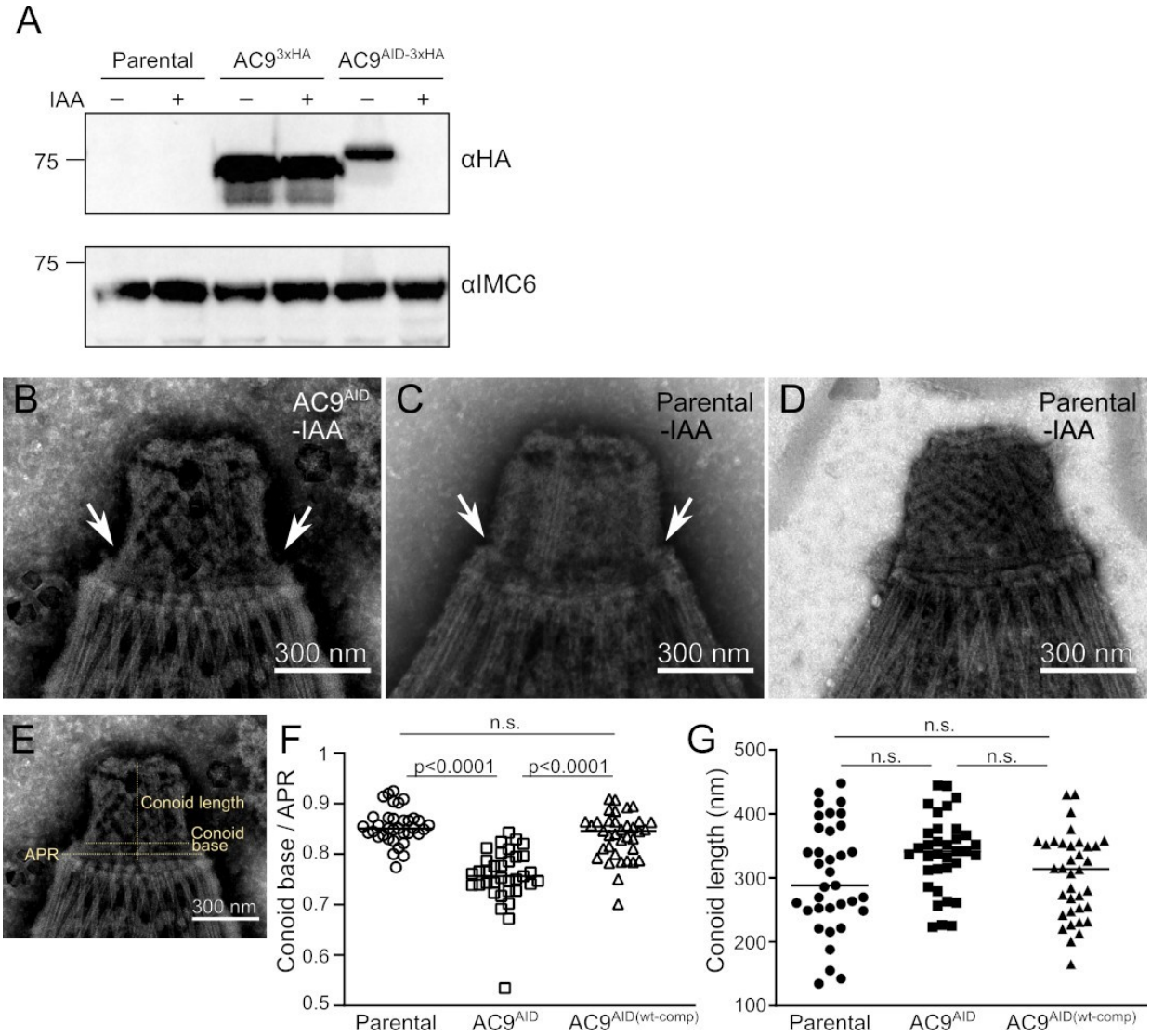

Figure S1. (A) IAA-independent reduction in AC9 protein levels upon AID tagging. Lysates from equal numbers of extracellular parasites of the indicated strains were separated by SDS-PAGE and probed with either anti-HA or anti-IMC6 (loading control). Quantification of band intensities indicates AC9$^{AID\text{-}3xHA}$ levels are 39% of AC9^{3xHA} even when grown without IAA. Western blot also verifies undetectable levels of AC9 after overnight grown in IAA. (B) AC9^{AID} tagging (in the absence of IAA) exacerbates an ultrastructural artifact in TEM sample preparation (arrows) where conoid base slightly detaches from apical polar ring (APR). Note that similar preparations of parental parasites exhibit a similar phenotype (C), though most show stable conoids (D). This observation led us to quantify n=35 conoid TEMs from 2 independent sample preparations for each strain using the rubric in (E); note image is identical to (B). (F) There is a slight, but significant reduction in the ratio of the width of the conoid base over the APR width in AC^{AID} parasites as compared with parental and rescue strains. (G) We observed no significant difference in conoid extension lengths between the three strains. Significance estimated by 1-way ANOVA with Tukey's test.

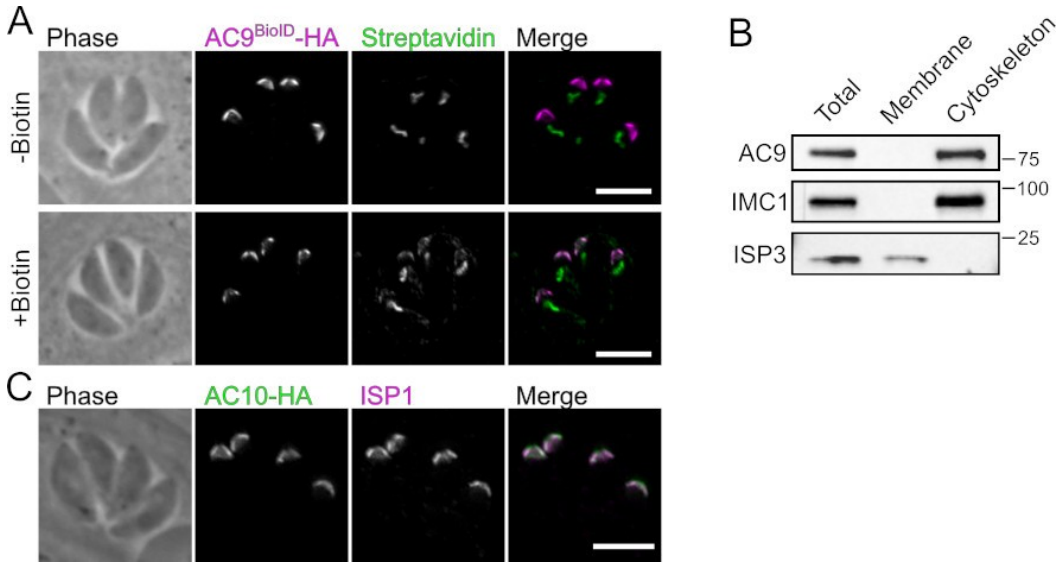

Figure S2. Preparation of apical cap cytoskeleton for BioID. (A) AC9^{BioID}-3xHA (magenta) actively biotinylates proteins at the apical cap when parasites are grown in the presence of 150 µM biotin, as detected by streptavidin staining (green). Note that the parasite apicoplast contains natively biotinylated proteins that are recognized by streptavidin. (B) Cytoskeletal components of the apical cap such as AC9 and IMC1 are enriched by detergent fractionation, while membrane-associated apical cap proteins, such as ISP3, are de-enriched. (C) Of the top hits in our BioID dataset (Supplemental Data 1) was one previously unidentified apical cap protein, TGGT1_292950, which, when endogenously tagged at its C-terminus with 3xHA (green) was verified to localize to the apical cap (ISP1; magenta). All scale bars: 5 µm.

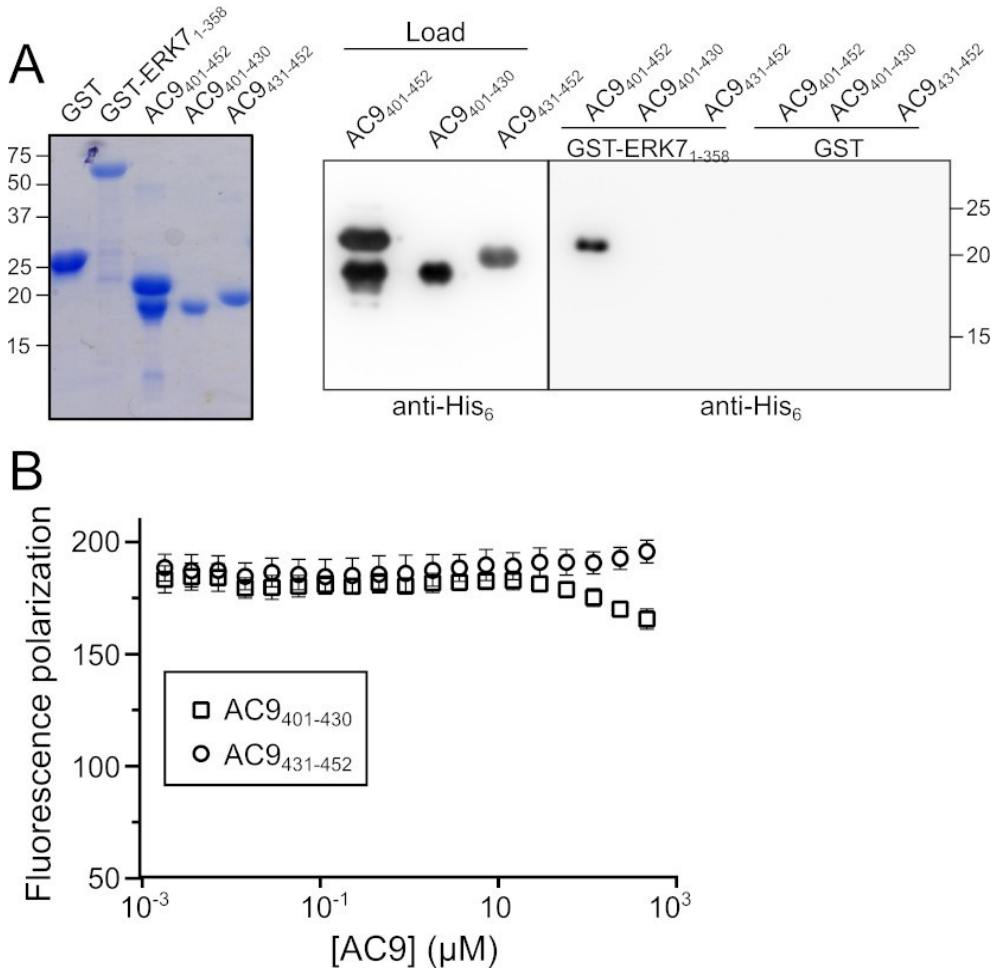

Figure S3. AC9 binds the ERK7 kinase domain. (A) (Left panel) Coomassie stained gel of purified proteins used to test binding. (Right panel) His_6-SUMO fusions of the indicated AC9 fragments were incubated with GST or GST-ERK7 bound to glutathione sepharose resin, washed, and detected by western blot with anti-His_6 antibody. Only $AC9_{401-452}$ showed detectable binding to ERK7. (B) Fluorescence polarization competition in which $AC9_{401-430}$ and $AC9_{431-452}$ were titrated against fluorescein-labeled $AC9_{419-452}$ bound to TgERK7. Note that neither the N-terminal nor C-terminal fragments of the AC9 ERK7-binding region were able to efficiently compete with $AC9_{419-452}$ for binding, indicating the fragments have affinities >1 mM for the kinase.

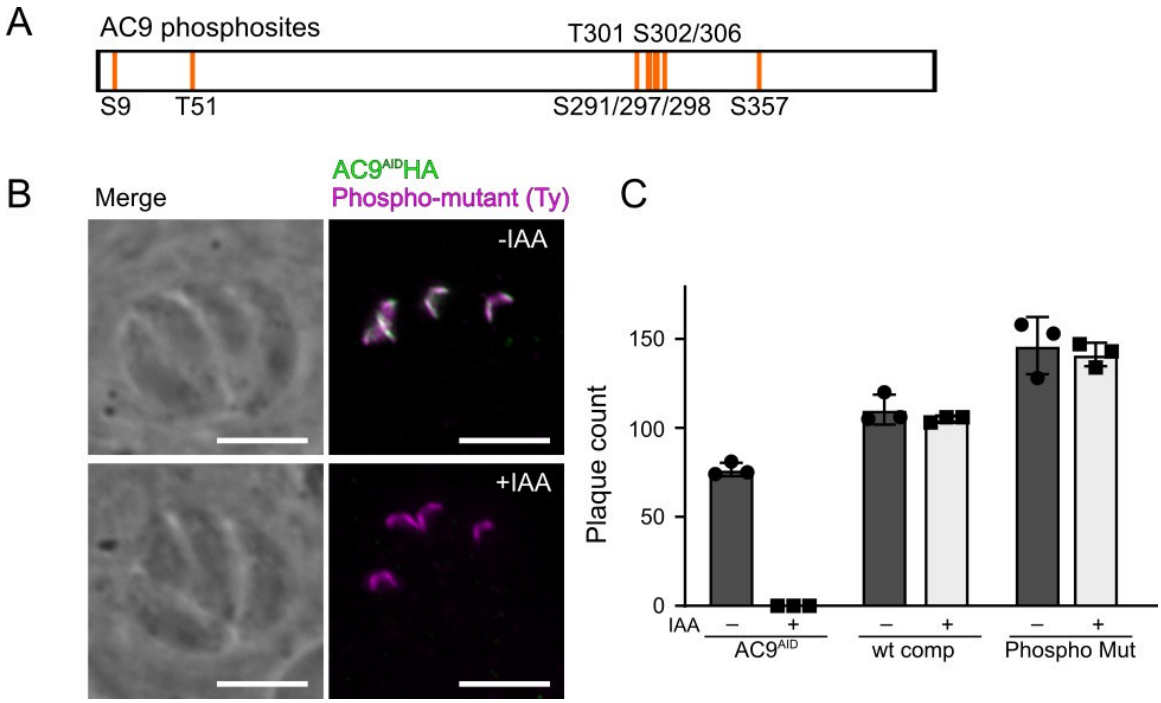

Figure S4. Phosphorylation of AC9 is not required for its function. (A) Location of known phosphorylated Ser/Thr on AC9 that have been mutated to Ala in this study. (B) Phospho-mutant AC9 correctly localizes to the apical cap in the AC9^{AID} background. Scale bars: 5 μm. (C) The phospho-mutant is able to fully rescue plaque formation in the AC9^{AID} background, indistinguishably from complementation with a wild-type copy of AC9.

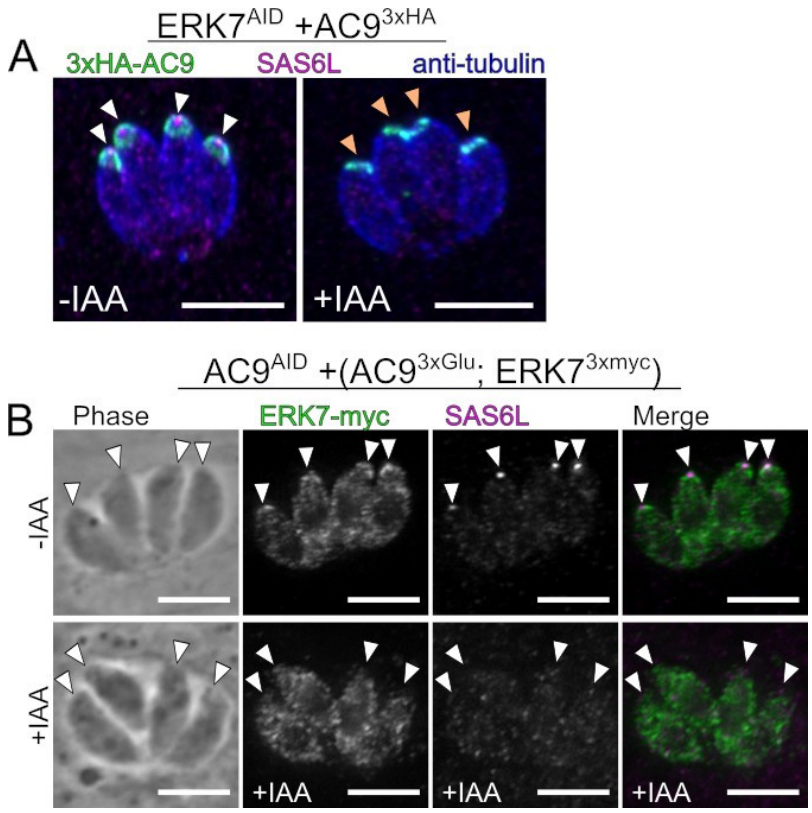

Figure S5. (A) AC9 localization is unaffected by ERK7 degradation. ERK7^{AID}(3xHA-AC9) parasites were grown in the presence or absence of IAA and stained with anti-HA (AC9; green), anti-SAS6L (magenta), and anti-β-tubulin (blue). Note anti-β-tubulin does not stain conoid, likely due to antigen accessibility. Images are maximum intensity projects of confocal stacks. White arrowheads indicate SAS6L-positive conoid puncta. Orange arrowheads indicate expected localization of missing SAS6L puncta in ERK7$^{AID/IAA}$ parasites. (B) AC9^{AID}(+AC9^{3xGlu}; ERK7-3xmyc) parasites were grown in the presence or absence of IAA and stained with anti-myc (ERK7; green) and anti-SAS6L (magenta), a marker for the parasite conoid. Arrows indicate the parasite apical end. Note the bright SAS6L foci in the -IAA parasites that are lost in +IAA. All scale bars: 5 μm.

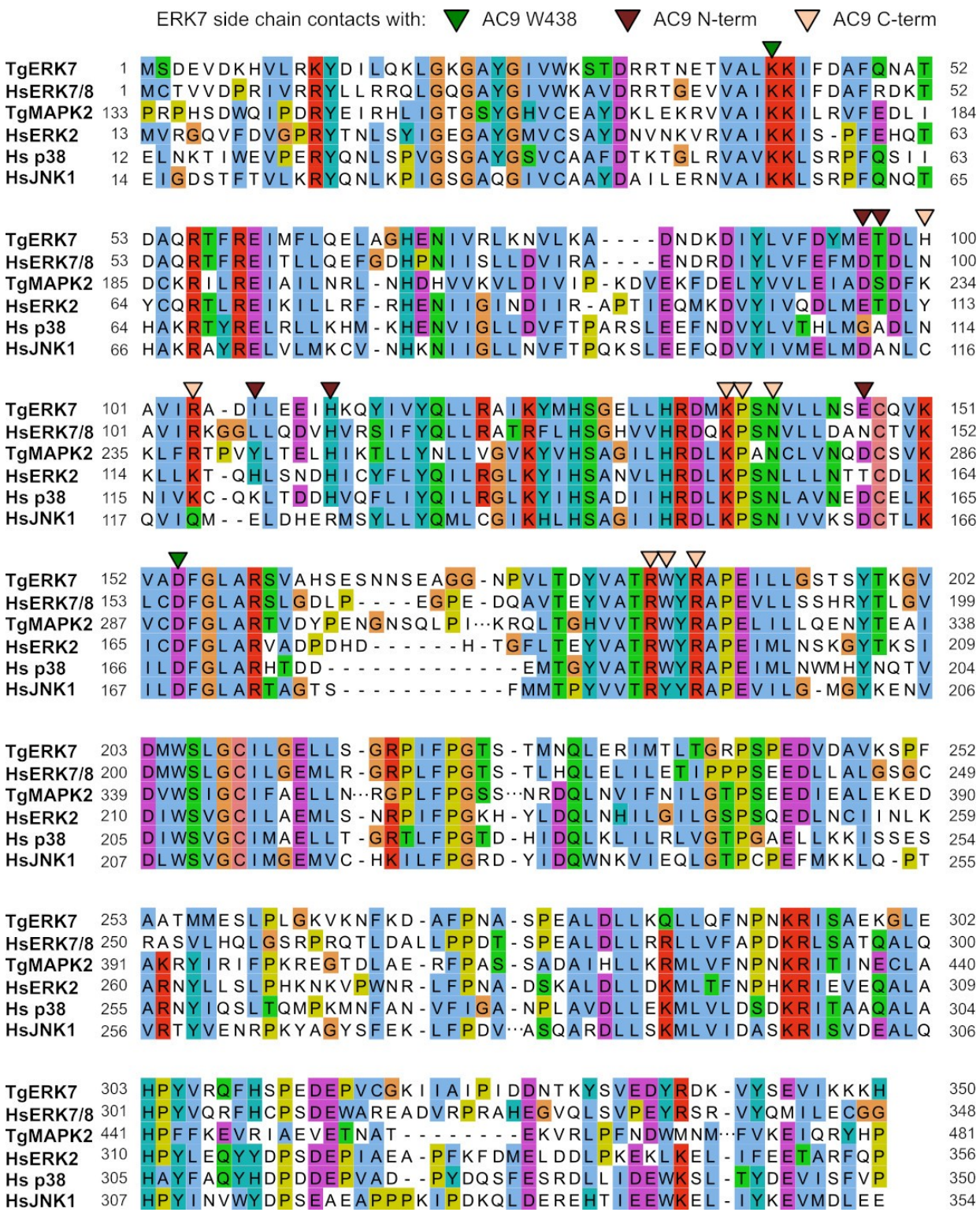

Figure S6. Alignment of TgERK7 and TgMAPK2 kinase domains with human MAPKs. TgERK7 side chains that make contact with AC9$_{419\text{-}452}$ in our crystal structure are marked as indicated. Large gaps were removed from alignment and are indicated with ellipses.

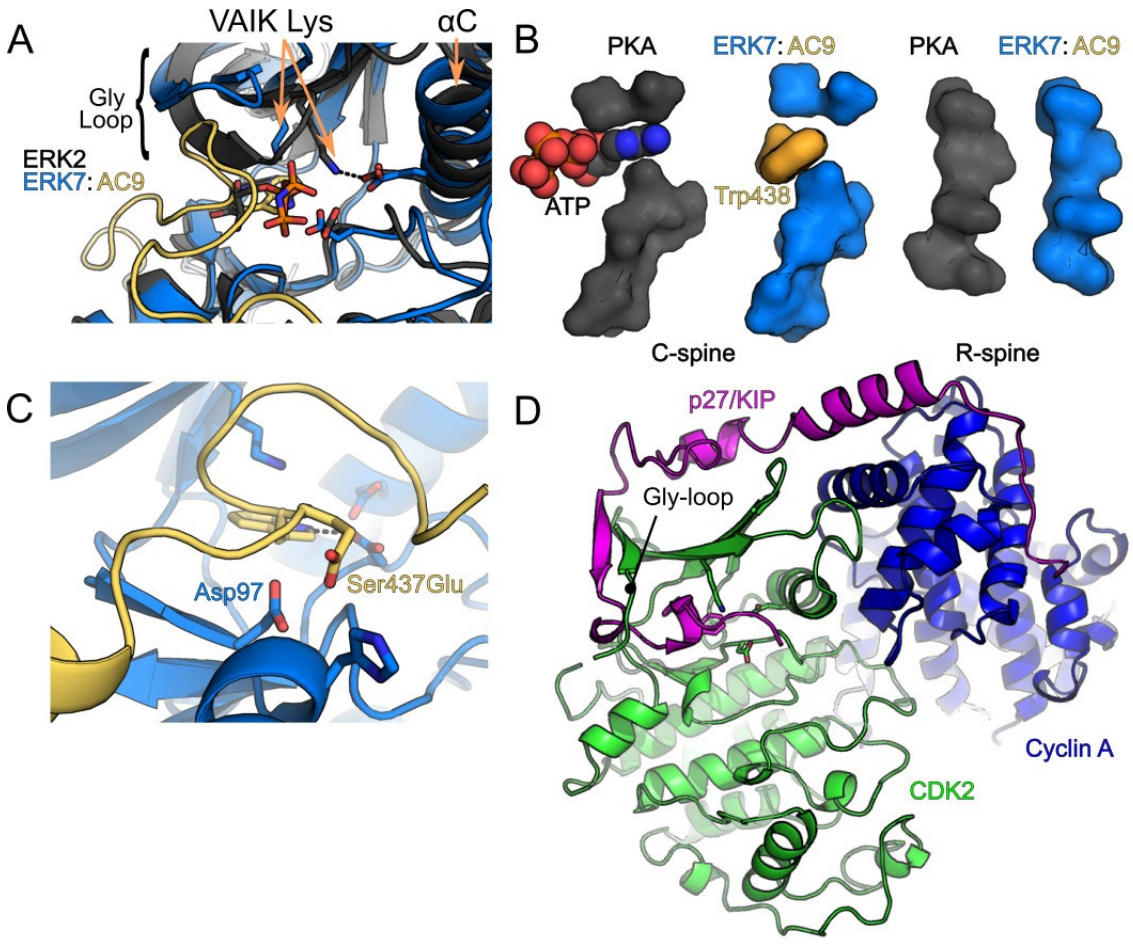

Figure S7. Comparison of ERK7:AC9 with other kinase structures. (A) The structure of activated, AMP-PNP-bound ERK2 (black; 6OPG) is overlaid with ERK7:AC9 (blue and yellow) and the Gly-loop, catalytic lysine, and αC helices are indicated. Note that the ERK7:AC9 Gly-loop is held in an inactive conformation by AC9, which keeps the αC-Glu from salt bridging with the VAIK Lys.(B) The "C-spines" (PKA: V57, A70, M128, L172, L173, I174, L227, M231; TgERK7: V27, A40, L99, V142, L143, L144, I210, L214) and "R-spines" (PKA: L95, L106, Y164, F185; TgERK7: L64, L76, H134, F155) of activated, ATP-bound PKA (black; 1ATP) is shown in comparison to ERK7:AC9 (blue and yellow). While the R-spine is intact, the C-spine is not fully complete by Trp438; ERK7 is not in an active conformation when bound to AC9, as the Gly-loop is in an open conformation, and the VAIK:α-C Glu salt bridge are not formed (see (A) and Figure 5). In addition, AC9 displaces the ERK7 activation loop (see Figure 5D,E). (C) Mutation of AC9 Ser437 to Glu would clash with the side chain of Asp98 (<3.5 Å between the carboxylate side chains) when AC9 is in the optimal conformation for binding ERK7. (D) Overview of the CDK2:p27/KIP:Cyclin inhibitory complex (1JSU). p27 (magenta) wraps around the cyclin A (blue) and CDK2 (green), unfolding the CDK2 Gly-loop and inserting it's C-terminal residues into the active site, replacing nucleotide.

Data collection		Refinement	
Wavelength	1.541	**Reflections used in refinement**	39043 (3083)
Resolution range	29.89 - 2.1 (2.175 - 2.1)	**Reflections used for R-free**	1718 (141)
Space group	P 1	**R-work**	0.1583 (0.1787)
Unit cell	50.8897 52.9379 67.8003 82.55 84.5785 81.35	**R-free**	0.2119 (0.2329)
Total reflections	93549 (4051)	**CC(work)**	0.961 (0.919)
Unique reflections	39049 (3083)	**CC(free)**	0.924 (0.809)
Multiplicity	2.4 (1.3)	**Number of non-hydrogen atoms**	5986
Completeness (%)	96.68 (76.39)	**macromolecules**	5468
Mean I/sigma(I)	15.17 (3.48)	**ligands**	20
Wilson B-factor	17.81	**solvent**	498
R-merge	0.05342 (0.1976)	**Protein residues**	682
R-meas	0.0665 (0.2744)	**RMS(bonds)**	0.004
R-pim	0.03903 (0.1898)	**RMS(angles)**	0.61
CC1/2	0.997 (0.894)	**Ramachandran favored (%)**	98.33
CC*	0.999 (0.972)	**Ramachandran allowed (%)**	1.67
		Ramachandran outliers (%)	0.00
		Rotamer outliers (%)	0.17
		Clashscore	1.45
		Average B-factor	29.43
		macromolecules	29.18
		ligands	44.08
		solvent	31.59
		Number of TLS groups	16

Table S1. Data collection and refinement statistics. Statistics for the highest-resolution shell are shown in parentheses.

Dataset S1. List of top AC9-BioID hits identified by mass spectrometry.
Proteins were ranked by NSAF. Proteins are included in this list if the ratio of the control (RH):AC9 < 0.5. Gene IDs and corresponding descriptions are from ToxoDB.

Gene ID	Rank	AC9 (NSAF)	RH-Control (NSAF)	Description
TGGT1_246950	1	1255.7094	0	AC9 (bait protein)
TGGT1_292950	2	1099.4067	0	AC10 (this study)
TGGT1_229640	3	949.1479	0	AC8
TGGT1_250820	4	840.1329	132.52401	AC2
TGGT1_231640	5	828.4337	387.00963	IMC1
TGGT1_251850	6	792.8808	0	AC6
TGGT1_289750	7	684.42114	274.05682	RPL40
TGGT1_230340	8	578.14675	49.67099	AAP4
TGGT1_214880	9	575.777	0	AC4
TGGT1_312090	10	499.07174	0	RPL23
TGGT1_263520	11	449.1775	167.86957	SPM1
TGGT1_225690	12	420.1986	0	AC7
TGGT1_231630	13	404.61747	104.2871	IMC4
TGGT1_225080	14	404.25975	151.0826	RPS18
TGGT1_231080	15	375.38402	0	RPL38
TGGT1_262690	16	355.29304	165.97807	RPL27
TGGT1_308860	17	347.14413	108.11415	AC3
TGGT1_271930	18	323.4078	151.0826	IMC20
TGGT1_233010	19	309.85456	0	ERK7
TGGT1_239400	20	309.0909	0	IMC28
TGGT1_222220	21	308.70743	82.408695	IMC7
TGGT1_278870	22	303.53635	0	MyoF
TGGT1_219820	23	287.59062	115.15743	Hypothetical protein
TGGT1_236650	24	286.6569	107.1313	DBP2
TGGT1_249250	25	281.53802	0	RPL35A
TGGT1_310440	26	277.97034	0	MORN1
TGGT1_286420B	27	277.48388	0	Hypothetical protein
TGGT1_320030	28	276.74588	109.69562	Localizes to the apical complex (PMID: 29269729)
TGGT1_313790	29	266.1574	0	Hypothetical protein
TGGT1_264430	30	262.99711	0	Hypothetical protein
TGGT1_290920	31	260.86667	24.373202	Hypothetical protein
TGGT1_314820	32	259.16924	0	ATP synthase (ToxoDB)
TGGT1_217890	33	257.4062	0	Hypothetical protein
TGGT1_212260	34	251.53938	0	Hypothetical protein
TGGT1_315510	35	246.7742	0	APR1
TGGT1_231070	36	244.0281	0	IMC basal complex (PMID: 27696623)
TGGT1_359490	37	243.4069	0	Hypothetical protein
TGGT1_280370	38	232.03765	0	Hypothetical protein
TGGT1_311430	39	228.9471	0	Hypothetical protein
TGGT1_236950	40	225.23042	0	Hypothetical protein
TGGT1_294800B	41	223.77733	0	Hypothetical protein
TGGT1_205250	42	216.28626	85.086236	ROP18
TGGT1_230210	43	213.96892	42.087297	IMC10
TGGT1_410360	44	213.77802	0	MAF1
TGGT1_206690	45	207.25427	0	GAPM2B
TGGT1_214575	46	205.64517	0	Hypothetical protein
TGGT1_220270	47	198.85208	79.624617	IMC6
TGGT1_223790	48	188.62766	0	Localizes to the cytoplasm (PMID: 29269729)
TGGT1_227600	49	188.25228	0	RPL34
TGGT1_316340	50	181.66733	0	IMC22

Dataset S2. Oligonucleotides used in this study.

Primers

Name	Description	Sequence (5'-3')
P1	AC9-C-terminal-tagging-HDR_F	GTCGGGGAACCGCGAACCGAGTGAATATCCGCAGGGAATGGGAAGTGGAGGACGGGAATTC
P2	AC9-C-terminal-tagging-HDR_F	CTCGCAGCGTGTCGCACTGAACTCTTGTGCGGAGAGAGCGACGGCCAGTGAATTGTAATA
P3	AC9-tagging-pU6-Universal gRNA_F	AAGTTATGTGTTCCTCAAATGTCAGG
P4	AC9-tagging-pU6-Universal gRNA_R	AAAACCTGACATTTGAGGAACACATA
P5	ERK7-C-terminal-tagging-HDR_F	TTCTCTTTTTTTTCAGTCTGCGTCCAAGACATACAACAGCGGAAGTGGAGGACGGGAATT
P6	ERK7-C-terminal-tagging-HDR_R	GCTTTCTCCACCTTCGCTTTCGGTGGAAGTCTTGCGAGCGACGGCCAGTGAATTGTAATA
P7	ERK7-tagging-pU6-Universal gRNA_F	AAGTTGCAAAAGCAAAGATTCAGACG
P8	ERK7-tagging-pU6-Universal gRNA_R	AAAACGTCTGAATCTTTGCTTTTGCA
P9	AC10-C-terminal-tagging-HDR_F	GCTGTGTCGGTGTCCTCCGTACTGCAATTAAAGGCGAGAGGAAGTGGAGGACGGGAATTC
P10	AC10-C-terminal-tagging-HDR_R	GAGGATATCCCTGCAATCTGACAAACATCACGTTTCGCCGACGGCCAGTGAATTGTAATA
P11	AC10-tagging-pU6-Universal gRNA_F	AAGTTgTAAGGGTGCAAGAGTTGATGG
P12	AC10-tagging-pU6-Universal gRNA_R	AAAACCATCAACTCTTGCACCCTTAcA

Synthetic genes

Name	Description	Sequence (5'-3')
AC9-Glutamate-Mutant	qBlock (Quintara Biosciences) of AC9 C-terminus used to mutate Ser419, Thr420, and Ser437 to glutamates	CGCCGGCGGCAAGTCGCGTGTCAGTTCTGTTGAACTCTGAAGAAATTCGACCTTCTTCGC GACCCACGTCGGCTCCGCACTCCTCGCGATCATGTGCGTCTCAGAATCAATCAGGCATC GCACAGGCGAGCGTGGAGAGCTCCACTTCTCTCTCACAGCAAGTCTGCGGGCAGGCGA GTCGTGAGTCTGCGGAGTCGACGCAGGCGCAGGAAAGGAAATTCGGGGAAGCGGAAAG TGGGCGACTTCTCAACGGGGATGCCGCAGGGGCTCGCGACGGTGCAACTCGAGAACAT GTGGAGAGCGACCACGAGTCTGTGTCGGAGAGGTCCTCGCATAGCAGTCGATCTAGCGA ATCAGAGTTCTTTTCTTCGTCAGCAGGCTCTTCTCCGCGGCTCTCGCTACGAGCTCCACC AGCCAAGgaggagCGACCCAAATTTGTTCCTTGTCTGTCGACTGCAGCTGCAGGTGCGGG TgaaTGGATGTCGGGGAACCGCGAACCGAGTGAATATCCGCAGGGAATGgcggccgc
AC9-N-term-phospho-Mutant	gBlock (IDT) used to mutate the first 2 phosphosites to alanines	agatctATGGACGTCTCCGGTCGAGGCTTTgcgGGTCCTCTCAGAAGCCAGGCGACACGTG CAAGAGCGTCGCAGCTCGTCAGACCTAACACTGGCGCCAGGGTCGCTGCTCTTCGGCC CTTGCCCGACGATTCGGCGAAACCGTCTCCACTCAAGgcgTCACAAATGTCCAAAATAAA TTTTCACCTCGAGGAG
AC9-C-term-phospho-Mutant	gBlock (IDT) used to mutate the remaining 7 phosphosites to alanines	CGCCGGCGGCAAGTCGCGTGTCAGTTCTGTTGAACgcgGAAGAAATTCGACCTgcggcgCG ACCCgcggcgGCTCCGCACgcgTCGCGATCATGTGCGTCTCAGAATCAATCAGGCATCGCA CAGGCGAGCGTGGAGAGCTCCACTTCTCTCTCACAGCAAGTCTGCGGGCAGGCGAGTC GTGAGTCTGCGGAGTCGACGCAGGCGCAGGAAAGGAAATTCGGGGAAGCGGAAgcgGGG CGACTTCTCAACGGGGATGCCGCAGGGGCTCGCGACGGTGCAACTCGAGAACATGTGG AGAGCGACCACGAGTCTGTGTCGGAGAGGTCCTCGCATAGCAGTCGATCTAGCGAATCA GAGTTCTTTTCTTCGTCAGCAGGCTCTTCTCCGCGGCTCTCGCTACGAGCTCCACCAGC CAAGTCCACGCGACCCAAATTTGTTCCTTGTCTGTCGACTGCAGCTGCAGGTGCGGGTT CTTGGATGTCGGGGAACCGCGAACCGAGTGAATATCCGCAGGGAATGgcggccgc

Chapter 3

–

Multivalent interactions drive the *Toxoplasma* AC9:AC10:ERK7 complex to concentrate ERK7 in the apical cap

AMERICAN SOCIETY FOR MICROBIOLOGY | mBio®

RESEARCH ARTICLE

Multivalent Interactions Drive the *Toxoplasma* AC9:AC10:ERK7 Complex To Concentrate ERK7 in the Apical Cap

Peter S. Back,[a] William J. O'Shaughnessy,[b] Andy S. Moon,[c] Pravin S. Dewangan,[b] Michael L. Reese,[b,d] Peter J. Bradley[a,c]

[a]Molecular Biology Institute, University of California, Los Angeles, California, USA
[b]Department of Pharmacology, University of Texas Southwestern Medical Center, Dallas, Texas, USA
[c]Department of Microbiology, Immunology, and Molecular Genetics, University of California, Los Angeles, California, USA
[d]Department of Biochemistry, University of Texas Southwestern Medical Center, Dallas, Texas, USA

Peter S. Back and William J. O'Shaughnessy contributed equally to this work. Author order was determined alphabetically. Peter J. Bradley and Michael L. Reese are co-principal investigators for this work.

ABSTRACT The *Toxoplasma* inner membrane complex (IMC) is a specialized organelle that is crucial for the parasite to establish an intracellular lifestyle and ultimately cause disease. The IMC is composed of both membrane and cytoskeletal components, further delineated into the apical cap, body, and basal subcompartments. The apical cap cytoskeleton was recently demonstrated to govern the stability of the apical complex, which controls parasite motility, invasion, and egress. While this role was determined by individually assessing the apical cap proteins AC9, AC10, and the mitogen-activated protein kinase ERK7, how the three proteins collaborate to stabilize the apical complex is unknown. In this study, we use a combination of deletion analyses and yeast two-hybrid experiments to establish that these proteins form an essential complex in the apical cap. We show that AC10 is a foundational component of the AC9:AC10:ERK7 complex and demonstrate that the interactions among them are critical to maintaining the apical complex. Importantly, we identify multiple independent regions of pairwise interaction between each of the three proteins, suggesting that the AC9:AC10:ERK7 complex is organized by multivalent interactions. Together, these data support a model in which multiple interacting domains enable the oligomerization of the AC9:AC10:ERK7 complex and its assembly into the cytoskeletal IMC, which serves as a structural scaffold that concentrates ERK7 kinase activity in the apical cap.

IMPORTANCE The phylum Apicomplexa consists of obligate, intracellular parasites, including the causative agents of toxoplasmosis, malaria, and cryptosporidiosis. Hallmarks of these parasites are the IMC and the apical complex, both of which are unique structures that are conserved throughout the phylum and required for parasite survival. The apical cap portion of the IMC has previously been shown to stabilize the apical complex. Here, we expand on those studies to determine the precise protein-protein interactions of the apical cap complex that confer this essential function. We describe the multivalent nature of these interactions and show that the resulting protein oligomers likely tether ERK7 in the apical cap. This study represents the first description of the architecture of the apical cap at a molecular level, expanding our understanding of the unique cell biology that drives *Toxoplasma* infections.

KEYWORDS *Toxoplasma gondii*, inner membrane complex, apical complex, protein-protein interactions, multivalent interactions

The phylum Apicomplexa contains a large group of obligate intracellular parasites of medical and veterinary importance (1). Human parasites include *Toxoplasma*

Editor Jon P. Boyle, University of Pittsburgh

Address correspondence to Peter J. Bradley, pbradley@ucla.edu, or Michael L. Reese, michael.reese@utsouthwestern.edu.

The authors declare no conflict of interest.

Received 2 November 2021
Accepted 11 January 2022
Published 8 February 2022

gondii, which causes toxoplasmosis in immunocompromised people and congenitally infected neonates; *Plasmodium* spp., which causes malaria; and *Cryptosporidium* spp., which causes diarrheal disease in children (2–4). Important animal pathogens include *Neospora* spp., *Eimeria* spp., *Theileria* spp., and *Babesia* spp., which together account for enormous economic losses in the poultry and cattle industries (5–7). These apicomplexan parasites require specialized machinery to actively invade their mammalian host cells, establish an intracellular niche, and cause disease. The alveoli are one such structure and are formed from a series of flattened membranous vesicles that underlies the plasma membrane. The alveoli represent a hallmark of the broader superphylum Alveolata that includes ciliates, dinoflagellates, and apicomplexan parasites (8).

In apicomplexans, the alveoli are called the inner membrane complex (IMC). The IMC is a peripheral membrane system with two well-described roles: a platform to anchor the glideosome, the actin-myosin motor complex that interacts with micronemal adhesins secreted onto the parasite surface for gliding motility, and a scaffold for endodyogeny, an internal budding process of replication (9, 10). The IMC is situated between the plasma membrane and cortical microtubules at the periphery of the cell and consists of a series of flattened membrane vesicles and an underlying cytoskeletal network of intermediate filament-like proteins called the alveolins (11, 12). The membrane vesicles are organized into rectangular plates along the body of the parasite, culminating in a single cone-shaped plate at the apex called the apical cap (13, 14). Because both the apical cap and body sections of the IMC are composed of similar membrane and cytoskeletal components, they were previously believed to be one unified structure. However, the discovery of an array of new IMC proteins revealed that the apical cap contains a unique cohort of proteins, suggesting a specialized function for this region (12, 15–19). Recent analyses of a group of these proteins revealed a third IMC function: regulating the biogenesis and stability of the apical complex (20–22).

The apical complex is a group of cytoskeletal structures at the apex of the parasite that includes the microtubule-based conoid, the flanking apical polar ring (APR), and two preconoidal rings (18, 23, 24). The striking basket-shaped ultrastructure of the conoid allowed it to be readily described in the tissue cyst-forming coccidian subgroup of the Apicomplexa (e.g., *Toxoplasma*, *Sarcocystis*, and *Eimeria*). Remarkably, the apical complex, including the conoid, has been described in early-branching alveolates that are not members of the Apicomplexa, suggesting the structure is more ancient than originally appreciated (25, 26). Indeed, while the conoid was originally presumed to be missing from Haemosporidia (1, 27), recent studies have identified a reduced conoid complex in multiple stages of *Plasmodium*, suggesting that this structure is conserved throughout the Apicomplexa (28–30). Moreover, the apical complex contains orthologs of cilium-associated proteins, leading to a potential link between the apical complex of apicomplexan parasites and more typical eukaryotic cilia (28, 31–34). Numerous studies have demonstrated that the apical complex regulates the secretion of specialized organelles called micronemes and rhoptries, which govern parasite motility, attachment, invasion, and egress (35). While the trigger for rhoptry secretion at the apical complex is unknown, calcium signaling cascades have been shown to coordinate both microneme secretion and conoid extrusion, suggesting a connection between the two activities (36). The conoid has also been implicated in initiating motility via several calmodulin-like proteins, the myosin motor protein MyoH, and the essential formin protein FRM1 (37–39). In addition, several APR-localizing proteins were shown to be important in controlling microneme release, indicating that these flanking cytoskeletal structures also contribute to the function of the apical complex (18, 40, 41).

While the molecular composition and function of the apical complex is becoming clearer, how it is formed and maintained is largely a mystery. Recently, three apical cap proteins (AC9, AC10, and ERK7) were identified as essential for the maturation of the apical complex (20–22). Depleting any one of these proteins eliminates the conoid in mature parasites, resulting in a complete block in motility, invasion, and egress. Importantly, AC9 was shown to accomplish this by recruiting the conserved mitogen-

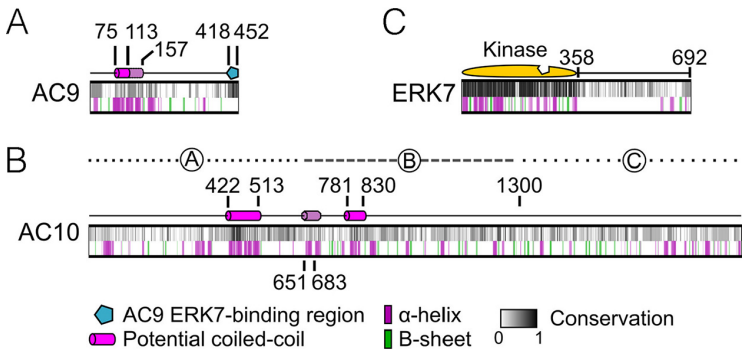

FIG 1 Overview of AC9, AC10, and ERK7 domains. (A) Diagram of AC9 illustrates a predicted coiled-coil (CC) domain (residues 75 to 113), conserved α-helices flanking the CC domain (residues 113 to 157), and the ERK7-binding region (residues 418 to 452). (B) Diagram of AC10 contains two predicted CC domains (CC1, 422 to 513, and CC2, 781 to 830) as well as a short conserved α-helix (651 to 683). Regions A (2 to 650), B (651 to 1300), and C (1301 to 1979) delineate the divisions of AC10 used for yeast two-hybrid (Y2H) assays. (C) Diagram of ERK7 showing the kinase domain (1 to 358) including the active site (notched region) and the C terminus (359 to 692). All three diagrams contain a grayscale representation of the degree of conservation as well as secondary structure predictions, which are depicted by purple and green bars. Conservation calculations are based on multiple-sequence alignments of AC9, AC10, and ERK7 sequences from *T. gondii*, *N. caninum*, *B. besnoitia*, *C. suis*, *E. maxima*, and *E. tenella*.

activated protein (MAP) kinase ERK7 to the apical cap and regulating its kinase activity (22). Thus, it is evident that AC9, AC10, and ERK7 work in conjunction to facilitate the apical complex maturation and function. However, how these proteins interact and coordinate at the apical cap to confer their functions remains unknown. In this study, we explore the organization and mechanism of this essential protein complex. We show that AC10 recruits both AC9 and ERK7 to the apical cap, suggesting it is the anchor for the complex. We combine yeast two-hybrid (Y2H) experiments to examine direct pairwise interactions with deletion analyses in parasites to assess the functional importance of these interactions. Through these experiments, we reveal multiple domains in AC9 and AC10 that are critical for assembling the complex at the apical cap and for the maturation of the conoid. Importantly, we show that these domains mediate independent pairwise interactions between AC9, AC10, and ERK7. Thus, we propose that these multimeric interactions drive the oligomerization of the AC9:AC10:ERK7 complex into the apical cap cytoskeleton, which tethers ERK7 to the site of its essential function in coordinating the proper biogenesis of the apical complex.

RESULTS

AC10 is essential for recruitment of the AC9:AC10:ERK7 complex to the apical cap. While AC9, AC10, and ERK7 were recently shown to be essential for apical complex assembly and stabilization (20–22), the interactions between the three proteins and how they are organized in the apical cap remain poorly understood (an overview of these proteins is shown in Fig. 1). To explore their interactions, we generated parasites with AC10 tagged with an auxin-inducible degron fused to 3×HA, AC9 tagged with 3×Myc, and ERK7 tagged with 3×Ty (triple-tagged: $AC10^{AID\text{-}3\times HA}$/$AC9^{3\times Myc}$/$ERK7^{3\times Ty}$). As shown previously, the $AC10^{AID\text{-}3\times HA}$ fusion protein targets correctly to the apical cap, degrades efficiently upon addition of auxin (IAA), and results in the loss of AC9 from the apical cap (Fig. 2A and B) (21). Our triple-tagged parasites allowed us to additionally demonstrate that $AC10^{AID\text{-}3\times HA}$ knockdown removes ERK7 from the apical cap, although its cytoplasmic staining is retained (Fig. 2B). We used line intensity scans to quantify the levels of ERK7 at the apical cap versus the bulk cytosol, which clearly demonstrated a loss in concentrated apical cap signal upon AC10 knockdown (Fig. S2). Consistent with the AC9 and ERK7 staining patterns, Western blot analyses showed that AC9 is predominantly degraded while ERK7 levels appear to remain stable (Fig. 2C) (21). In agreement with previous studies (21), depletion of AC10 results in the elimination of the conoid (Fig. 2D), which is lethal

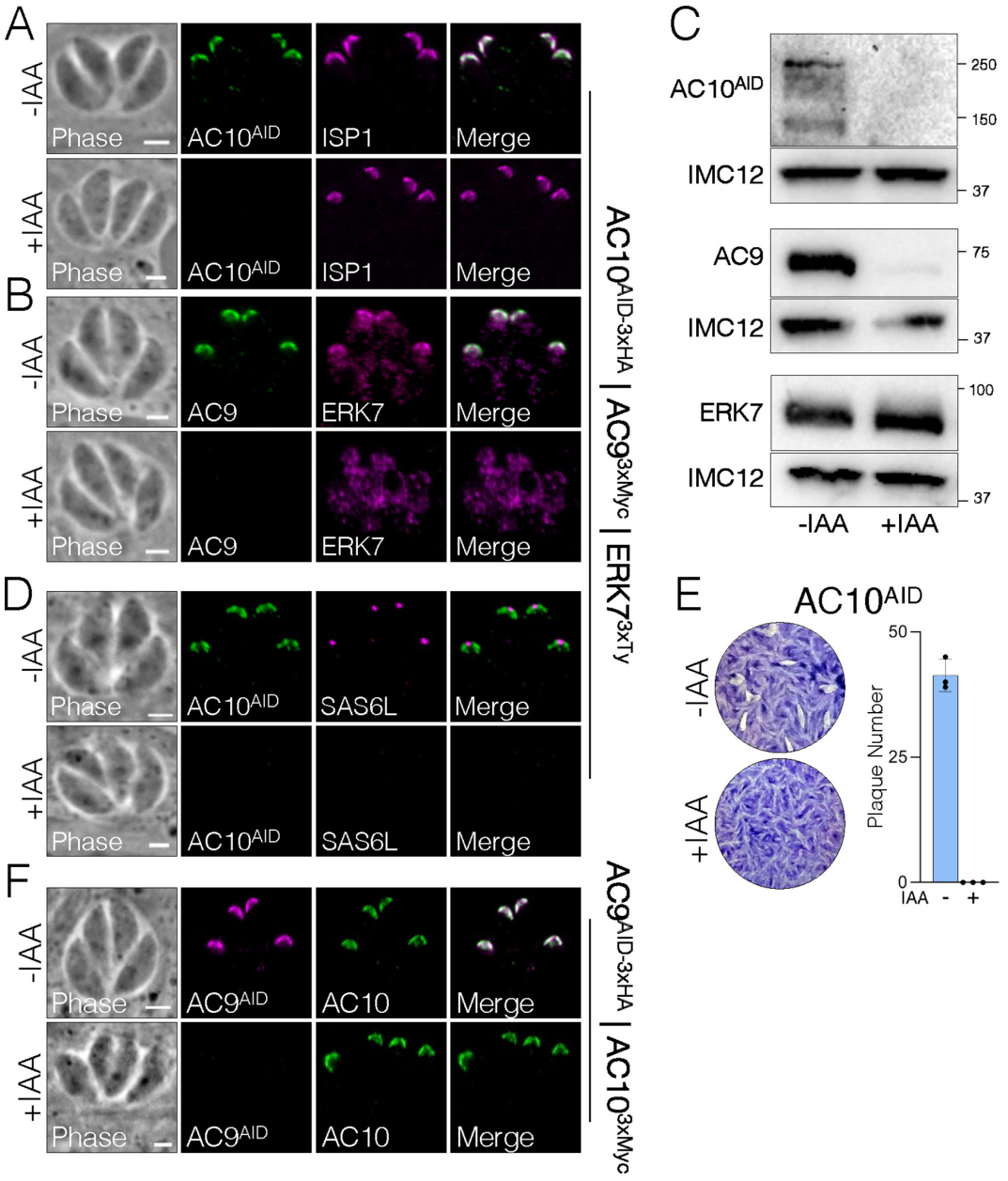

FIG 2 AC10 is an essential component of the apical cap. (A) Immunofluorescence assay (IFA) of triple-tagged parasites ($AC10^{AID\text{-}3\times HA}$ | $AC9^{3xMyc}$ | $ERK7^{3xTy}$) shows that endogenous $AC10^{AID\text{-}3\times HA}$ colocalizes with the apical cap marker ISP1 and is efficiently depleted upon addition of IAA (3-indoleacetic acid). Green, rabbit anti-HA; magenta, mouse anti-ISP1. (B) IFA showing that the depletion of $AC10^{AID\text{-}3\times HA}$ results in the absence of AC9 and the loss of ERK7 from the apical cap. Green, rabbit anti-Myc; magenta, mouse anti-Ty. (C) Western blot analysis confirms efficient degradation of $AC10^{AID\text{-}3\times HA}$ and the concomitant nearly complete degradation of AC9 upon $AC10^{AID\text{-}3\times HA}$ knockdown. ERK7 levels are not substantially affected. $AC10^{AID\text{-}3\times HA}$, mouse anti-HA; AC9, mouse anti-Myc; ERK7, mouse anti-Ty. Rabbit anti-IMC12 was used as a loading control, and validation of this antibody is shown in Fig. S1. (D) $AC10^{AID\text{-}3\times HA}$ knockdown results in the elimination of the conoid, detected by SAS6L. Green, rabbit anti-HA; magenta, mouse anti-SAS6L. (E) Representative plaque assay images and quantification of plaque numbers illustrate a complete loss of plaque formation upon $AC10^{AID\text{-}3\times HA}$ depletion. (F) Using parasites tagged with $AC9^{AID\text{-}3\times HA}$ and $AC10^{3xMyc}$, IFA shows that conditional knockdown of AC9 (+IAA) does not affect the localization of AC10. Green, mouse anti-Myc; magenta, rabbit anti-HA. All scale bars are 2 μm.

for the parasites (Fig. 2E), as it renders them immotile and noninvasive. In addition, we confirmed that the knockdown of AC9 does not affect the localization of AC10 (Fig. 2F) (21), indicating that AC10 does not rely on AC9 for apical cap localization. These results demonstrate that AC10 is essential for recruiting both AC9 and ERK7 to the apical cap and suggest that AC10 is the foundational component of the AC9:AC10:ERK7 complex.

AC9 is recruited to the apical cap through a direct interaction with AC10. Like most IMC components, AC9 and AC10 lack significant homology to other proteins. Both proteins contain large stretches of predicted intrinsic disorder as well as predicted coiled-coil (CC) domains toward their N termini (Fig. 1A and B). In addition, we previously identified a well-conserved sequence in the AC9 C terminus that is required to recruit ERK7 to the apical cap and acts as a competitive inhibitor of ERK7 kinase activity by occupying both the kinase scaffolding and active sites (22). Since AC10 likely recruits AC9 to the apical cap, we reasoned that the AC9 CC domain is required for this interaction. In the background of our AC9$^{AID\text{-}3\times HA}$ strain (22), we expressed a second copy of AC9 driven by the ISC6 promoter and targeted to the UPRT locus (AC9^{wt}) (Fig. 3A and B) (42). As expected, expression of AC9^{wt} rescued the AC9$^{AID\text{-}3\times HA}$ knockdown phenotype, as assessed by SAS6L staining of the conoid and plaque assay (Fig. 3C to E). We also created a strain expressing AC9 in which the core of the predicted CC domain had been deleted (residues Δ75 to 113, AC9$^{\Delta CC}$) (Fig. 3F). Consistent with the high conservation of this region (Fig. 1A), AC9$^{\Delta CC}$ was not correctly targeted to the apical cap and, thus, it was unable to rescue the effects of AC9$^{AID\text{-}3\times HA}$ degradation (Fig. 3G to I). Because AC9$^{\Delta CC}$ staining was faint, we assessed its stability by Western blotting and found that it is expressed at the appropriate size, but its protein level is greatly diminished (Fig. S3A). This low level of AC9$^{\Delta CC}$ is likely the result of turnover upon loss of binding to its partner, AC10, as loss of AC9 is also seen following AC10^{AID} knockdown (Fig. 2C). While we and others have demonstrated a potential interaction between AC9 and AC10 through proximity biotinylation (21, 22), this interaction may either be direct or through an intermediate protein. To test whether AC9 directly binds AC10, we used a Y2H system in which stable interactions drive the expression of the HIS3 marker. Full-length AC9 was expressed as an N-terminal fusion with the LexA DNA binding domain, and AC10 was expressed as an N-terminal fusion with the GAL4 activating domain. As AC10 is a large protein of 1,979 residues, we split the protein into thirds and tested each portion for activation: AC10^{A} containing residues 2 to 650, AC10^{B} containing residues 651 to 1300, and AC10^{C} containing residues 1301 to 1979 (Fig. 1B). Intriguingly, we found that AC9 interacts with two independent regions of AC10, robustly binding both AC10^{A} and AC10^{B}; however, we observed no growth under restrictive conditions with the C-terminal AC10^{C} region (Fig. 3J; all Y2H data are shown in Table 1). These data suggest AC10^{C} does not bind AC9, although we cannot rule out that AC10^{C} is not stable in yeast and is therefore unavailable for binding.

To test whether the AC9 CC domain was required for this interaction, we deleted this region from the full-length Y2H construct (AC9$^{\Delta CC}$). Consistent with its inability to rescue the AC9$^{AID\text{-}3\times HA}$ knockdown phenotype in parasites, AC9$^{\Delta CC}$ was unable to bind either AC10^{A} or AC10^{B} (Fig. 3K). Moreover, the AC9 CC domain alone was sufficient to bind AC10^{A} in the Y2H assay, although it could not interact with AC10^{B}. The α-helical region of AC9 C terminal to the predicted CC is one of the more highly conserved areas in the protein (Fig. 1A). We therefore extended our Y2H construct to include this region (AC9$^{70\text{-}157}$), which now robustly interacted with both AC10^{A} and AC10^{B} (Fig. 3K). Taken together, these data demonstrate that the conserved α-helical sequence containing the predicted AC9 CC domain is driving interaction with at least two independent sites on AC10, and these interactions are required for forming the functional ternary complex in the apical cap.

The N-terminal third of AC10 binds both AC9 and ERK7 and is required for efficient recruitment of ERK7 to the apical cap. As AC9^{CC} binds AC10 at multiple distinct sites within the first two-thirds of the protein (Fig. 3J), we sought to further delineate which regions of AC10 are required for this interaction. Since AC10^{A} encompasses

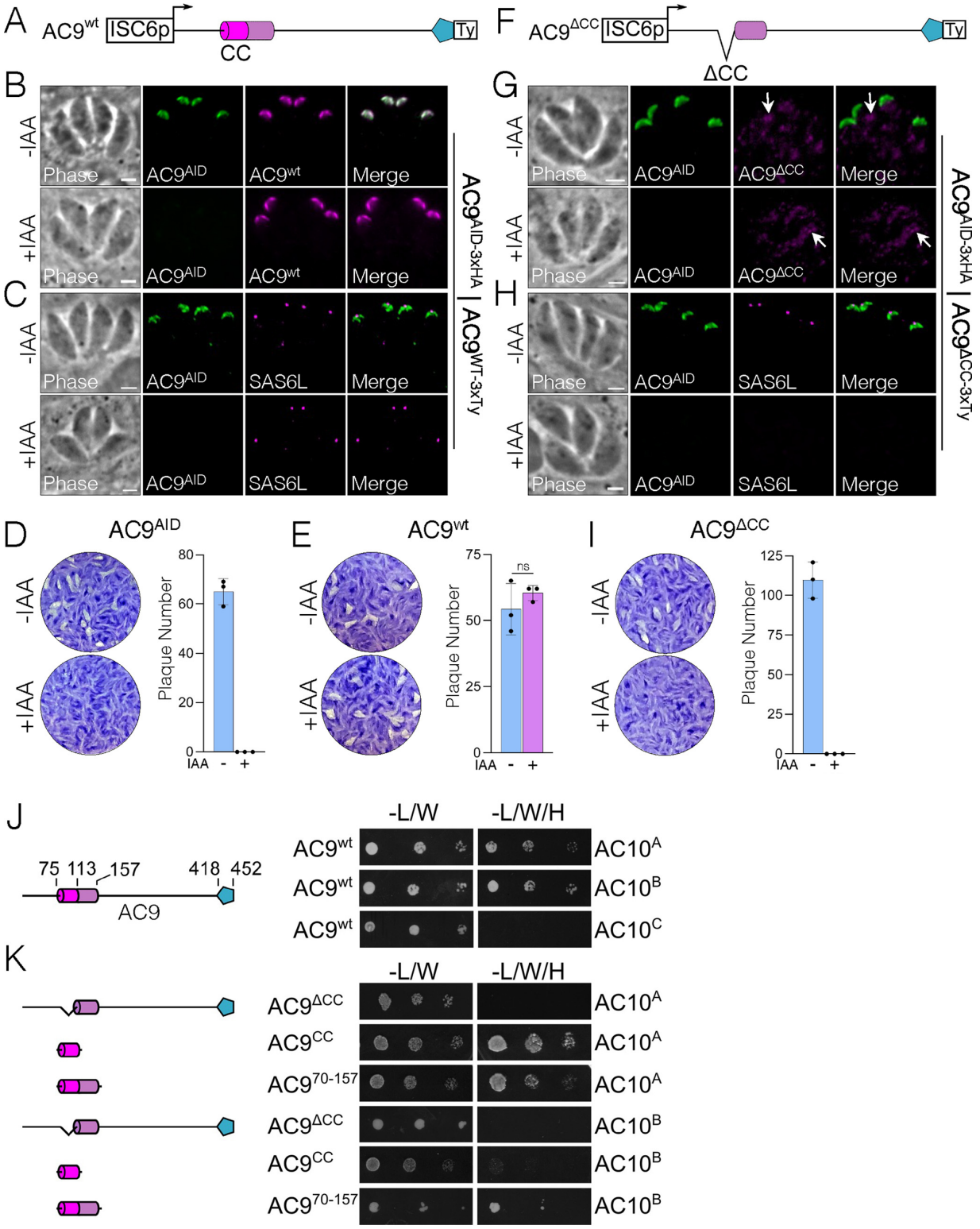

FIG 3 AC9 coiled-coil domain is necessary for localization and function. (A) Diagram of full-length AC9 driven by the ISC6 promoter and a C-terminal 3×Ty epitope tag. The AC9 CC domains, α-helices, and ERK7-binding region are highlighted as described for Fig. 1A. (B) IFAs show that the full-length

(Continued on next page)

TABLE 1 Overview of yeast two-hybrid data[a]

Bait	Prey	Growth
$AC9^{wt}$	$AC10^{A}$	+++
$AC9^{wt}$	$AC10^{B}$	+++
$AC9^{wt}$	$AC10^{C}$	–
$AC9^{wt}$	$AC10^{A\Delta CC1}$	–
$AC9^{wt}$	$AC10^{AC9BD_{(651-683)}}$	+++
$AC9^{wt}$	$AC10^{684-1300}$	++
$AC9^{wt}$	$AC10^{684-1300(\Delta CC2)}$	++
$AC9^{\Delta CC}$	$AC10^{A}$	–
$AC9^{CC}$	$AC10^{A}$	+
$AC9^{70-157}$	$AC10^{A}$	+++
$AC9^{\Delta CC}$	$AC10^{B}$	–
$AC9^{CC}$	$AC10^{B}$	+
$AC9^{70-157}$	$AC10^{B}$	+++
$AC9^{wt}$	$AC10^{CC1}$	–
$AC9^{wt}$	$AC10^{684-913}$	–
$AC9^{wt}$	$AC10^{914-1300}$	–
$ERK7^{Kinase}$	$AC10^{A}$	+++
$ERK7^{Kinase}$	$AC10^{B}$	–
$ERK7^{Kinase}$	$AC10^{C}$	–
$ERK7^{Kinase}$	$AC10^{A\Delta CC1}$	++
$ERK7^{C\text{-}term}$	$AC10^{A}$	–
$ERK7^{C\text{-}term}$	$AC10^{B}$	++
$ERK7^{C\text{-}term}$	$AC10^{C}$	–

[a]Bait and prey constructs and their relative growth on selective media are noted.

the most conserved stretch of residues in AC10 and includes a predicted CC domain (Fig. 1B), we generated a Y2H construct in which CC1 was deleted from this region [residues Δ422 to 513, $AC10^{A(\Delta CC1)}$]. The Y2H assay showed that $AC10^{A(\Delta CC1)}$ was unable to interact with full-length AC9, demonstrating that CC1 is necessary for binding (Fig. 4A). $AC10^{CC1}$ alone was not, however, sufficient to bind AC9, suggesting that this region does not form a simple coiled-coil interaction with AC9 (Fig. 4A).

To interrogate the functional domains of AC10 in parasites, we expressed full-length AC10 fused to a V5 epitope tag driven by its endogenous promoter and targeted to the UPRT locus ($AC10^{wt}$) (Fig. 4B). As expected, the $AC10^{wt}$ complementation construct correctly localized to the apical cap (Fig. 4C), fully rescued the plaque defect (Fig. 4D), properly recruited both AC9 and ERK7 (Fig. 4E), and restored SAS6L staining to the conoid upon $AC10^{AID\text{-}3\times HA}$ degradation (Fig. 4F). Thus, this complementation system serves as a platform to assess the functional domains of AC10.

To assess the role of $AC10^{CC1}$ in parasites, we deleted CC1 from the full-length construct ($AC10^{\Delta CC1}$) and expressed it in the $AC10^{AID\text{-}3\times HA}$ strain (Fig. 4G). While $AC10^{\Delta CC1}$ targeted correctly (Fig. 4H), this complemented strain was unable to form plaques upon $AC10^{AID\text{-}3\times HA}$ degradation, demonstrating that CC1 is essential for AC10 function (Fig. 4I). Consistent with the lack of plaque formation, $AC10^{\Delta CC1}$ did not recruit ERK7 to the apical cap upon $AC10^{AID\text{-}3\times HA}$ degradation (Fig. 4J), resulting in the loss of SAS6L signal (Fig. 4K). However, we still observed AC9 recruitment in $AC10^{\Delta CC1}$ parasites upon $AC10^{AID\text{-}3\times HA}$ degradation (Fig. 4J). This observation was surprising, as we have

FIG 3 Legend (Continued)

complementation ($AC9^{wt}$) targets correctly to the apical cap and is not affected by the knockdown of endogenous $AC9^{AID\text{-}3\times HA}$. Green, rabbit anti-HA; magenta, mouse anti-Ty. (C) Staining with SAS6L indicates that the conoid is restored via complementation. Green, rabbit anti-HA; magenta, mouse anti-SAS6L. (D and E) Representative plaque assays and quantification of plaque numbers demonstrate that $AC9^{AID\text{-}3\times HA}$ depletion results in no plaques, while complementation with $AC9^{wt}$ fully restores the plaque defect. (F) Diagram of $AC9^{\Delta CC}$ with residues 75 to 113 deleted from the $AC9^{wt}$ construct. (G) $AC9^{\Delta CC}$ fails to localize to the apical cap with faint, dispersed cytoplasmic staining (arrows) upon knockdown of endogenous $AC9^{AID\text{-}3\times HA}$. Green, rabbit anti-HA; magenta, mouse anti-Ty. (H) As expected from its mislocalization, $AC9^{\Delta CC}$ fails to rescue SAS6L staining upon $AC9^{AID\text{-}3\times HA}$ knockdown. Green, rabbit anti-HA; magenta, mouse anti-SAS6L. All scale bars are 2 μm. (I) Representative plaque assays and their quantifications demonstrate that complementation with $AC9^{\Delta CC}$ cannot rescue the plaque defect. (J) Yeast expressing $AC9^{wt}$ and the indicated AC10 constructs were grown under permissive (-L/W) or restrictive (-L/W/H) conditions to assess interaction. A corresponding diagram of full-length AC9 is shown. (K) Y2H assessing the interaction of AC9 mutants with the indicated AC10 sequence, as described for panel J. Corresponding diagrams of AC9 deletion constructs are shown.

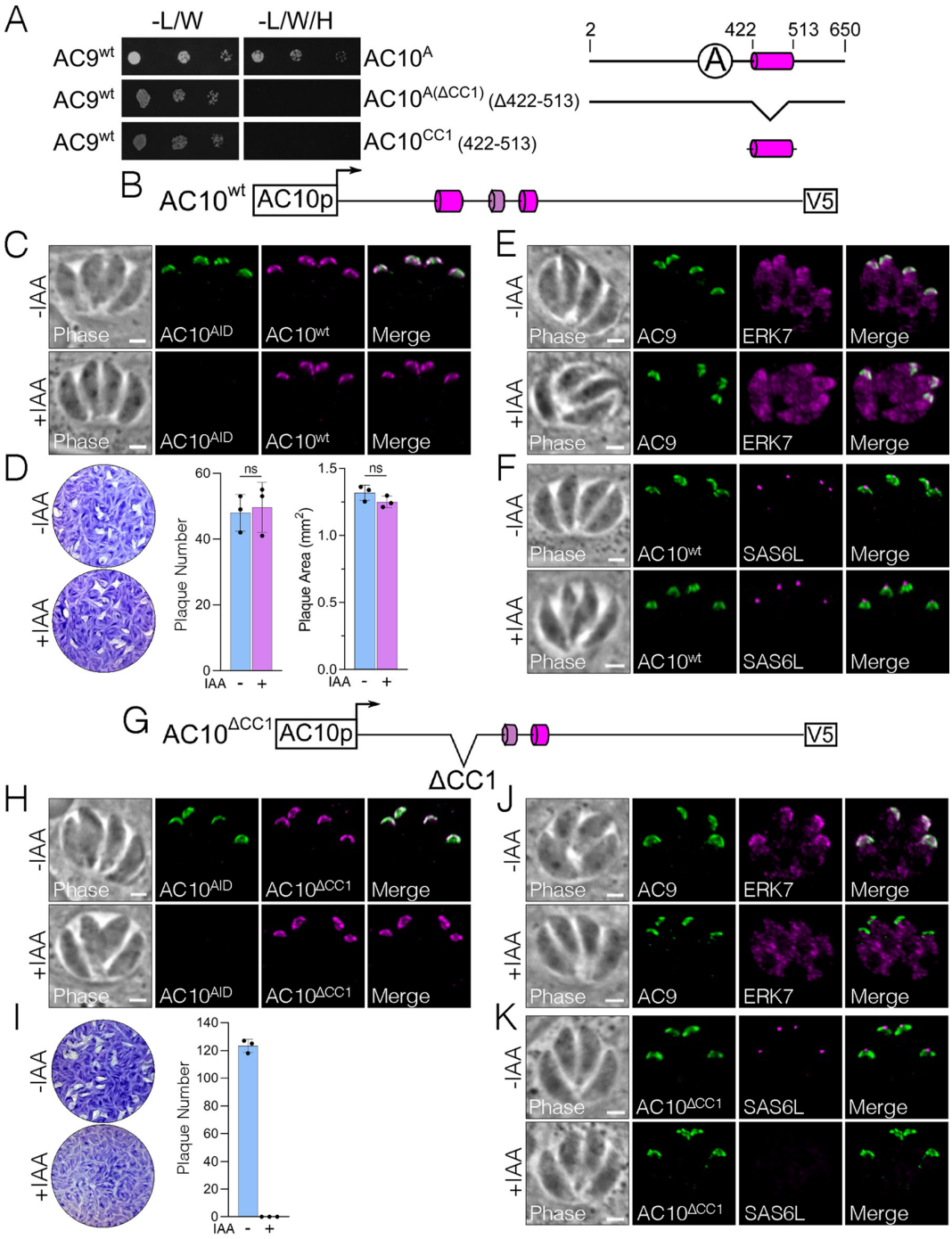

FIG 4 AC10 CC1 binds both AC9 and ERK7 and is essential for apical cap function. (A) Y2H assessing interaction of full-length AC9 with the indicated AC10 constructs, which are shown with corresponding diagrams. The data for AC9:AC10^{A} are shown again from Fig. 3J to facilitate a direct comparison. (B) Diagram of the full-length AC10 with a C-terminal V5 epitope tag (denoted AC10^{wt}). (C) IFA shows that AC10^{wt} localizes properly to the apical cap, which is not affected by knockdown of the endogenous AC10$^{AID\text{-}3\times HA}$. Green, rabbit anti-HA; magenta, mouse anti-V5. (D) Representative plaque assay images and the corresponding quantification of plaque number and plaque size illustrate that AC10^{wt} fully rescues the lytic ability of AC10$^{AID\text{-}3\times HA}$ knockdown. Statistical significance was calculated using two-sample two-tailed *t* tests. (E) IFA demonstrates that AC10^{wt} rescues AC9 and ERK7 localization in the apical cap. Green, rabbit anti-Myc; magenta, mouse anti-Ty. (F) IFA using SAS6L shows that AC10^{wt} restores the conoid with IAA. Green, rabbit anti-V5; magenta, mouse anti-SAS6L. (G) Diagram of AC10$^{\Delta CC1}$ with residues 422 to 513 deleted from the AC10^{wt} construct. (H) IFA shows that AC10$^{\Delta CC1}$ targets properly to the

(Continued on next page)

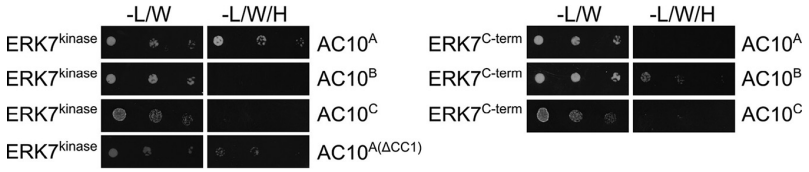

FIG 5 Both regions of ERK7 interact with multiple regions of AC10. Y2H assay was used to assess interaction of ERK7^{kinase} (2-358) or ERK7$^{C\text{-}term}$ (359-652) with the indicated AC10 constructs.

previously shown that the AC9 C terminus forms a tight interaction with ERK7 and is required for its recruitment to the apical cap (22). These data suggest that AC10^{CC1} also directly binds ERK7 independently of the AC10 recruitment of AC9 to the apical cap.

We tested this hypothesis using our Y2H assay and found that AC10^{A} was indeed able to bind the ERK7 kinase domain (Fig. 5). In contrast to the interaction with AC9, in which AC10^{CC1} was required, we found that AC10$^{A(\Delta CC1)}$ was still able to bind ERK7 in the Y2H assay, although the interaction was attenuated. In addition to AC10^{A} interacting with the ERK7 kinase domain, we were surprised to find that AC10^{B} also interacted with the intrinsically disordered C terminus of ERK7, suggesting that ERK7 forms multivalent interactions with AC10. Thus, the Y2H and functional data indicate that multiple AC10 regions mediate interactions with both AC9 (Fig. 3 and 4) and ERK7 (Fig. 5). Among these interactions, AC10^{CC1} is required for the efficient recruitment of ERK7 to the apical cap independently of AC9, and this interaction is essential for the formation of the mature conoid.

A short, conserved sequence in AC10 is essential to bind and recruit AC9 to the apical cap. Because the AC10$^{\Delta CC1}$ strain was still able to recruit AC9 to the apical cap, we sought to identify additional regions in AC10 that are required for AC9 recruitment. Our Y2H experiments identified regions in AC10^{B} that independently bound AC9 (Fig. 3J). To identify a minimal region that was sufficient for AC9 binding, we focused on a short, conserved sequence within AC10^{B} that is predicted to form an α-helix (Fig. 1B) and has a heptad repeat similar to that seen in coiled-coil domains (Fig. 6A). Y2H analysis showed that residues 651 to 683 were sufficient to robustly interact with AC9 (Fig. 6B), leading us to label this region the AC9 binding domain (AC10$^{AC9\text{-}BD}$). To test the importance of this region for AC10 function in parasites, we complemented the AC10$^{AID\text{-}3\times HA}$ strain with a construct in which AC9-BD had been deleted [AC10$^{\Delta(AC9\text{-}BD)}$] (Fig. 6C). We found that while the truncated protein localized properly to the apical cap (Fig. 6D), it was unable to rescue the plaque defect upon AC10$^{AID\text{-}3\times HA}$ knockdown (Fig. 6E). We also observed that both AC9 and ERK7 were absent from the apical cap upon AC10$^{AID\text{-}3\times HA}$ degradation (Fig. 6F), resulting in the loss of the conoid (Fig. 6G). These results suggest that AC10$^{AC9\text{-}BD}$ forms a short coiled-coil with AC9^{CC}, and this interaction is absolutely required for recruitment of the AC9:ERK7 complex to the apical cap in parasites.

A third AC9 binding site on AC10 is required for full parasite fitness. While AC10$^{AC9\text{-}BD}$ was sufficient to bind AC9 in our Y2H assay (Fig. 6B), AC10^{B} also contains the second predicted CC domain spanning residues 781 to 830 (Fig. 1B and 7A). To assess the importance of CC2, we first generated a construct with AC9-BD deleted from AC10^{B} (AC10$^{684\text{-}1300}$) and found that this region still interacted with AC9 (Fig. 7A). We then deleted CC2 from AC10$^{684\text{-}1300}$ (AC10$^{684\text{-}1300,\Delta CC2}$), which resulted in a somewhat attenuated interaction with AC9 in our Y2H assay. We additionally found that a

FIG 4 Legend (Continued)
apical cap regardless of AC10$^{AID\text{-}3\times HA}$ knockdown. Green, rabbit anti-HA; magenta, mouse anti-V5. (I) Plaque assays demonstrate that AC10$^{\Delta CC1}$ cannot rescue the parasite's lytic ability. (J) IFA shows that AC9 is present in the apical cap, while ERK7 is mislocalized to the cytoplasm upon knockdown of AC10$^{AID\text{-}3\times HA}$. Green, rabbit anti-Myc; magenta, mouse anti-Ty. (K) IFA illustrates that AC10$^{\Delta CC1}$ does not rescue SAS6L localization, indicating the absence of the conoid. Green, rabbit anti-V5; magenta, mouse anti-SAS6L. All scale bars are 2 μm.

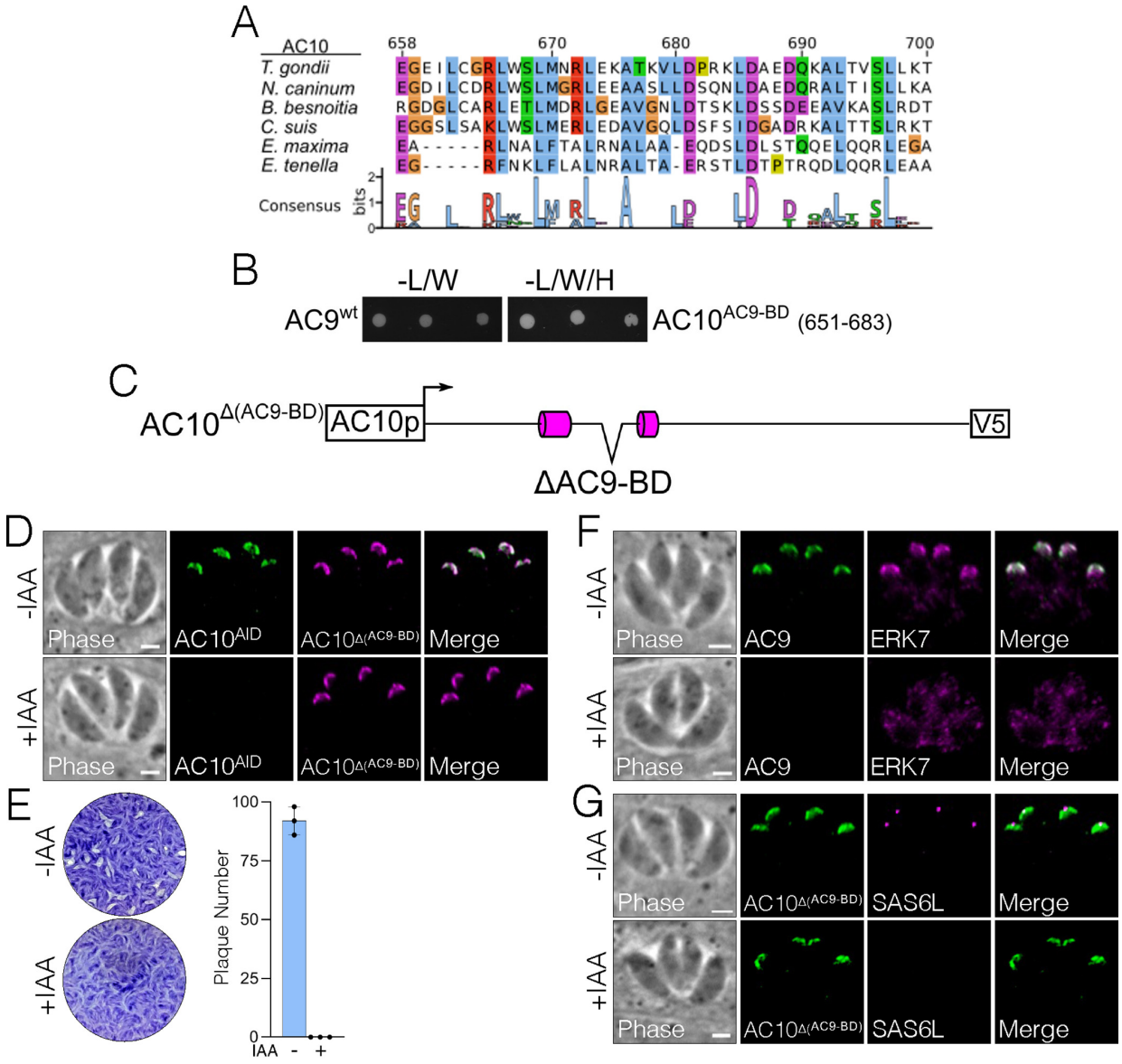

FIG 6 Conserved AC9 binding domain within AC10 is essential for AC10 function. (A) Multiple-sequence alignments and accompanying sequence logo mapped to TgAC10$^{658\text{-}700}$. Conserved residues are highlighted by class (blue, hydrophobic; purple, acidic; red, basic; green, polar; orange, Gly; yellow, Pro). (B) Y2H showing interaction of full-length AC9 with the AC10$^{AC9\text{-}BD}$ (residues 651 to 683). (C) Diagram of AC10$^{\Delta(AC9\text{-}BD)}$ with residues 651 to 683 deleted from the AC10^{wt} construct. (D) AC10$^{\Delta(AC9\text{-}BD)}$ localizes properly to the apical cap with or without IAA. Green, rabbit anti-HA; magenta, mouse anti-V5. (E) Plaque assays show that AC10$^{\Delta(AC9\text{-}BD)}$-complemented parasites cannot form plaques upon knockdown of endogenous AC10$^{AID\text{-}3\times HA}$. (F) AC10$^{\Delta(AC9\text{-}BD)}$ cannot rescue the recruitment of either AC9 or ERK7 to the apical cap. Green, rabbit anti-Myc; magenta, mouse anti-Ty. (G) IFA shows that SAS6L cannot be restored when complemented with AC10$^{\Delta(AC9\text{-}BD)}$. Green, rabbit anti-V5; magenta, mouse anti-SAS6L. All scale bars are 2 μm.

portion of AC10^{B} containing CC2 (AC10$^{684\text{-}913}$) is not sufficient for interacting with AC9. These Y2H results suggest that CC2 contains minor AC9 binding regions and that the remaining residues in AC10^{B} provide additional binding sites, further supporting the hypothesis that AC9 and AC10 interact via multiple contact points.

We then asked whether deletion of CC2 in the context of an otherwise full-length protein would affect AC10 function in parasites. We generated AC10$^{\Delta CC2}$ (residues Δ781 to 830) and expressed it in the triple-tagged AC10$^{AID\text{-}3\times HA}$ line (Fig. 7B). As with our other deletion constructs, AC10$^{\Delta CC2}$ protein localized correctly to the apical cap

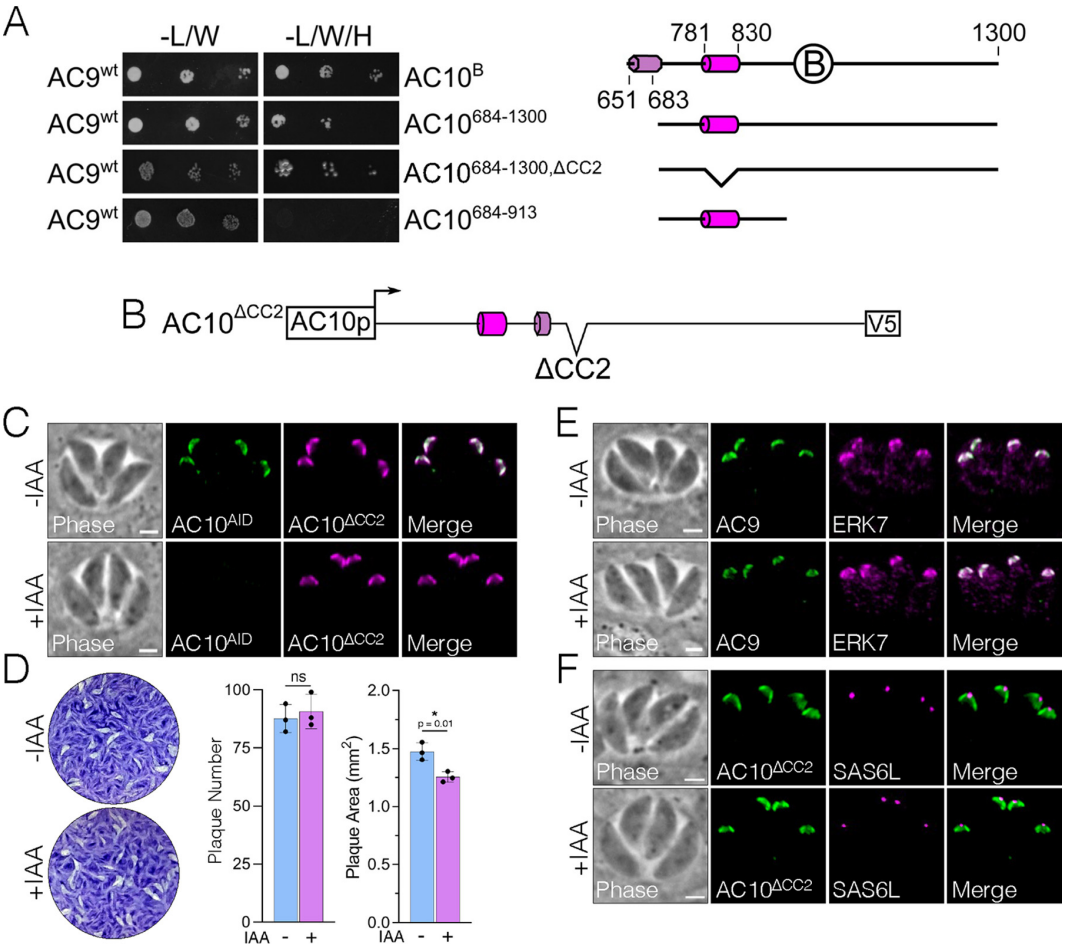

FIG 7 Deletion of CC2 within AC10 results in subtle plaque defects. (A) Y2H to assess interaction of full-length AC9 with the indicated AC10 mutants. Corresponding diagrams of AC10 deletion constructs are shown. (B) Diagram of AC10$^{\Delta CC2}$ with residues 781 to 830 deleted from the AC10^{wt} construct. (C) IFA shows that AC10$^{\Delta CC2}$ localizes to the apical cap and is not affected by AC10$^{AID\text{-}3\times HA}$ knockdown. Green, rabbit anti-HA; magenta, mouse anti-V5. (D) Plaque assays indicate that AC10$^{\Delta CC2}$ complementation does not fully rescue the growth defect (15% reduction). Statistical significance was calculated using two-sample two-tailed *t* tests, and *P* values are noted on the graph. (E) AC9 and ERK7 staining with or without IAA shows that AC10$^{\Delta CC2}$ can still recruit members of the complex to the apical cap. Green, rabbit anti-Myc; magenta, mouse anti-Ty. (F) IFA illustrates that AC10$^{\Delta CC2}$ restores SAS6L staining at the conoid. Green, rabbit anti-V5; magenta, mouse anti-SAS6L. All scale bars are 2 μm.

(Fig. 7C). Upon degradation of AC10$^{AID\text{-}3\times HA}$, AC10$^{\Delta CC2}$ mostly rescued parasite fitness in a plaque assay, with a small but reproducible 15% reduction in plaque size (Fig. 7D). Consistent with this minor impact on the lytic cycle, both AC9 and ERK7 localizations were unaffected (Fig. 7E) and the conoid appeared intact (Fig. 7F). These data suggest that binding of AC9 and other potential interactors at this site, while not required for full parasite fitness, is still functionally relevant.

AC10 N- and C-terminal deletions reveal additional domains for full apical cap function. The functional regions of AC10 described above only occupy about half of the 1,979-residue protein. Notably, AC10 orthologs in other Sarcocystidae are of various lengths and display low sequence identity through the majority of the protein (Fig. 1B). To determine if the remainder of the protein harbored any additional regions important for function, we first deleted the N-terminal region of AC10 up to 36 residues N terminal to AC10^{CC1} (residues 387 to 1979, AC10$^{\Delta N\text{-}term}$) (Fig. 8A). The AC10$^{\Delta N\text{-}term}$ protein localized properly to the apical cap independently of AC10$^{AID\text{-}3\times HA}$ degradation (Fig. 8B). Upon AC10$^{AID\text{-}3\times HA}$ depletion, parasites with AC10$^{\Delta N\text{-}term}$ displayed a substantial fitness defect by

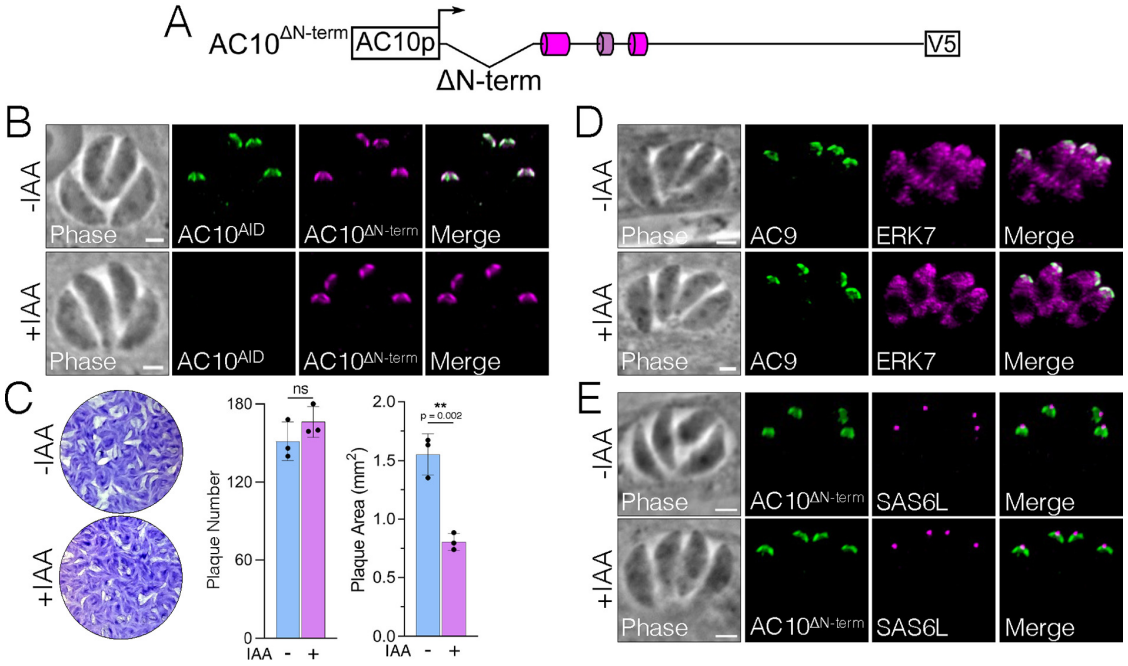

FIG 8 N-terminal deletion of AC10 results in a substantial plaque defect. (A) Diagram of AC10$^{\Delta N\text{-term}}$ with residues 2 to 386 deleted from the AC10^{wt} construct. (B) IFA shows that AC10$^{\Delta N\text{-term}}$ targets properly to the apical cap with or without IAA. Green, rabbit anti-HA; magenta, mouse anti-V5. (C) Plaque assays show that AC10$^{\Delta N\text{-term}}$ partially rescues the growth defect, resulting in smaller plaques upon AC10$^{AID\text{-}3\times HA}$ knockdown (48% reduction). Statistical significance was calculated using two-sample two-tailed *t* tests, and *P* values are noted on the graph. (D) IFA illustrates that AC9 and ERK7 are present in the apical cap with or without IAA. Green, rabbit anti-Myc; magenta, mouse anti-Ty. (E) SAS6L staining indicates that the conoid is present with or without IAA. Green, rabbit anti-V5; magenta, mouse anti-SAS6L. All scale bars are 2 μm.

plaque assay (48% reduction in plaque size) (Fig. 8C). However, AC10$^{\Delta N\text{-term}}$ appears to be sufficient for recruiting both AC9 and ERK7 to the apical cap (Fig. 8D), resulting in the presence of a conoid as demonstrated by apical SAS6L staining (Fig. 8E). Thus, while this N-terminal region is not strictly required for recruiting AC9:ERK7 and maturation of the conoid, its deletion reduces parasite fitness, indicating that this region is important for full AC10 function.

We next focused on the C-terminal region of AC10. Due to the lack of identifiable features in this region, we deleted the C-terminal half of the protein, which includes AC10^{C} plus the portion of AC10^{B} C terminal to the CC domains (residues Δ914 to 1979, AC10$^{\Delta C\text{-term}}$) (Fig. 9A). Upon examining the localization of AC10$^{\Delta C\text{-term}}$, we noticed striking, cell cycle-dependent variation. In mature parasites, AC10$^{\Delta C\text{-term}}$ localized to the apical cap regardless of AC10$^{AID\text{-}3\times HA}$ depletion (Fig. 9B). However, in budding parasites, AC10$^{\Delta C\text{-term}}$ was largely absent from the maternal apical cap while remaining intact in the daughter buds (Fig. 9C). Thus, we assessed the localization of AC9 and ERK7 in mature parasites expressing AC10$^{\Delta C\text{-term}}$ and found that only a small amount of AC9 could be detected in the apical cap upon AC10$^{AID\text{-}3\times HA}$ knockdown (Fig. 9D). ERK7 also appeared to be dramatically diminished from the apical cap in mature parasites (Fig. 9D). In budding parasites, while both AC9 and ERK7 were drastically reduced in mature apical caps, the signal appeared largely intact in daughter buds, similar to the localization of AC10$^{\Delta C\text{-term}}$ (Fig. 9E). Somewhat surprisingly, despite these substantial localization defects, the conoid still appeared to be intact by SAS6L staining, suggesting that the amounts of AC9, AC10$^{\Delta C\text{-term}}$, and ERK7 in the apical cap are sufficient to stabilize the conoid (Fig. 9F). Nevertheless, plaque assays revealed that parasites expressing AC10$^{\Delta C\text{-term}}$ suffered a severe defect in parasite fitness upon AC10$^{AID\text{-}3\times HA}$ degradation (85% reduction in plaque size) (Fig. 9G).

We next sought to determine whether the C-terminal half of AC10 described above

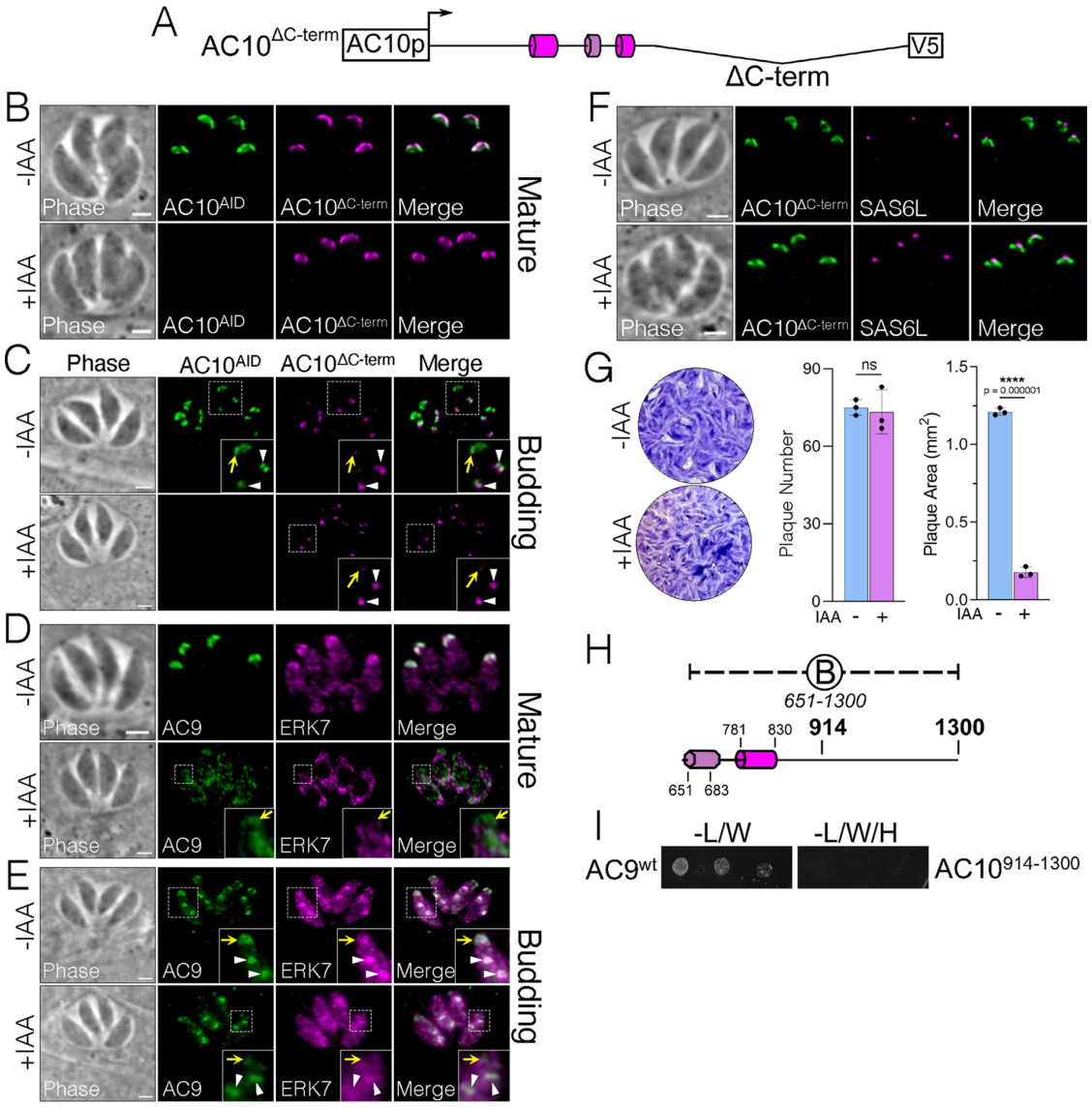

FIG 9 C-terminal deletion of AC10 diminishes maternal apical cap localization and causes severe fitness defects. (A) Diagram of AC10$^{\Delta C\text{-term}}$ with residues 914 to 1979 deleted from the AC10^{wt} construct. (B) IFA shows that mature parasites have proper AC10$^{\Delta C\text{-term}}$ localization with or without IAA. Green, rabbit anti-HA; magenta, mouse anti-V5. (C) In contrast, actively budding parasites have substantially diminished AC10$^{\Delta C\text{-term}}$ localization in maternal apical caps (inset, yellow arrows), while AC10$^{\Delta C\text{-term}}$ localization to daughter buds is unaffected (inset, white arrowheads). Green, rabbit anti-HA; magenta, mouse anti-V5. (D) IFA depicts that both AC9 and ERK7 are substantially mislocalized to the cytoplasm in mature parasites with IAA (insets, yellow arrows). Green, rabbit anti-Myc; magenta, mouse anti-Ty. (E) In budding parasites, IFAs show severely decreased levels of AC9 in the maternal apical cap (insets, yellow arrows) but intact localization in daughter buds (insets, white arrowheads). ERK7 appears absent from the apical cap upon depletion of AC10$^{AID\text{-}3\times HA}$. Green, rabbit anti-Myc; magenta, mouse anti-Ty. (F) IFAs demonstrate that SAS6L staining appears intact upon degradation of AC10$^{AID\text{-}3\times HA}$. Green, rabbit anti-V5; magenta, mouse anti-SAS6L. All scale bars are 2 μm. (G) Plaque assays show extremely small plaques upon knockdown of AC10$^{AID\text{-}3\times HA}$ (85% reduction). Statistical significance was calculated using two-sample two-tailed *t* tests, and *P* values are noted on the graph. (H) Diagram illustrating the AC10$^{914\text{-}1300}$ construct used in the following Y2H assay. (I) Y2H to assess the interaction of full-length AC9 with AC10$^{914\text{-}1300}$.

binds directly to AC9. We created a Y2H construct spanning AC10 residues 914 to 1300 to interrogate the C-terminal portion of AC10^{B} (AC10$^{914\text{-}1300}$) (Fig. 9H). Despite the defects in AC9 and ERK7 recruitment in AC10$^{\Delta C\text{-term}}$ parasites, we found that neither AC10$^{914\text{-}1300}$ (Fig. 9I) nor the remainder of the AC10 C terminus (AC10^{C}) interacts with AC9 (Fig. 3J). Together, these results suggest that while the AC10 C terminus does not

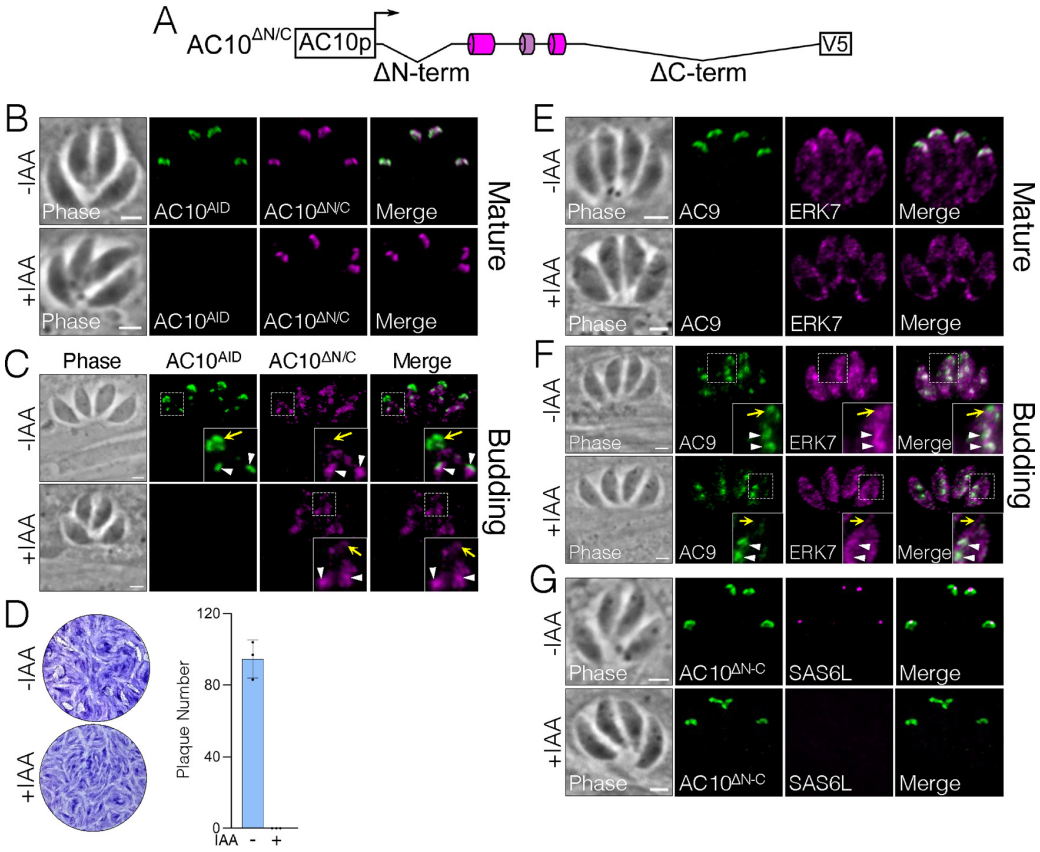

FIG 10 Combination of N- and C-terminal deletions is essential for apical cap function. (A) Diagram of AC10$^{\Delta N/C}$ combining the AC10$^{\Delta N\text{-term}}$ (residues 2 to 337) and AC10$^{\Delta C\text{-term}}$ (residues 914 to 1979) deletions from the AC10^{wt} construct. (B) IFAs illustrate that AC10$^{\Delta N/C}$ localizes properly to the apical caps in mature parasites with or without IAA. Green, rabbit anti-HA; magenta, mouse anti-V5. (C) IFAs show that AC10$^{\Delta N/C}$ appears to be almost completely absent from the maternal apical cap of budding parasites upon depletion of AC10$^{AID\text{-}3\times HA}$ (insets, yellow arrows). However, in daughter apical caps, AC10$^{\Delta N/C}$ remains intact even upon depletion of endogenous AC10$^{AID\text{-}3\times HA}$ (insets, white arrowheads). Green, rabbit anti-HA; magenta, mouse anti-V5. (D) Plaque assays show that deleting both N- and C-terminal regions from AC10 eliminates plaque formation. (E) IFAs display the absence of AC9 and ERK7 from mature apical caps. Green, rabbit anti-Myc; magenta, mouse anti-Ty. (F) IFAs show that AC9 and ERK7 remain intact in daughter apical caps (insets, white arrowheads) but appear completely eliminated from maternal apical caps upon knockdown of AC10$^{AID\text{-}3\times HA}$ (insets, yellow arrows). Green, rabbit anti-Myc; magenta, mouse anti-Ty. (G) IFAs display absence of SAS6L upon AC10$^{AID\text{-}3\times HA}$ knockdown. Green, rabbit anti-V5; magenta, mouse anti-SAS6L. All scale bars are 2 μm.

directly interact with AC9, it contains important regions for maintaining the integrity of the AC9:AC10:ERK7 complex.

Since deletion of either the N or C termini of AC10 only partially disrupted function, we assessed whether the combination of these regions is essential by deleting both regions simultaneously (residues Δ2 to 337 and Δ914 to 1979, AC10$^{\Delta N/C}$) (Fig. 10A). As with AC10$^{\Delta C\text{-term}}$, AC10$^{\Delta N/C}$ localized properly in mature parasites (Fig. 10B), and during replication, the signal was diminished specifically in maternal apical caps upon addition of auxin (Fig. 10C). Unlike AC10$^{\Delta C\text{-term}}$, however, this construct could not rescue the plaque defect at all (Fig. 10D). Western blot analysis demonstrated that the difference between AC10$^{\Delta C\text{-term}}$ and AC10$^{\Delta N/C}$ does not appear to be due to expression levels (Fig. S3B). Consistent with the complete loss of function of AC10$^{\Delta N/C}$, both AC9 and ERK7 were absent from the maternal apical caps of both mature and budding parasites (Fig. 10E and F). In addition, we observed reduced AC9 and ERK7 signal in the apical caps of daughter buds (Fig. 10F). In agreement with the lack of ability to form plaques, AC10$^{\Delta N/C}$ parasites were completely missing apical SAS6L staining upon AC10$^{AID\text{-}3\times HA}$

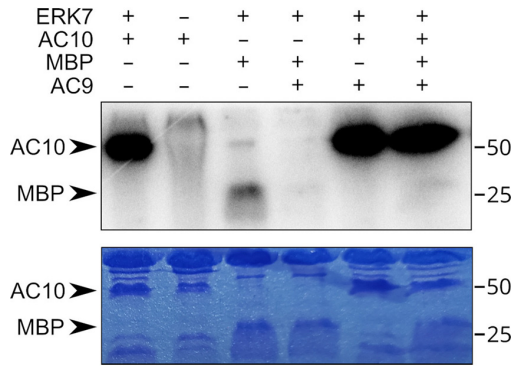

FIG 11 ERK7 robustly phosphorylates AC10 *in vitro*. Autoradiogram and corresponding Coomassie-stained gel of an *in vitro* kinase assay in which 1 μM ERK7 was used to phosphorylate 10 μM AC10$^{313\text{-}569}$ or the generic substrate MBP. In the rightmost 3 lanes, 10 μM inhibitory AC9$^{418\text{-}452}$ was added to the reaction. Note that the rightmost lane contains both MBP and AC10 as the substrates.

depletion (Fig. 10G). Together, these results demonstrate that the cumulative effect of deleting both N- and C-terminal regions renders AC10 nonfunctional.

AC10 effectively competes with AC9 as an ERK7 substrate. Because AC10 binds both AC9 and ERK7 (Fig. 4 to 6), and ERK7 localization (22) and kinase activity (20) are both essential for a functional conoid, we asked whether AC10 is phosphorylated by ERK7. Notably, AC10 has 396 phosphorylatable residues (Ser/Thr), and 57 of these residues have been identified as phosphorylated in parasites in published phosphoproteomics data sets (43), including 10 high-probability MAP kinase sites spread throughout the AC10 sequence. We created a bacterial expression construct of the N-terminal region of AC10 that is bound by both AC9 and ERK7. We found that this recombinantly expressed and purified AC10 was robustly phosphorylated by ERK7 (Fig. 11). Remarkably, the AC10 protein was phosphorylated to a much greater degree than myelin basic protein (MBP), a typical generic substrate used to test MAPK activity (44).

We previously demonstrated that AC9 binds ERK7 with an approximate dissociation constant (K_D) of 20 nM and robustly inhibits ERK7 activity (22). This led us to propose a model by which AC9 increases the specificity of ERK7 for its substrates, as true substrates must not only bind the active site but also compete with AC9 for scaffolding interaction. We therefore tested whether the AC10 interaction with ERK7 can overcome inhibition by the AC9$^{418\text{-}452}$ peptide (Fig. 11). As expected, addition of equimolar AC9$^{418\text{-}452}$ to the kinase reaction completely blocks MBP phosphorylation by ERK7. We found, however, that AC10 phosphorylation is undiminished by the addition of AC9.

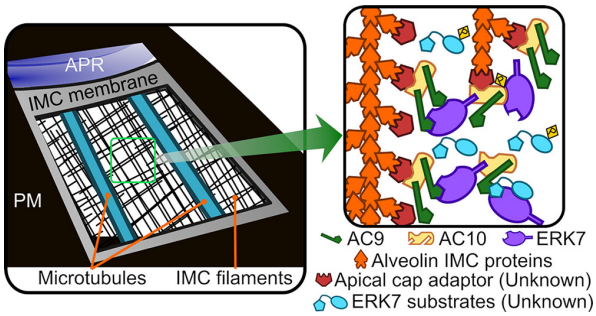

FIG 12 Model for AC9:AC10:ERK7 complex oligomerization in the apical cap. AC9, AC10, and ERK7 oligomerize with the IMC cytoskeleton filaments that are associated with the cytosolic leaflet of the IMC membrane. AC10 recruits the other two proteins to the IMC, possibly through interaction with an undescribed adaptor protein. Because AC10 has multiple binding sites for both AC9 and ERK7, which also interact with one another, the three proteins likely form an irregular oligomer. These interactions concentrate ERK7 at the apical cap while allowing it to bind and phosphorylate its substrates and thereby facilitate the stability of the apical complex.

Furthermore, when we included equimolar AC9, AC10, and MBP in the kinase reaction, we saw that MBP phosphorylation was still fully inhibited while AC10 was still robustly phosphorylated. These data strongly suggest AC10 is a legitimate substrate of ERK7 and that one function of ERK7 kinase activity is to regulate the conformation and assembly of the AC10 complex.

DISCUSSION

In this study, we explore the organization and function of the AC9:AC10:ERK7 ternary complex. We demonstrated that both AC9 and ERK7 are dependent on AC10 to be recruited to the apical cap, suggesting that AC10 is an anchor for the complex. However, it remains unclear how AC10 itself is targeted to the apical cap. One possibility is that other apical cap proteins recruit AC10. Similar to AC10, six of the known apical cap proteins (AC2, AC3, AC4, AC5, AC7, and AC8) are associated with the IMC cytoskeletal network (15). Unlike AC9 and AC10, these other apical cap proteins were predicted to be dispensable based on a genome-wide CRISPR screen (45). Thus, it is possible that these apical cap proteins play redundant roles in organizing the AC9:AC10:ERK7 complex. It is also possible that there are undiscovered components of this protein complex or ones that serve to tether AC10 to the apical cap.

To determine how AC9, AC10, and ERK7 interact, we focused on identifiable domains using a combination of pairwise Y2H (Table 1) and complementation assays to assess direct binding and functional relevance. AC10 appears to recruit AC9 (Fig. 2) (21), which in turn recruits ERK7 through a conserved C-terminal motif that serves to both concentrate ERK7 at the apical cap and regulate its kinase activity (22). Our Y2H and complementation assays revealed a conserved helical sequence at the AC9 N terminus that was both necessary and sufficient to bind AC10 and was required for AC9's localization at the apical cap (Fig. 2). Remarkably, this single region of AC9 was able to bind multiple sites on AC10 (Fig. 3 and 7). In addition, AC10 can independently interact with both the kinase domain and C-terminal regions of ERK7 (Fig. 5). AC10 therefore seems to act as a large scaffolding molecule that recruits multiple copies of each AC9 and ERK7. Furthermore, combined with the multiple binding sites on AC10 for both AC9 and ERK7, because each component of the AC9:AC10:ERK7 complex can interact with the other, it seems likely that AC10 functions to nucleate oligomerization of this complex (Fig. 12). Importantly, AC9, AC10, and ERK7 each has been demonstrated to fractionate with the detergent-insoluble parasite cytoskeleton (20, 21), and their oligomerization is consistent with the characteristic meshwork of the IMC cytoskeleton. The AC10 binding region of AC9 is a predicted coiled-coil ($AC9^{CC}$), and we identified two regions of AC10 ($AC10^{CC1}$ and $AC10^{AC9\text{-}BD}$) with coiled-coil-like properties that are required for AC9 interaction and essential for AC10 function in parasites. Notably, predicted coiled-coil domains have also been shown to be essential in other IMC proteins (46–48), suggesting this is a general theme of IMC cytoskeleton assembly.

Deletion of the short $AC10^{AC9\text{-}BD}$ sequence blocks AC9 recruitment to the apical cap in parasites (Fig. 6). However, AC9 localization was largely unperturbed in $AC10^{\Delta CC1}$ parasites while ERK7 was unable to be recruited to the apical cap (Fig. 4). Remarkably, Y2H revealed that the N-terminal third of AC10 was able to physically interact with both AC9 and the ERK7 kinase domain, although the $AC10^{CC1}$ region itself was only required for AC9 binding (Fig. 4A and 5). This differential effect of $AC10^{\Delta CC1}$ on AC9 and ERK7 binding to this region suggests that the binding interfaces occupy different surfaces of a folded domain. We also found that this N-terminal region of AC10 was robustly phosphorylated by ERK7 *in vitro* and was unaffected by AC9 inhibition (Fig. 11). Together, these data indicate that AC10 is an ERK7 substrate in parasites and that its phosphorylation functions in regulating the assembly of the AC9:AC10:ERK7 complex into the apical cap cytoskeleton.

While AC10 is found throughout coccidia, its length and much of its sequence are not well conserved (Fig. 1B). Nevertheless, there are stretches of conserved sequence in the N- and C-terminal regions that are outside those we identified as critical for

interacting with AC9 and ERK7. We found that neither of these regions of AC10 was essential to function, although deletion of either reduced parasite fitness (Fig. 8C and 9G). Notably, AC10$^{\Delta C\text{-term}}$ parasites showed the fragility of the AC9:AC10:ERK7 complex, in which the initial recruitment to the apical cap was largely unaffected in daughter cells (Fig. 9C), but the complex appeared disrupted in mature parasites (Fig. 9D and E). While AC10$^{\Delta C\text{-term}}$ parasites showed a substantial loss of function, the complex was still able to function in facilitating maturation of the conoid (Fig. 9G). In contrast, deletion of both the N- and C-terminal regions of AC10 rendered the AC9:AC10:ERK7 complex nonfunctional, as the daughter conoids were lost (Fig. 10G) and parasites were nonviable (Fig. 10D). Therefore, it appears that these regions of AC10 either recruit other, undescribed components of the apical cap cytoskeleton or form nonessential interactions that facilitate AC9:AC10:ERK7 oligomerization.

This study builds on an increasingly robust body of evidence that the apical cap acts as an essential platform to facilitate the assembly and maintenance of the apical complex (20–22). A previously proposed model suggested that AC9 and AC10 act primarily to stabilize the *Toxoplasma* subpellicular microtubules due to the distribution of AC9 and AC10 proteins along the longitudinal rows of the microtubules (21). While our data support the idea that AC9 and AC10 form filaments in the apical cap cytoskeleton, this model was developed prior to establishing a connection with the MAP kinase ERK7 and its essential role in apical complex maturation (20). We have previously shown that an AC9 mutant that is unable to recruit ERK7 to the apical cap cannot rescue the AC9 knockdown (22). We have built upon that finding here, demonstrating a loss of the conoid in mutant AC10 parasites that can recruit AC9, but not ERK7, to the apical cap (Fig. 4J and K). Taken together, our data suggest a different model in which the ERK7-dependent phosphorylation of AC10 promotes functional assembly of the AC9:AC10:ERK7 complex at the apical cap (Fig. 12). It is likely that ERK7 then phosphorylates other substrates after being recruited at this site, which may include critical components of the apical complex.

MATERIALS AND METHODS

***T. gondii* and host cell culture.** *T. gondii* RHΔ*ku80*Δ*hxgprt* (parental) and subsequent strains were grown on confluent monolayers of human foreskin fibroblasts (HFFs; ATCC) at 37°C and 5% CO_2 in Dulbecco's modified Eagle medium (DMEM) supplemented with 5% fetal bovine serum (Gibco), 5% cosmic calf serum (HyClone), and 1× penicillin-streptomycin-L-glutamine (Gibco). Constructs containing selectable markers were selected using 1 μM pyrimethamine (dihydrofolate reductase-thymidylate synthase [DHFR-TS]), 50 μg/ml mycophenolic acid-xanthine (HXGPRT), or 40 μM chloramphenicol (CAT) (49–51). Removal of HXGPRT was negatively selected using 350 μg/ml 6-thioxanthine (6-TX), and homologous recombination to the UPRT locus was negatively selected using 5 μM 5-fluorodeoxyuridine (FUDR) (42).

Antibodies. The hemagglutinin epitope was detected with mouse monoclonal antibody (MAb) HA.11 (diluted 1:1,000) (item no. 901515; BioLegend) or rabbit polyclonal antibody (pAb) anti-HA (diluted 1:1,000) (catalog no. PI715500; Invitrogen). The Ty1 epitope was detected with mouse MAb BB2 (diluted 1:1,000) (52). The c-Myc epitope was detected with mouse MAb 9E10 (diluted 1:1,000) (53) or rabbit pAb anti-Myc (diluted 1:1,000) (catalog no. PA1981; Invitrogen). The V5 epitope was detected with mouse MAb anti-V5 (diluted 1:1,000) (catalong no. R96025; Invitrogen). *Toxoplasma*-specific antibodies include mouse MAb m-IMC1 (diluted 1:500) (54), mouse MAb anti-ISP1 (diluted 1:1,000) (55), and rabbit pAb anti-IMC6 (diluted 1:2,000) (46).

Production of IMC12 antibody. The IMC12 coding sequence was cloned into the pET His6 TEV LIC bacterial expression vector (Addgene plasmid number 29653; Scott Gradia) using primers P32 to P35. The construct was transformed into BL21(DE3) *Escherichia coli*, and protein was induced with 1 mM isopropyl-β-D-thiogalactopyranoside (IPTG) and purified using nickel-nitrilotriacetic acid (Ni-NTA) agarose under denaturing conditions as described previously (56). The sample was then dialyzed into PBS to remove the urea, and rabbit antisera were produced by Cocalico Biologicals.

Immunofluorescence assay and Western blotting. Confluent HFF cells were grown on glass coverslips and infected with *T. gondii*. After 18 to 24 h, the coverslips were fixed with 3.7% formaldehyde in PBS and processed for immunofluorescence assay (IFA) as described previously (56). Primary antibodies were detected by species-specific secondary antibodies conjugated to Alexa Fluor 488/594 (ThermoFisher). Coverslips were mounted in Vectashield (Vector Labs, Burlingame, CA), viewed with an Axio Imager.Z1 fluorescence microscope (Zeiss), and processed with ZEN 2.3 software (Zeiss). Processing with the ZEN software included deconvolution as well as adaptation of the magenta pseudocolor from the 594 fluorophore.

For Western blotting, parasites were lysed in 1× Laemmli sample buffer with 100 mM dithiothreitol

(DTT) and boiled at 100°C for 10 min. Lysates were resolved by SDS-PAGE and transferred to nitrocellulose membranes, and proteins were detected with the appropriate primary antibody and corresponding secondary antibody conjugated to horseradish peroxidase. Chemiluminescence was induced using the SuperSignal West Pico substrate (Pierce) and imaged on a ChemiDoc XRS+ (Bio-Rad).

Endogenous epitope tagging. For C-terminal endogenous tagging, a pU6-Universal plasmid containing a protospacer against the 3′ untranslated region (UTR) approximately 100 to 200 bp downstream of the stop codon was generated for AC9, AC10, and ERK7, as described previously (57). A homology-directed repair (HDR) template was PCR amplified using the LIC vectors $p^{3\times HA}$-mAID.LIC-HXGPRT, p3xMyc.LIC-DHFR, and p2xStrep3xTy.LIC-HXGPR, which include the epitope tag, 3′ UTR, and a selection cassette (58). The HDR templates include 40 bp of homology immediately upstream of the stop codon or 40 bp of homology within the 3′ UTR downstream of the CRISPR/Cas9 cut site. This template was amplified in 400 μl, purified by phenol-chloroform extraction, ethanol precipitated, and electroporated into RH*Δhxgprt*Δ*ku80* parasites, along with 50 μg of the pU6-Universal plasmid. Successful tagging was confirmed by IFA, and clonal lines of tagged parasites were obtained through limiting dilution. AC10, AC9, and ERK7 were tagged using CRISPR/Cas9 with primers P1 to P12. This process was followed to generate the triple-tagged parasites ($AC10^{AID\text{-}3\times HA}$ | $AC9^{3xMyc}$ | $ERK7^{3xTy}$).

Complementation of AC9 and AC10. The AC9 wild-type complementation construct (22) was used as the template for creating a deletion of the CC domain. The online NEBasechanger (https://nebasechanger.neb.com/) was used to design primers, and the Q5 site-directed mutagenesis kit (NEB) was used to generate pUPRTKO-ISC6pro-$AC9^{\Delta CC}$-3xTy (primers P13 and P14). Both the $AC9^{wt}$ and $AC9^{\Delta CC}$ constructs were linearized with DraIII-HF (NEB), transfected into $AC9^{AID\text{-}3\times HA}$ parasites along with a universal pU6 that targets the UPRT coding region, and selected with 5 μg/ml FUDR for replacement of UPRT as described previously (42).

For AC10, the endogenous promoter as well as the full coding region was PCR amplified from genomic DNA. This was cloned into the pUPRTKO vector (22) with Gibson assembly (primers P15 to P18), resulting in pUPRTKO-AC10pro-$AC10^{wt}$-1xV5. The online NEBuilder tool was used to design these Gibson primers (https://nebuilder.neb.com/#!/). This complementation vector was then linearized with PsiI-v2 (NEB), transfected into triple-tagged parasites, and selected with FUDR. Clones expressing the pUPRTKO-AC10pro-$AC10^{wt}$-1xV5 vector were screened by IFA, and a V5-positive clone was designated $AC10^{wt}$. For most of the AC10 deletion constructs, pUPRTKO-AC10pro-$AC10^{wt}$-1xV5 was used as the template for the Q5 site-directed mutagenesis kit (NEB) (primers P19 to P28). For the $AC10^{\Delta N/C}$ construct, Gibson assembly was used with pUPRTKO-AC10pro-$AC10^{wt}$-1xV5 as the template for the vector (primers P29 and P30), and wild-type cDNA was used as a template for the insert (primers P31and P32). The same processes for linearization, transfection, and selection as described above were followed for all deletion constructs.

Plaque assays. Six-well plates with HFF monolayers were infected with equal numbers of individual strains grown with or without 500 μM IAA. Plaques were allowed to form for 7 days, fixed with ice-cold methanol, and stained with crystal violet. The areas of 30 plaques per condition were measured using ZEN software (Zeiss). All plaque assays were performed in triplicate for each condition. Graphical and statistical analyses were performed using Prism GraphPad 8.0. Multiple two-tailed *t* tests were used to compare the standard deviation-centered means with or without IAA, and statistical significance was determined using the Holm-Sidak method.

Pairwise yeast two-hybrid. ERK7 and AC9 sequences were cloned into the pB27 vector (Hybrigenics SA) as N-terminal fusions with the LexA DNA binding domain by Gibson assembly or enzyme inverse mutagenesis. AC10 sequences were cloned into the pP6 vector (Hybrigenics SA) as N-terminal fusions with the GAL4 activating domain. AC9 and AC10 constructs were created by Gibson assembly using *Toxoplasma* expression constructs as the template, and additional truncations were made by enzyme inverse mutagenesis with primers P36 to P56. ERK7 truncations were created from a full-length pB27 construct provided by Hybrigenics using primers P57 and P58. Synthetic dropout medium was purchased from Sunrise Science. To test for interactions, pairs of constructs were transformed into the L40 strain of *S. cerevisiae* [*MAT***a** *his3Δ200trp1-901 leu2-3112 ade2 LYS2*::(*4lexAop-HIS3*) *URA3*::(*8lexAop-lacZ*) *GAL4*; gift of Melanie Cobb]. Strains were grown overnight in permissive (−Leu/−Trp) medium, normalized to their optical density at 600 nm (OD_{600}), and spotted in 5× dilutions in both permissive and restrictive (−Leu/−Trp/−His) media. Relative growth in the two conditions was assessed after 3 to 4 days incubation at 30°C.

Protein expression and purification. All recombinant proteins were expressed as N-terminal fusions to His_6-SUMO in Rosetta2(DE3) bacteria overnight at 16°C overnight after induction with 300 mM IPTG. Cells were resuspended in binding buffer (50 mM Tris, pH 8.6, 500 mM NaCl, 15 mM Imidazole) and lysed by sonication. His_6-tagged protein was affinity purified using Ni-NTA resin (Qiagen), which was washed with binding buffer. Protein was eluted in 20 mM Tris, pH 8.6, 100 mM NaCl, 150 mM imidazole. Protein was diluted 1:1 with 20 mM Tris, pH 8.6, and purified by anion exchange on a HiTrapQ column. For ERK7 kinase and $AC9^{418\text{-}452}$, anion exchange peaks were pooled, incubated with ULP1 protease for 30 min, and diluted 1:1 in water, and the cleaved SUMO was separated from the protein of interest by anion exchange. The flowthrough was concentrated and purified by size exclusion chromatography, after which it was flash-frozen in 10 mM HEPES, pH 7.0, 300 mM NaCl for storage.

***In vitro* kinase assay.** ERK7 kinase activity was assessed using 1 μM purified ERK7 kinase, 5 mM $MgCl_2$, 200 μM cold ATP, 10 mM DTT, 1 mg/ml bovine serum albumin, 300 mM NaCl, 20 mM HEPES, pH 7.0, 10% glycerol. Reactions were started by adding a hot ATP mix that contained 10 μCi [γ^{32}P]ATP and 5 μg MBP and/or 10 μM $AC10^{313\text{-}569}$ as the substrate and in the presence or absence of 10 μM $AC9^{418\text{-}452}$. The 25-μl reaction mixtures were incubated in a 30°C water bath for 30 min. Reactions were

stopped by adding 5 μl 6× SDS buffer; 10 μl of each reaction was then separated by SDS-PAGE. Gels were fixed and Coomassie stained, and the extent of phosphorylation was assessed by phosphorimager (GE Typhoon).

SUPPLEMENTAL MATERIAL

Supplemental material is available online only.

FIG S1, TIF file, 1.4 MB.

FIG S2, TIF file, 1.4 MB.

FIG S3, TIF file, 2 MB.

FIG S4, TIF file, 0.8 MB.

TABLE S1, PDF file, 0.03 MB.

ACKNOWLEDGMENTS

We thank Gary Ward for anti-IMC1 antibodies and members of the Reese and Bradley labs for helpful reading of the manuscript. This work was supported by the National Institute of Health (AI150715 to M.L.R. and AI064616 to P.J.B.). M.L.R. was also supported by the National Science Foundation (NSF; MCB1553334) and the Welch Foundation (I-2075-20210327). P.S.B. was supported by the Ruth L. Kirschstein National Research Service Award GM007185 and the Molecular Biology Institute (MBI) Whitcome Fellowship at UCLA.

REFERENCES

1. Levine ND, Corliss JO, Cox FEG, Deroux G, Grain J, Honigberg BM, Leedale GF, Loeblich AR, Lom IJ, Lynn D, Merinfeld EG, Page FC, Poljansky G, Sprague V, Vavra J, Wallace FG. 1980. A newly revised classification of the protozoa. J Protozool 27:37–58. https://doi.org/10.1111/j.1550-7408.1980.tb04228.x.
2. Hill DE, Chirukandoth S, Dubey JP. 2005. Biology and epidemiology of Toxoplasma gondii in man and animals. Anim Health Res Rev 6:41–61. https://doi.org/10.1079/ahr2005100.
3. Mackintosh CL, Beeson JG, Marsh K. 2004. Clinical features and pathogenesis of severe malaria. Trends Parasitol 20:597–603. https://doi.org/10.1016/j.pt.2004.09.006.
4. Sow SO, Muhsen K, Nasrin D, Blackwelder WC, Wu Y, Farag TH, Panchalingam S, Sur D, Zaidi AKM, Faruque ASG, Saha D, Adegbola R, Alonso PL, Breiman RF, Bassat Q, Tamboura B, Sanogo D, Onwuchekwa U, Manna B, Ramamurthy T, Kanungo S, Ahmed S, Qureshi S, Quadri F, Hossain A, Das SK, Antonio M, Hossain MJ, Mandomando I, Nhampossa T, Acácio S, Omore R, Oundo JO, Ochieng JB, Mintz ED, O'Reilly CE, Berkeley LY, Livio S, Tennant SM, Sommerfelt H, Nataro JP, Ziv-Baran T, Robins-Browne RM, Mishcherkin V, Zhang J, Liu J, Houpt ER, Kotloff KL, Levine MM. 2016. The burden of Cryptosporidium diarrheal disease among children <24 months of age in moderate/high mortality regions of sub-Saharan Africa and South Asia, utilizing data from the Global Enteric Multicenter Study (GEMS). PLoS Negl Trop Dis 10:e0004729. https://doi.org/10.1371/journal.pntd.0004729.
5. Dubey JP, Dubey J. 2003. Review of Neospora caninum and neosporosis in animals. Korean J Parasitol 41:1–16. https://doi.org/10.3347/kjp.2003.41.1.1.
6. Kivaria FM. 2006. Estimated direct economic costs associated with tick-borne diseases on cattle in Tanzania. Trop Anim Health Prod 38:291–299. https://doi.org/10.1007/s11250-006-4181-2.
7. Sharman PA, Smith NC, Wallach MG, Katrib M. 2010. Chasing the golden egg: vaccination against poultry coccidiosis. Parasite Immunol 32:590–598. https://doi.org/10.1111/j.1365-3024.2010.01209.x.
8. Gould SB, Tham W-H, Cowman AF, McFadden GI, Waller RF. 2008. Alveolins, a new family of cortical proteins that define the protist infrakingdom Alveolata. Mol Biol Evol 25:1219–1230. https://doi.org/10.1093/molbev/msn070.
9. Frénal K, Dubremetz J-F, Lebrun M, Soldati-Favre D. 2017. Gliding motility powers invasion and egress in Apicomplexa. Nat Rev Microbiol 15:645–660. https://doi.org/10.1038/nrmicro.2017.86.
10. Francia ME, Striepen B. 2014. Cell division in apicomplexan parasites. Nat Rev Microbiol 12:125–136. https://doi.org/10.1038/nrmicro3184.
11. Harding CR, Meissner M. 2014. The inner membrane complex through development of Toxoplasma gondii and Plasmodium. Cell Microbiol 16:632–641. https://doi.org/10.1111/cmi.12285.
12. Anderson-White BR, Ivey FD, Cheng K, Szatanek T, Lorestani A, Beckers CJ, Ferguson DJP, Sahoo N, Gubbels M-J. 2011. A family of intermediate filament-like proteins is sequentially assembled into the cytoskeleton of Toxoplasma gondii. Cell Microbiol 13:18–31. https://doi.org/10.1111/j.1462-5822.2010.01514.x.
13. Porchet E, Torpier G. 1977. Freeze fracture study of Toxoplasma and Sarcocystis infective stages. Z Parasitenkd 54:101–124. https://doi.org/10.1007/BF00380795.
14. Mann T, Beckers C. 2001. Characterization of the subpellicular network, a filamentous membrane skeletal component in the parasite Toxoplasma gondii. Mol Biochem Parasitol 115:257–268. https://doi.org/10.1016/s0166-6851(01)00289-4.
15. Chen AL, Kim EW, Toh JY, Vashisht AA, Rashoff AQ, Van C, Huang AS, Moon AS, Bell HN, Bentolila LA, Wohlschlegel JA, Bradley PJ. 2015. Novel components of the Toxoplasma inner membrane complex revealed by BioID. mBio 6:e02357-14. https://doi.org/10.1128/mBio.02357-14.
16. Chen AL, Moon AS, Bell HN, Huang AS, Vashisht AA, Toh JY, Lin AH, Nadipuram SM, Kim EW, Choi CP, Wohlschlegel JA, Bradley PJ. 2017. Novel insights into the composition and function of the Toxoplasma IMC sutures. Cell Microbiol 19:10.1111/cmi.12678. https://doi.org/10.1111/cmi.12678.
17. Frénal K, Polonais V, Marq J-B, Stratmann R, Limenitakis J, Soldati-Favre D. 2010. Functional dissection of the apicomplexan glideosome molecular architecture. Cell Host Microbe 8:343–357. https://doi.org/10.1016/j.chom.2010.09.002.
18. Hu K, Johnson J, Florens L, Fraunholz M, Suravajjala S, DiLullo C, Yates J, Roos DS, Murray JM. 2006. Cytoskeletal components of an invasion machine—the apical complex of Toxoplasma gondii. PLoS Pathog 2:e13. https://doi.org/10.1371/journal.ppat.0020013.
19. Gilk SD, Raviv Y, Hu K, Murray JM, Beckers CJM, Ward GE. 2006. Identification of PhIL1, a novel cytoskeletal protein of the Toxoplasma gondii pellicle, through photosensitized labeling with 5-[^{125}I]iodonaphthalene-1-azide. Eukaryot Cell 5:1622–1634. https://doi.org/10.1128/EC.00114-06.
20. O'Shaughnessy WJ, Hu X, Beraki T, McDougal M, Reese ML. 2020. Loss of a conserved MAPK causes catastrophic failure in assembly of a specialized cilium-like structure in Toxoplasma gondii. Mol Biol Cell 31:881–888. https://doi.org/10.1091/mbc.E19-11-0607.
21. Tosetti N, Dos Santos Pacheco N, Bertiaux E, Maco B, Bournonville L, Hamel V, Guichard P, Soldati-Favre D. 2020. Essential function of the alveolin network in the subpellicular microtubules and conoid assembly in Toxoplasma gondii. Elife 9:e56635. https://doi.org/10.7554/eLife.56635.
22. Back PS, O'Shaughnessy WJ, Moon AS, Dewangan PS, Hu X, Sha J, Wohlschlegel JA, Bradley PJ, Reese ML. 2020. Ancient MAPK ERK7 is regulated by an unusual inhibitory scaffold required for Toxoplasma apical

complex biogenesis. Proc Natl Acad Sci U S A 117:12164–12173. https://doi.org/10.1073/pnas.1921245117.
23. Morrissette NS, Sibley LD. 2002. Cytoskeleton of apicomplexan parasites. Microbiol Mol Biol Rev 66:21–38. https://doi.org/10.1128/MMBR.66.1.21-38.2002.
24. Hu K, Roos DS, Murray JM. 2002. A novel polymer of tubulin forms the conoid of Toxoplasma gondii. J Cell Biol 156:1039–1050. https://doi.org/10.1083/jcb.200112086.
25. Okamoto N, Keeling PJ. 2014. The 3D structure of the apical complex and association with the flagellar apparatus revealed by serial TEM tomography in Psammosa pacifica, a distant relative of the apicomplexa. PLoS One 9:e84653. https://doi.org/10.1371/journal.pone.0084653.
26. Füssy Z, Masařová P, Kručinská J, Esson HJ, Oborník M. 2017. Budding of the alveolate alga vitrella brassicaformis resembles sexual and asexual processes in apicomplexan parasites. Protist 168:80–91. https://doi.org/10.1016/j.protis.2016.12.001.
27. Scholtyseck E, Mehlhorn H, Friedhoff K. 1970. The fine structure of the conoid of sporozoa and related organisms. Z F Parasitenkunde 34:68–94. https://doi.org/10.1007/BF00629180.
28. Wall RJ, Roques M, Katris NJ, Koreny L, Stanway RR, Brady D, Waller RF, Tewari R. 2016. SAS6-like protein in Plasmodium indicates that conoid-associated apical complex proteins persist in invasive stages within the mosquito vector. Sci Rep 6:28604–28612. https://doi.org/10.1038/srep28604.
29. Wall RJ, Zeeshan M, Katris NJ, Limenitakis R, Rea E, Stock J, Brady D, Waller RF, Holder AA, Tewari R. 2019. Systematic analysis of Plasmodium myosins reveals differential expression, localisation, and function in invasive and proliferative parasite stages. Cell Microbiol 21:e13082. https://doi.org/10.1111/cmi.13082.
30. Koreny L, Zeeshan M, Barylyuk K, Tromer EC, van Hooff JJE, Brady D, Ke H, Chelaghma S, Ferguson DJP, Eme L, Tewari R, Waller RF. 2021. Molecular characterization of the conoid complex in Toxoplasma reveals its conservation in all apicomplexans, including Plasmodium species. PLoS Biol 19:e3001081. https://doi.org/10.1371/journal.pbio.3001081.
31. de Leon JC, Scheumann N, Beatty W, Beck JR, Tran JQ, Yau C, Bradley PJ, Gull K, Wickstead B, Morrissette NS. 2013. A SAS-6-like protein suggests that the Toxoplasma conoid complex evolved from flagellar components. Eukaryot Cell 12:1009–1019. https://doi.org/10.1128/EC.00096-13.
32. Francia ME, Dubremetz J-F, Morrissette NS. 2015. Basal body structure and composition in the apicomplexans Toxoplasma and Plasmodium. Cilia 5:3. https://doi.org/10.1186/s13630-016-0025-5.
33. Lentini G, Dubois DJ, Maco B, Soldati-Favre D, Frénal K. 2019. The roles of Centrin 2 and Dynein Light Chain 8a in apical secretory organelles discharge of Toxoplasma gondii. Traffic 20:583–600. https://doi.org/10.1111/tra.12673.
34. Francia ME, Jordan CN, Patel JD, Sheiner L, Demerly JL, Fellows JD, de Leon JC, Morrissette NS, Dubremetz J-F, Striepen B. 2012. Cell division in apicomplexan parasites is organized by a homolog of the striated rootlet fiber of algal flagella. PLoS Biol 10:e1001444. https://doi.org/10.1371/journal.pbio.1001444.
35. Blader IJ, Coleman BI, Chen C-T, Gubbels M-J. 2015. Lytic cycle of Toxoplasma gondii: 15 years later. Annu Rev Microbiol 69:463–485. https://doi.org/10.1146/annurev-micro-091014-104100.
36. Carmen MGD, Mondragón M, González S, Mondragón R. 2009. Induction and regulation of conoid extrusion in Toxoplasma gondii. Cell Microbiol 11:967–982. https://doi.org/10.1111/j.1462-5822.2009.01304.x.
37. Graindorge A, Frénal K, Jacot D, Salamun J, Marq JB, Soldati-Favre D. 2016. The conoid associated motor MyoH is indispensable for Toxoplasma gondii entry and exit from host cells. PLoS Pathog 12:e1005388. https://doi.org/10.1371/journal.ppat.1005388.
38. Long S, Brown KM, Drewry LL, Anthony B, Phan IQH, Sibley LD. 2017. Calmodulin-like proteins localized to the conoid regulate motility and cell invasion by Toxoplasma gondii. PLoS Pathog 13:e1006379. https://doi.org/10.1371/journal.ppat.1006379.
39. Tosetti N, Dos Santos Pacheco N, Soldati-Favre D, Jacot D. 2019. Three F-actin assembly centers regulate organelle inheritance, cell-cell communication and motility in Toxoplasma gondii. Elife 8:e42669. https://doi.org/10.7554/eLife.42669.
40. Leung JM, He Y, Zhang F, Hwang Y-C, Nagayasu E, Liu J, Murray JM, Hu K. 2017. Stability and function of a putative microtubule-organizing center in the human parasite Toxoplasma gondii. Mol Biol Cell 28:1361–1378. https://doi.org/10.1091/mbc.e17-01-0045.
41. Katris NJ, van Dooren GG, McMillan PJ, Hanssen E, Tilley L, Waller RF. 2014. The apical complex provides a regulated gateway for secretion of invasion factors in Toxoplasma. PLoS Pathog 10:e1004074. https://doi.org/10.1371/journal.ppat.1004074.
42. Donald RG, Roos DS. 1995. Insertional mutagenesis and marker rescue in a protozoan parasite: cloning of the uracil phosphoribosyltransferase locus from Toxoplasma gondii. Proc Natl Acad Sci U S A 92:5749–5753. https://doi.org/10.1073/pnas.92.12.5749.
43. Treeck M, Sanders JL, Elias JE, Boothroyd JC. 2011. The phosphoproteomes of Plasmodium falciparum and Toxoplasma gondii reveal unusual adaptations within and beyond the parasites' boundaries. Cell Host Microbe 10:410–419. https://doi.org/10.1016/j.chom.2011.09.004.
44. Brad AH, David CS. 2016. Enzyme activity assays for protein kinases: strategies to identify active substrates. Curr Drug Discov Technol 13:2–15. https://doi.org/10.2174/1570163813666160115125930.
45. Sidik SM, Huet D, Ganesan SM, Huynh M-H, Wang T, Nasamu AS, Thiru P, Saeij JPJ, Carruthers VB, Niles JC, Lourido S. 2016. A genome-wide CRISPR screen in Toxoplasma identifies essential apicomplexan genes. Cell 166:1423–1435. https://doi.org/10.1016/j.cell.2016.08.019.
46. Choi CP, Moon AS, Back PS, Jami-Alahmadi Y, Vashisht AA, Wohlschlegel JA, Bradley PJ. 2019. A photoactivatable crosslinking system reveals protein interactions in the Toxoplasma gondii inner membrane complex. PLoS Biol 17:e3000475. https://doi.org/10.1371/journal.pbio.3000475.
47. Torres JA, Pasquarelli RR, Back PS, Moon AS, Bradley PJ. 2021. Identification and molecular dissection of IMC32, a conserved Toxoplasma inner membrane complex protein that is essential for parasite replication. mBio 12:e03622-20. https://doi.org/10.1128/mBio.03622-20.
48. Lupas AN, Bassler J. 2017. Coiled coils–a model system for the 21st century. Trends Biochem Sci 42:130–140. https://doi.org/10.1016/j.tibs.2016.10.007.
49. Donald RGK, Carter D, Ullman B, Roos DS. 1996. Insertional tagging, cloning, and expression of the Toxoplasma gondii hypoxanthine-xanthine-guanine phosphoribosyltransferase gene: use as a selectable marker for stable transformation. J Biol Chem 271:14010–14019. https://doi.org/10.1074/jbc.271.24.14010.
50. Donald RG, Roos DS. 1993. Stable molecular transformation of Toxoplasma gondii: a selectable dihydrofolate reductase-thymidylate synthase marker based on drug-resistance mutations in malaria. Proc Natl Acad Sci U S A 90:11703–11707. https://doi.org/10.1073/pnas.90.24.11703.
51. Kim K, Soldati D, Boothroyd JC. 1993. Gene replacement in Toxoplasma gondii with chloramphenicol acetyltransferase as selectable marker. Science 262:911–914. https://doi.org/10.1126/science.8235614.
52. Bastin P, Bagherzadeh A, Matthews KR, Gull K. 1996. A novel epitope tag system to study protein targeting and organelle biogenesis in Trypanosoma brucei. Mol Biochem Parasitol 77:235–239. https://doi.org/10.1016/0166-6851(96)02598-4.
53. Evan GI, Lewis GK, Ramsay G, Bishop JM. 1985. Isolation of monoclonal antibodies specific for human c-myc proto-oncogene product. Mol Cell Biol 5:3610–3616. https://doi.org/10.1128/mcb.5.12.3610-3616.1985.
54. Wichroski MJ, Melton JA, Donahue CG, Tweten RK, Ward GE. 2002. Clostridium septicum alpha-toxin is active against the parasitic protozoan Toxoplasma gondii and targets members of the SAG family of glycosylphosphatidylinositol-anchored surface proteins. Infect Immun 70:4353–4361. https://doi.org/10.1128/IAI.70.8.4353-4361.2002.
55. Beck JR, Rodriguez-Fernandez IA, de Leon JC, Huynh M-H, Carruthers VB, Morrissette NS, Bradley PJ. 2010. A novel family of Toxoplasma IMC proteins displays a hierarchical organization and functions in coordinating parasite division. PLoS Pathog 6:e1001094. https://doi.org/10.1371/journal.ppat.1001094.
56. Bradley PJ, Ward C, Cheng SJ, Alexander DL, Coller S, Coombs GH, Dunn JD, Ferguson DJ, Sanderson SJ, Wastling JM, Boothroyd JC. 2005. Proteomic analysis of rhoptry organelles reveals many novel constituents for host-parasite interactions in Toxoplasma gondii. J Biol Chem 280:34245–34258. https://doi.org/10.1074/jbc.M504158200.
57. Sidik SM, Hackett CG, Tran F, Westwood NJ, Lourido S. 2014. Efficient genome engineering of Toxoplasma gondii using CRISPR/Cas9. PLoS One 9:e100450. https://doi.org/10.1371/journal.pone.0100450.
58. Huynh M-H, Carruthers VB. 2009. Tagging of endogenous genes in a Toxoplasma gondii strain lacking Ku80. Eukaryot Cell 8:530–539. https://doi.org/10.1128/EC.00358-08.

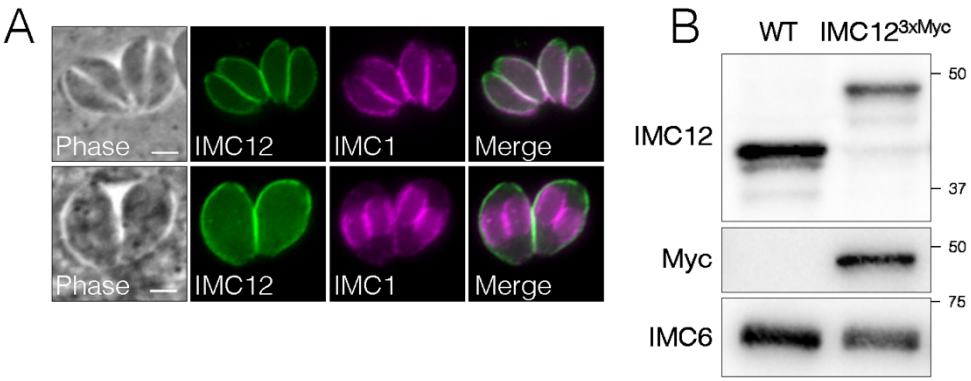

Supplemental Figure S1. Antibody validation for IMC12. (A) IFAs show the IMC12 antibody colocalized with IMC1. Upper panels show mature parasites, while the lower panels show ones in the process of budding, highlighting that IMC12 localizes exclusively to the maternal IMC. Green, rabbit anti-IMC12; magenta, mouse anti-IMC1. IFA scale bars are 2 μm. (B) Western blot analysis validates the efficacy of the IMC12 antibody. Endogenously tagged IMC12^{3xMyc} parasites display the upshift in protein size due to the mass of the epitope tag compared to untagged parasites, solidifying the identity of the band detected by the IMC12 antibody. IMC12 detected with rabbit anti-IMC12; IMC12^{3xMyc} detected with mouse anti-Myc. Rabbit anti-IMC6 was used as a loading control.

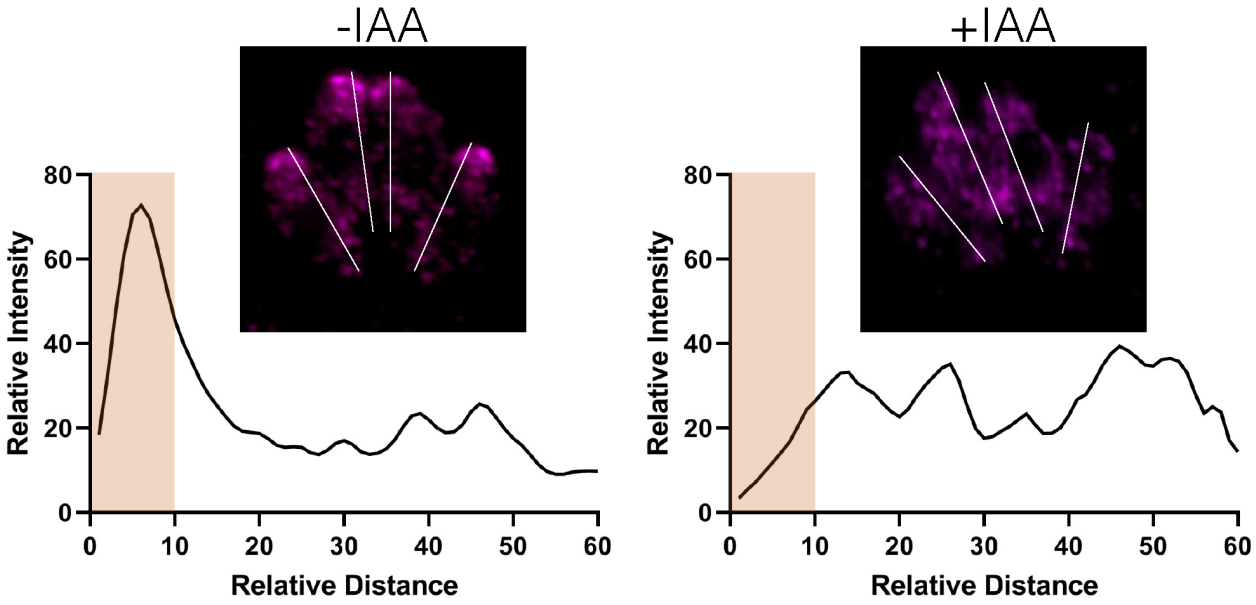

Supplemental Figure S2. Line intensity scans of ERK7 localization. Fluorescence intensity was measured across the indicated white lines, and the resulting relative intensity values from the four lines were averaged to produce the line intensity graph. Orange shading depicts the approximate position of the apical cap.

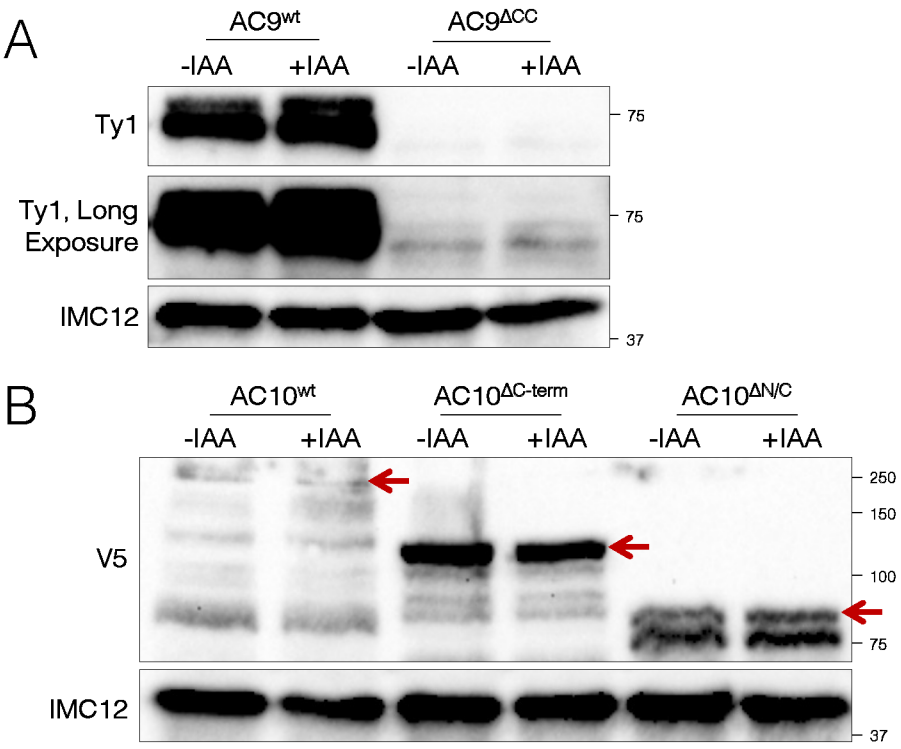

Supplemental Figure S3. Relative protein expression levels of mislocalized AC9 and AC10. (A) Western blot of whole-cell lysates showing the protein expression levels of $AC9^{wt}$ and $AC9^{\Delta CC}$ with or without IAA. $AC9^{wt}$ and $AC9^{\Delta CC}$ were detected with mouse anti-Ty1, and rabbit anti-IMC12 was used as a loading control. (B) Western blot showing migration of the indicated AC10 complementation constructs with or without IAA. $AC10^{wt}$ undergoes substantial breakdown during processing (also see Fig. 2C). Red arrows indicate the likely primary translation product for each construct. AC10 constructs were detected with mouse anti-V5, and rabbit anti-IMC12 was used as a loading control.

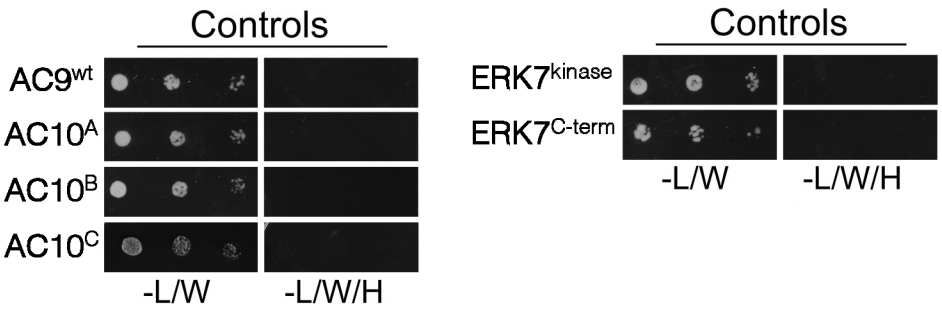

Supplemental Figure S4. Control Y2H experiments. Y2H demonstrates a lack of autoactivation of the indicated constructs. Each construct is coexpressed with the corresponding empty bait or prey vectors, as appropriate.

Supplemental Table 1: Oligonucleotides used in this study.

Purpose	Name	Description	Sequence 5'-3'
AC10 (TGGT1_292950) tagging	P1	AC10 gRNA-tagging sense	AAGTTgTAAGGGTGCAAGAGTTGATGG
	P2	AC10 gRNA-tagging antisense	AAAACCATCAACTCTTGCACCCTTAcA
	P3	AC10 5' HDR template	GCTGAAGACTCGCCTGATAAAGCTCACGAAGGCAAACACGGGAAGTGGAGGACGGGAATT
	P4	AC10 3' HDR template	AGTCCACTGCTGCTCCTCGAGCAGTCTGGGAGATTTGGCGACGGCCAGTGAATTGTAATA
AC9 (TGGT1_246950) tagging	P5	AC9 gRNA-tagging sense	AAGTTATGTGTTCCTCAAATGTCAGG
	P6	AC9 gRNA-tagging antisense	AAAACCTGACATTTGAGGAACACATA
	P7	AC9 5' HDR template	GTCGGGGAACCGCGAACCGAGTGAATATCCGCAGGGAATGGGAAGTGGAGGACGGGAATTC
	P8	AC9 3' HDR template	CTCGCAGCGTGTCGCACTGAACTCTTGTGCGGAGAGAGCGACGGCCAGTGAATTGTAATA
ERK7 (TGGT1_233010) tagging	P9	ERK7 gRNA-tagging sense	AAGTTGCAAAAGCAAAGATTCAGACG
	P10	ERK7 gRNA-tagging antisense	AAAACGTCTGAATCTTTGCTTTTGCA
	P11	ERK7 5' HDR template	TTCTCTTTTTTTTCAGTCTGCGTCCAAGACATACAACAGCGGAAGTGGAGGACGGGAATT
	P12	ERK7 3' HDR template	GCTTTCTCCACCTTCGCTTTCGGTGGAAGTCTTGCGAGCGACGGCCAGTGAATTGTAATA
AC9 CC deletion construct	P13	AC9 CCdel mut fwd	AAGGAGGCGTTTGCACGCAG
	P14	AC9 CCdel mut rev	GGCTGCTGCAGCCGGGTC
AC10 promoter and full length complementation	P15	pUPRTKO vector fwd	GCGGCCGCCTACCCGTAC
	P16	pUPRTKO vector rev	ATGCATATGCGATGTCGAACCCTCG
	P17	AC10pro-coding fwd	gttcgacatcgcatatgcatCCCCACTCGTTCCTCGATG
	P18	AC10pro-coding rev	tcgtacgggtaggcggccgcTCTCGCCTTTAATTGCAGTACG
AC10 CC1 deletion construct	P19	AC10CC1 Q5del fwd	CTGACGCATGCAGTGGAC
	P20	AC10CC1 Q5del rev	GTCACCGCAGGTGGCATC
AC10 AC9-BD deletion construct	P21	AC10-AC9bd Q5del fwd	AAACTAGACGCTGAAGAC
	P22	AC10-AC9bd Q5del rev	GTTATCTTCTGCACTGCC
AC10 CC2 deletion construct	P23	AC10CC2 Q5del fwd	GAAAGTACAGGAAGTCGTG
	P24	AC10CC2 Q5del rev	ACAGACATTCGATCGTTG
AC10 N-term deletion construct	P25	AC10N-term Q5del fwd	GGAGACACGCGTCCGCAT
	P26	AC10N-term Q5del rev	CATCGCAACTTCCTCCTTTTCG
AC10 C-term deletion construct	P27	AC10C-term Q5del fwd	GCGGCCGCCGGCAAACCT
	P28	AC10C-term Q5del rev	GGACTGAGCAGGTAGAACTGAAAGGGATAGAGG
AC10 N/C deletion construct	P29	pUPRTKO-AC10wt-vector-fwd	GCGGCCGCCGGCAAACCT
	P30	pUPRTKO-AC10wt-vector-rev	CATCGCAACTTCCTCCTTTTCGCAAAAAGATGTGTTCTTTC
	P31	AC10N-Cdel fwd	aaaaggaggaagttgcgatgCTTACGCGTCTAGATTTG
	P32	AC10N-Cdel rev	ataggtttgccggcggccgcGGACTGAGCAGGTAGAAC
IMC12 pET28 construct for antibody production	P32	IMC12-pET28 fwd	TAATAACATTGGAAGTGGATAAC
	P33	IMC12-pET28 rev	TGCATTGGATTGGAAGTAC
	P34	IMC12-coding fwd	tgtacttccaatccaatgcaGCAACCGAGTTCGTCGTTC
	P35	IMC12-coding rev	atccacttccaatgttattaCTGGGGCATGGAGTCGAC
Yeast-2-hybrid	P36	f pB27* ga/PhQC [58]	TAAGGGCCACTGGGGCCCC
	P37	r pB27 ga/PhQC [59]	TCCGGCCCCGAATTCCAGC
	P38	f pP6 3p ga/PhQC [57]	CTCGAGTAGCTAGTGTCTAGAG
	P39	r pP6 5p ga/PhQC [57]	ATTCGTGGCCCCTGCGG
	P40	f AC9(D2) pb27-ga [58]	ctggaattcggggccggaGACGTCTCCGGTCGAGGC
	P41	r AC9(M452*) pb27-ga	gggccccagtggcccttaCATTCCCTGCGGATATTCACTCG
	P42	f AC9(P70) blunt [61]	CCGGCTGCAGCAGCCATTC
	P43	r AC9(Q113*) blunt [59]	tcaCTGCTCCTCCAAGCTTTTGAAAG
	P44	r AC9(A157*) blunt [59]	tcaGGCAAAGCCTTGAATGGTTGAGG
	P45	f AC10(V2) pP6-ga [57]	gccgcaggggccacgaat GTGACTGCAGTACCCAATCCTTC
	P46	r AC10(N650*) pP6-ga [57]	ctagacactagctactcgag tca GTTATCTTCTGCACTGCCTTTGAC
	P47	f AC10(E651) pP6-ga [59]	gccgcaggggccacgaatGAAGACAGCACAGAGAGCCAG
	P48	r AC10(T1300*) pP6-ga [59]	ctagacactagctactcgagtcaGGTGGTACGCGTCGCTATTC
	P49	f AC10(S1301) pP6-ga [57]	gccgcaggggccacgaatTCCCCTTTTCAGCGGGGAG
	P50	r AC10(R1979*) pP6-ga [57]	ctagacactagctactcgagTCATCTCGCCTTTAATTGCAGTAC
	P51	f AC10(K684) blunt [59]	AAACTAGACGCTGAAGACCAGAAG
	P52	r AC10(R683) blunt [58]	GCGTGGATCAAGCACCTTGG
	P53	r AC10(S913*) blunt [58/62]	tcaGGACTGAGCAGGTAGAACTG
	P54	f AC10(W914) blunt [59/64]	TGGAATACTACGTCTGTGTCCGC
	P55	r AC10(C780 no*) [57/61]	ACAGACATTCGATCGTTGCTG
	P56	f AC10(E831) [57/61]	GAAAGTACAGGAAGTCGTGCG
	P57	r TgERK7(A358*) blunt [61]	tcaAGCTGTGCGGTGTCGCCG
	P58	f TgERK7(G359) blunt [59]	GGTTCTTCCGGCCGCCACC

Supplemental Table S1. Oligonucleotides used in this study. All primer sequences are shown in the 5' to 3' orientation.